



HAL
open science

QCD resummations for gaugino-pair hadroproduction

Jonathan Debove

► **To cite this version:**

Jonathan Debove. QCD resummations for gaugino-pair hadroproduction. High Energy Physics - Experiment [hep-ex]. Université Joseph-Fourier - Grenoble I, 2010. English. NNT: . tel-00522972

HAL Id: tel-00522972

<https://theses.hal.science/tel-00522972>

Submitted on 4 Oct 2010

HAL is a multi-disciplinary open access archive for the deposit and dissemination of scientific research documents, whether they are published or not. The documents may come from teaching and research institutions in France or abroad, or from public or private research centers.

L'archive ouverte pluridisciplinaire **HAL**, est destinée au dépôt et à la diffusion de documents scientifiques de niveau recherche, publiés ou non, émanant des établissements d'enseignement et de recherche français ou étrangers, des laboratoires publics ou privés.

UNIVERSITÉ DE GRENOBLE
ÉCOLE DOCTORALE DE PHYSIQUE

Thèse de Doctorat

Spécialité: Physique Subatomique et Astroparticules

présentée par
Jonathan Debove

en vue de l'obtention du grade de
Docteur ès Science de l'Université de Grenoble

**QCD resumptions for gaugino-pair
hadroproduction**

soutenue le 8 septembre 2010 au
LABORATOIRE DE PHYSIQUE SUBATOMIQUE ET DE COSMOLOGIE

devant le jury composé de

Prof. Johann Collot	Université de Grenoble	Président du jury
Dr. Benjamin Fuks	Université de Strasbourg	Examineur
Prof. Michael Klasen	Université de Grenoble	Directeur de thèse
Dr. Jean-Loïc Kneur	LPTA Montpellier	Rapporteur
Dr. Yves Sirois	LLR Palaiseau	Examineur
Prof. Werner Vogelsang	Université de Tübingen	Rapporteur

Résumé

Ce document a pour vocation de présenter mon travail de thèse sur les resommations en Chromo-Dynamique Quantique (QCD) pour la production hadronique de paires de jauginos.

Dans le premier chapitre, nous introduisons quelques motivations pour étendre le Modèle Standard (MS) de la physique des particules, telles que le problème de hiérarchie et l'absence de candidat pour former la matière noire observée dans l'univers. Parmi les extensions possibles, nous mentionnons l'ajout de la supersymétrie (SUSY) qui permet, en plus de résoudre les problèmes précédemment cités, l'unification des trois couplages de jauges du MS. Le MS Supersymétrique Minimal (MSSM) est l'extension la plus simple du MS qui inclut la SUSY. Ainsi, nous présentons les limites et contraintes actuelles sur les paramètres du MSSM provenant à la fois des données cosmologiques sur la matière noire et des diverses expériences aux collisionneurs.

Le second chapitre traite du MSSM. Tout d'abord, nous introduisons la SUSY via la superalgèbre. Puis, nous nous concentrons sur le MSSM et présentons son contenu en particule, sa densité de Lagrange et la brisure douce de la SUSY. Enfin, nous décrivons les états propres de masse et les mélanges induits par la brisure de la symétrie électrofaible, en particulier, ceux des états neutralinos et charginos.

Les techniques nécessaires aux resommations pour la production de paires de jauginos sont présentées dans le troisième chapitre. Les notations sont introduites via la présentation de résultats majeurs de la QCD perturbative que sont la liberté asymptotique et le théorème de factorisation. Nous détaillons ensuite les formalismes de resommations au seuil et en impulsion transverse, abordant les différentes refactorisations qui mènent à la resommation des logarithmes dominants. Plusieurs techniques et améliorations des formalismes de resommations sont aussi exposées.

Les chapitres 4 et 5 sont dédiés à la production hadronique des paires de jauginos. Dans le chapitre 4, nous présentons nos calculs perturbatifs aux ordres dominant et sous-dominant en QCD. A l'ordre dominant, nous donnons les résultats analytiques des sections efficaces partoniques polarisées, et nous présentons une étude numérique des sections efficaces totales et des asymétries simple/double-spin pour la production de différentes paires de jauginos aux collisionneurs RHIC, Tevatron et LHC. A l'ordre sous-dominant, les corrections QCD supersymétriques sont étudiées. Nous présentons tout d'abord notre calcul des corrections virtuelles en précisant le schéma de renormalisation des masses, des fonction d'onde et des matrices de mélange des quarks et des squarks (partenaires SUSY des quarks). Puis, nous détaillons le traitement des corrections réelles par les méthodes de soustractions des dipôles et des contributions dues aux squarks sur couche de masse. Numériquement, nous trouvons que les corrections sont importantes et positives aux collisionneurs actuels.

Notre analyse numérique des effets de resommations au seuil et en impulsion transverse pour la production de paires de jauginos est présentée au chapitre 5. Alors que les effets de seuil n'augmentent que peu la distribution en masse invariante et la section efficace totale, ils stabilisent grandement nos prédictions vis-à-vis des dépendances aux échelles de renormalisation et de factorisation. Concernant la distribution en impulsion transverse, la resommation permet d'obtenir des résultats convergents pour des petites impulsions transverses, contrairement aux résultats perturbatifs. Nous avons comparé nos distributions avec

celles obtenues avec des générateurs Monte-Carlo et nous avons étudié en détail l'impact des incertitudes dus aux fonctions de distributions de partons et aux effets non-perturbatifs.

Finalement, le chapitre 6 conclut sur l'apport de nos résultats pour la découverte des paires de jauginos et les perspectives futures quant aux développements des générateurs Monte-Carlo à l'ordre sous-dominant et des techniques de resommation.

Remerciements

Tout d'abord, je souhaiterais exprimer toute ma gratitude à mon directeur de thèse Michael Klasen pour m'avoir soutenu et toujours fait confiance. Je remercie également Benjamin Fuks pour son aide précieuse tout au long de ces trois années, et qui est aussi devenu un ami.

Je voudrais remercier particulièrement mes deux rapporteurs, Jean-Loïc Kneur et Werner Vogelsang, ainsi que l'ensemble de mon jury, Johann Collot et Yves Sirois, pour leur lecture attentive de ce manuscrit.

Mes sincères remerciements au groupe théorie du LPSC pour leur accueil pendant ces trois ans: Jaume Carbonell, Ingo Schienbein et Sabine Kraml. Je souhaite remercier aussi les précaires du groupe, Roberto Bonciani, Björn Herrmann, Tomas Jezo, Karol Kovařík et Carole Weydert, pour les nombreuses discussions que nous avons partagées. Et je remercie tout particulièrement mes amis du groupe QCD sur réseau: Vincent Drach et Pierre-Antoine Harraud.

Ma reconnaissance à Serge Kox, directeur du LPSC, ainsi qu'à Anic, Audrey, Cecile et Halima pour l'administration de mes nombreuses missions.

Je salue tous les autres doctorants du laboratoire pour les moments agréables que nous avons partagé, en particulier autour d'un café. Merci également à tous ceux qui ont pu ponctuellement contribuer à cette thèse et qui ne sont pas cités ici.

Merci enfin à mes parents et à Nolwen pour leur soutien et leurs encouragements pendant ces trois années d'étude.

QCD resummations for gaugino-pair hadroproduction

JONATHAN DEBOVE

8th September 2010

Contents

1	Introduction	1
2	Supersymmetry	5
2.1	The superalgebra	5
2.2	The Minimal Supersymmetric Standard Model	7
2.2.1	Field Content of the MSSM	7
2.2.2	Supersymmetric Lagrange density	7
2.2.3	Supersymmetry breaking	8
2.3	Mass eigenstates	9
2.3.1	Higgs sector	10
2.3.2	Sfermion sector	11
2.3.3	Gaugino/Higgsino sector	11
3	Resummation	15
3.1	Perturbative QCD	15
3.2	Resummation philosophy	18
3.3	Threshold resummation	19
3.3.1	Refactorisation	20
3.3.2	Exponentiation	20
3.3.3	NLL approximation	22
3.3.4	Improvement of the threshold resummation	22
3.3.5	Matching procedure	23
3.4	Transverse-momentum resummation	24
3.4.1	Refactorisation	24
3.4.2	Exponentiation	25
3.4.3	NLL approximation	26
3.4.4	Improvements of the resummation formalism	27
3.4.5	Matching procedure	27
3.5	Inverse transforms	28
4	Gaugino-pair production: Fixed-order calculations	31
4.1	LO cross section and spin asymmetries	31
4.1.1	Coupling definitions	31
4.1.2	Polarised partonic cross section	33
4.1.3	Numerical results	34
4.2	SUSY-QCD corrections	46
4.2.1	Virtual corrections	46

Contents

4.2.2	Real corrections	51
4.2.3	Numerical results	55
5	Gaugino-pair production: Resummed calculations	57
5.1	Benchmark points	57
5.2	Transverse-momentum distribution	59
5.2.1	Transverse-momentum resummation	59
5.2.2	Numerical results	60
5.3	Invariant-mass distribution	63
5.3.1	Threshold resummation	63
5.3.2	Numerical results	64
5.4	Total cross section	70
6	Conclusion	77

1

Introduction

The Standard Model of particle physics is based on the gauge group $SU(3)_C \times SU(2)_L \times U(1)_Y$ and includes both the strong and electroweak interactions [1, 2, 3, 4, 5]. At present, there are experimental evidences for all of its particles except for the Higgs boson, which continues to defy the scientific community. It is the last necessary piece to describe the observed electroweak symmetry breaking and is supposed to couple to every massive particle [6, 7]. Despite its great success in describing Nature, the Standard Model leaves several questions unanswered. From the point of view of particle physics, the most quoted argument is probably the hierarchy problem. It originates from the large difference between the electroweak scale of $\mathcal{O}(100 \text{ GeV})$ and the Planck scale of $\mathcal{O}(10^{19} \text{ GeV})$. This leads to *unnaturally* large radiative corrections to the scalar masses in the theory (in the Standard Model there is only one scalar boson, the Higgs boson). Therefore, the Standard Model parameters have to be fine-tuned to respect all electroweak precision data. On the cosmological side, the Standard Model does not include the dark matter, which is observed in the Universe. These considerations are taken as hints of new physics, which might appear at the scale of $\mathcal{O}(1 \text{ TeV})$.

Many models propose to extend the Standard Model in order to solve one or several of these problems. Among them, supersymmetry is probably the best-known and certainly the best studied extension [8, 9]. Linking bosons and fermions in an elegant formalism, supersymmetry allows for a natural solution of the hierarchy problem and for accurate unification of the three Standard Model gauge couplings at a high unification scale of $\mathcal{O}(10^{16} \text{ GeV})$. Furthermore, if R -parity is conserved, it provides a convincing candidate for the large amount of cold dark matter observed in the Universe. In the Minimal Supersymmetric Standard Model, this is generally the lightest neutralino ($\tilde{\chi}_1^0$), one of the spin-1/2 supersymmetric partners of the electroweak gauge bosons (gauginos) and of the Higgs bosons (Higgsinos), which mix to form four neutral (neutralino) and two charged (chargino) mass eigenstates. The gaugino/Higgsino decomposition of the neutralinos/charginos contains important information about the supersymmetry-breaking mechanism and plays a crucial role in the determination of the dark matter relic density Ω_{CDM} . With the precision measurements of the Cosmic Microwave Background, the satellites COBE and WMAP have imposed strong limits on Ω_{CDM} [10, 11], thus allowing for dramatic discriminations between different supersymmetric scenarios [12]. In Fig. 1.1, we show several constraints for minimal supergravity scenarios in the $m_0 - m_{1/2}$ plane, m_0 and $m_{1/2}$ being the universal scalar and gaugino mass, respectively.¹ The region allowed by the WMAP constraint is in-

¹The minimal supergravity parameters and supersymmetric particles are discussed in Sec. 2.2.3.

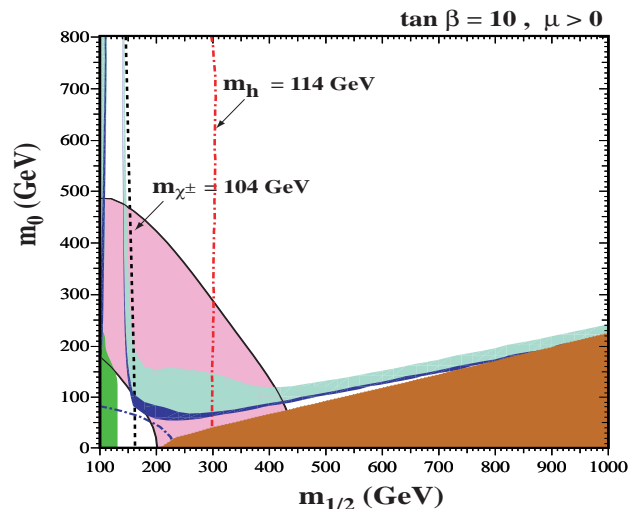


Figure 1.1: The $m_0 - m_{1/2}$ plane for $\tan \beta = 10$ and $\mu > 0$ [12]. The pre-WMAP (light blue), post-WMAP (dark blue) and $g_\mu - 2$ (pink) favoured regions are shown as well as $b \rightarrow s\gamma$ (green) and charged dark matter (brown) excluded regions. The different lines indicate the LEP constraints on the Higgs boson mass (red), chargino mass (black) and selectron mass (blue).

deed a very narrow band, and several regions are preferred: the bulk region at small m_0 and $m_{1/2}$, the focus point at very large m_0 , and the co-annihilation region just above the region excluded because of a charged dark matter (usually this is the lightest stau $\tilde{\tau}_1$).

Unfortunately, the collider constraints are less severe, and supersymmetric particles have yet to be found at high-energy accelerators. The Large Electron Positron (LEP) and Tevatron colliders have constrained the gauginos and scalar partners of the fermions (squarks/sleptons) to be heavier than a few tens and hundreds of GeV, respectively. In Fig. 1.2, we show the present limits for the search of the associated production of lightest chargino ($\tilde{\chi}_1^\pm$) and next-to-lightest neutralino ($\tilde{\chi}_2^0$) at the D0 and CDF experiments. The current Tevatron searches exclude only the low mass region of the parameter space (roughly $m_0 < 150$ GeV and $m_{1/2} < 250$ GeV), and the search for supersymmetric particles has thus become one of the defining tasks of the Large Hadron Collider (LHC) at CERN. In spite of difficulties in September 2008, due to a serious fault between two superconducting bending magnets, the proton beams were finally circulating in the LHC and first collisions were observed in November 2009. At present, the LHC is running with a centre-of-mass energy of 7 TeV and should collect 1 fb^{-1} by the end of 2011. A few W and Z bosons have already been seen, and the very first $t\bar{t}$ events are being analysed as you are reading this manuscript. Concerning supersymmetry, ATLAS and CMS should have enough data at the end of run one to double today's sensitivity to certain new discoveries, pushing the discovery range up to masses of 620 GeV [16]. The end of run one will see a longer shutdown for routine maintenance and repair completion, the goal being to reach first a centre-of-mass energy of 10 TeV, and then the LHC design energy and luminosity of 14 TeV and $10^{34} \text{ cm}^{-2}\text{s}^{-1}$, respectively.

In this document, we present precision calculations for gaugino-pair production at current hadron colliders. In the second chapter of this thesis, we introduce supersymmetry

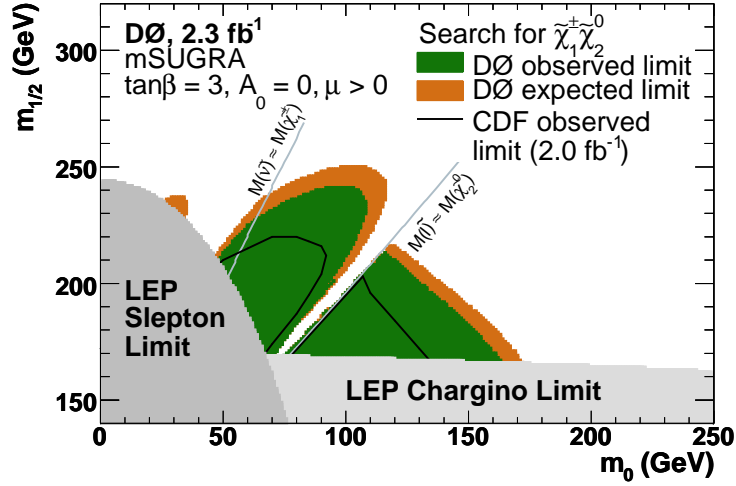


Figure 1.2: Region in the $m_0 - m_{1/2}$ plane excluded by the DØ analyses (green), by LEP searches for charginos (light grey) and sleptons (dark grey) [13], and by CDF (black line) [14]. The assumed minimal supergravity parameters are $A_0 = 0$ GeV, $\tan\beta = 3$ and $\mu > 0$ [15].

and concentrate on the simplest realistic model, the Minimal Supersymmetric Standard Model. We therefore present its particle content, its Lagrange density and the resulting mass eigenstates of the theory, emphasising the neutralino and chargino mass eigenstates. In chapter three, we present important features of perturbative QCD and focus on threshold and transverse-momentum resummations. The pioneering work of Collins, Soper and Sterman on all-order resummations [17, 18] as well as more recent improvements are detailed. Chapter four is devoted to our fixed-order calculations for gaugino-pair production. We study the polarised total cross sections and the supersymmetric QCD radiative corrections to the unpolarised cross sections. In chapter 5, we apply the resummation formalisms to the production of the gaugino pairs. Analytical and numerical results are detailed focusing on the transverse-momentum spectra, invariant-mass distributions, and total cross sections at both the Tevatron and the LHC. Our conclusion and outlook are presented in chapter 6.

1 Introduction

2

Supersymmetry

The Standard Model (SM) of particle physics, developed in the 70's, has known a great success in describing Nature. Based on the gauge-symmetry group $SU(3)_C \times SU(2)_L \times U(1)_Y$, it consistently includes both the electroweak and the strong interactions [1, 2, 3, 4, 5]. At present, its only missing piece is the discovery of the Higgs boson, responsible for the generation of the electroweak gauge-boson masses and the fermion masses through its Yukawa couplings [6, 7].

However, there are still several fundamental open questions, and many SM extensions propose to solve some of them. Among these extensions, the Minimal Supersymmetric SM (MSSM) is probably the most famous and best studied [8, 9]. Weak scale supersymmetry (SUSY) is indeed one of the most appealing extensions of the SM. It can break the electroweak symmetry radiatively, allows for its grand unification with the local gauge symmetry of strong interactions, offers a natural explanation of the large hierarchy between electroweak and gravitational interactions and appears naturally in string theories. From a theoretical point of view, the main motivation for SUSY is that it is the only way to extend the Poincaré symmetry with internal symmetries (as discussed in the next section).

This chapter is devoted to the presentation of the MSSM. We first introduce SUSY itself and then focus on the MSSM with its field content and its symmetries, broken or not, and finally its mass spectrum.

2.1 The superalgebra

It is known that Poincaré symmetry is realised in Nature and that symmetries play an important role in particle physics. Therefore, one may ask whether it is possible to extend the Poincaré group with internal symmetries. Recall that the generators of the Poincaré algebra satisfy the commutation relations

$$[P_\mu, P_\nu] = 0, \tag{2.1}$$

$$[P_\mu, M_{\nu\rho}] = i(g_{\mu\nu}P_\rho - g_{\mu\rho}P_\nu), \tag{2.2}$$

$$[M_{\mu\nu}, M_{\rho\sigma}] = -i(g_{\mu\rho}M_{\nu\sigma} - g_{\mu\sigma}M_{\nu\rho} + M_{\mu\rho}g_{\nu\sigma} - M_{\mu\sigma}g_{\nu\rho}), \tag{2.3}$$

where $g_{\mu\nu} = \text{diag}(1, -1, -1, -1)$ is the Minkowski metric, P_μ is the energy-momentum operator and $M_{\mu\nu}$ are the generators of angular momenta and Lorentz boosts.

In 1967, Coleman and Mandula published their so-called *no-go theorem*, where starting from an interacting four-dimensional quantum field theory with massive one-particle states

2 Supersymmetry

and assuming some non-zero scattering amplitudes, they proved that any Lie group which contains both the Poincaré group \mathcal{P} and an internal symmetry group \mathcal{G} must be a trivial direct product $\mathcal{P} \times \mathcal{G}$ [19]. This is well-known nowadays and it is actually realised in the SM with gauge symmetries, whose generators trivially commute with those of the Poincaré group. For instance, concerning the gauge group $SU(N)$, its generators T^a , with $1 \leq a \leq N^2 - 1$, satisfy the following commutation relations

$$[T^a, T^b] = if^{abc}T^c, \quad (2.4)$$

$$[T^a, P_\mu] = 0 = [T^a, M_{\mu\nu}], \quad (2.5)$$

where f^{abc} are the structure constants of the gauge group. And this would be the end of the story if nobody had managed to bypass this no-go theorem.

In 1975, Haag, Lopuszanski and Sohnius extended the Coleman-Mandula theorem by allowing not only commuting, but also anticommuting symmetry generators. They proved that there is a unique non-trivial extension of the Poincaré algebra which is called superalgebra [20]. The superalgebra is defined by the usual relations of the Poincaré algebra together with the new (anti)commutation relations

$$\{Q_\alpha^i, \bar{Q}_\beta^j\} = 2(\sigma^\mu)_{\alpha\beta}P_\mu\delta_{ij}, \quad (2.6)$$

$$\{Q_\alpha^i, Q_\beta^j\} = \varepsilon_{\alpha\beta}Z^{ij}, \quad (2.7)$$

$$[Q_\alpha^i, P_\mu] = 0, \quad (2.8)$$

$$[Q_\alpha^i, M_{\mu\nu}] = i(\sigma_{\mu\nu})_\alpha^\beta Q_\beta^i, \quad (2.9)$$

$$[Q_\alpha^i, T^a] = 0, \quad (2.10)$$

where Q_α^i , with $1 \leq i \leq \mathcal{N}$, are the \mathcal{N} SUSY generators, $Z^{ij} = -Z^{ji}$ are central charges which commute with all the generators of the superalgebra, and $\varepsilon_{\alpha\beta}$ is the two-dimensional antisymmetric tensor with $\varepsilon_{12} = 1$. Note that the SUSY generators carry a spinorial index ($\alpha = 1, 2$ in Weyl notation), thus changing the spin of the state they act on by one-half. Our conventions for the matrices σ^μ , $\bar{\sigma}^\mu$ and $\sigma^{\mu\nu}$ are

$$(\sigma^\mu)_{\alpha\dot{\alpha}} = (I, \sigma_x, \sigma_y, \sigma_z)_{\alpha\dot{\alpha}}, \quad (2.11)$$

$$(\bar{\sigma}^\mu)^{\dot{\alpha}\alpha} = \varepsilon^{\dot{\alpha}\beta}\varepsilon^{\alpha\gamma}(\sigma^\mu)_{\beta\gamma}, \quad (2.12)$$

$$(\sigma^{\mu\nu})_\alpha^\beta = \frac{1}{4}(\sigma^\mu\bar{\sigma}^\nu - \sigma^\nu\bar{\sigma}^\mu)_\alpha^\beta, \quad (2.13)$$

where I is the identity matrix and $\sigma_{x,y,z}$ are the usual Pauli matrices.

The particle states lie in the irreducible representations of the above superalgebra, namely the supermultiplets. Each of them contains an equal number of bosonic and fermionic degrees of freedom. As can be seen from Eqs. (2.8) and (2.10), the SUSY generators commute with both the squared mass operator P^2 and the generators of the gauge transformations. Thus, particles in the same supermultiplet have equal mass, electric charge, weak isospin and colour quantum numbers. In principle, there can be $\mathcal{N} \leq 4J$ distinct sets of SUSY generators, where J denotes the maximal spin of the particles involved in the theory. For instance for renormalisable gauge theories where $J = 1$, one should in principle consider the cases $1 \leq \mathcal{N} \leq 4$. However, for $\mathcal{N} \geq 2$, left-handed and right-handed fermionic states belong to the same supermultiplet and have equal weak isospin quantum number. Since we know that parity is violated by the weak interactions, only the case $\mathcal{N} = 1$ is viable phenomenologically.

2.2 The Minimal Supersymmetric Standard Model

Names	Superfield	Spin 0	Spin 1/2
Squarks/Quarks	Q	$\tilde{q}_L = (\tilde{u}_L, \tilde{d}_L)$	$q_L = (u_L, d_L)$
	U	\tilde{u}_R^\dagger	u_R^\dagger
	D	\tilde{d}_R^\dagger	d_R^\dagger
Sleptons/Leptons	L	$\tilde{l}_L = (\tilde{\nu}_L, \tilde{e}_L)$	$l_L = (\nu_L, e_L)$
	E	\tilde{e}_R^\dagger	e_R^\dagger
Higgs/Higgsinos	H_1	$h_1 = (H_1^0, H_1^-)$	$\tilde{h}_1 = (\tilde{H}_1^0, \tilde{H}_1^-)$
	H_2	$h_2 = (H_2^+, H_2^0)$	$\tilde{h}_2 = (\tilde{H}_2^+, \tilde{H}_2^0)$

Table 2.1: Chiral supermultiplets of the MSSM.

Names	Superfield	Spin 1/2	Spin 1
Gluinos/Gluons	G	\tilde{g}	g
Winos/W-bosons	W	$\tilde{W}^\pm, \tilde{W}^0$	W^\pm, W^0
Bino/B-boson	B	\tilde{B}^0	B^0

Table 2.2: Vector supermultiplets of the MSSM.

2.2 The Minimal Supersymmetric Standard Model

Although SUSY had appeared before in some articles published in the Soviet Union [21, 22], it was the work of Wess and Zumino in 1974 that triggered the great interest on SUSY [23]. It is fair to say that most of the SUSY extensions of the SM like the MSSM have followed the path set by their work [24, 25]. For a complete introduction to SUSY field theory with an emphasis on the MSSM see Refs. [9, 26].

2.2.1 Field Content of the MSSM

The MSSM is the minimal model which includes both the SM and $\mathcal{N} = 1$ SUSY. It is built on two kinds of supermultiplets. The first one is called the chiral supermultiplet. It is composed of a complex scalar field and a Weyl fermion. The second one contains also a Weyl fermion, but associated with a vector boson. It is called a vector supermultiplet.

The SM fermions, the quarks and the leptons, are incorporated in chiral supermultiplets, thus getting scalar partners called squarks and sleptons, respectively. In addition, to preserve SUSY and avoid gauge anomalies, two Higgs doublets are needed in the MSSM, unlike the SM. They are organised in chiral supermultiplets together with their fermionic partners, the Higgsinos. Finally, all the SM gauge bosons are associated with vector supermultiplets, and we call their SUSY partners the gauginos. The MSSM content of chiral and vector supermultiplets is summarised up in Tabs. 2.1 and 2.2 respectively.

2.2.2 Supersymmetric Lagrange density

In order to be more concise, we will denote the complex scalar and Weyl fermion within the chiral supermultiplets by ϕ and ψ , while the gauge bosons and the gauginos from vector supermultiplets will be denoted by A_μ and λ respectively. The Lagrange density of a

2 Supersymmetry

renormalisable SUSY theory is then given by

$$\begin{aligned} \mathcal{L}_{\text{susy}} = & (D_\mu \phi)_i^\dagger (D^\mu \phi)_i + i\psi_i \sigma_\mu (D^\mu \bar{\psi})_i + i\lambda^a \sigma_\mu (D^\mu \bar{\lambda})^a - \frac{1}{4} F_{\mu\nu}^a (F^a)^{\mu\nu} \\ & + \left[-ig\sqrt{2}\bar{\psi}_i \bar{\lambda}^a T_{ij}^a \phi_j - \frac{1}{2} \frac{\partial^2 W}{\partial \phi_i \partial \phi_j} \psi_i \psi_j + \text{h.c.} \right] - V(\phi_i, \phi_j^\dagger). \end{aligned} \quad (2.14)$$

The first line contains all the kinetic terms and the gauge interactions involving vector bosons. These interactions are hidden either in the covariant derivative $D_\mu = \partial_\mu + igA_\mu^a T^a$, which ensures the gauge invariance of the Lagrangian, or in the field strength tensor $F_{\mu\nu}^a = \partial_\mu A_\nu^a - \partial_\nu A_\mu^a - gf^{abc}A_\mu^b A_\nu^c$. The first term in the second line involves the interactions between scalars and fermions, and the second term, namely the scalar potential, is defined by

$$V(\phi_i, \phi_j^\dagger) = \sum_i \left| \frac{\partial W}{\partial \phi_i} \right|^2 + \frac{1}{2} \sum_a (g\phi_i^\dagger T_{ij}^a \phi_j + k^a)^2, \quad (2.15)$$

where the Fayet-Iliopoulos term k^a is non-zero for U(1) gauge fields only [27].

Having fixed the list of the chiral and vector supermultiplets in the previous section, the MSSM is then specified by the choice of its superpotential written in terms of the chiral superfields

$$W_{\text{MSSM}} = -E y_E L H_1 - D y_D Q H_1 + U y_U Q H_2 - \mu H_1 H_2. \quad (2.16)$$

For brevity, we have suppressed the possible flavour and gauge indices. The first three terms correspond to the Yukawa couplings and give rise to the (s)fermion masses. The last term, so-called the μ -term, is related to the Higgs(ino) masses.

In principle, when imposing only renormalisability and gauge invariance, we could have included four additional terms in the superpotential. However, three of them violate lepton number and the fourth violates baryon number, leading to serious problems with the present limits on proton decay. To avoid these, one must assume one or several additional symmetries. Usually, it is R -parity which is chosen. It is defined by

$$R = (-1)^{3B+L+2S}, \quad (2.17)$$

B and L being the baryon and lepton numbers and S the spin of the particle. Under this new quantum number, the SM particles have $R = 1$, while their SUSY partners have $R = -1$. Since R is multiplicative, only vertices with an even number of SUSY particles are allowed. They can therefore only be produced by pairs and may decay only into final states containing an odd number of SUSY particles. Consequently, the Lightest SUSY Particle (LSP) is stable and can only interact via (co-)annihilation processes. If in addition the LSP is electrically neutral and colourless, it can be a viable Dark Matter (DM) candidate, one of the missing pieces of the SM.

2.2.3 Supersymmetry breaking

At this stage, the action obtained from the Lagrange density of Eq. (2.14) is invariant under global SUSY transformations. Therefore all the SUSY particles have the very same mass as their SM partners. This is in contradiction with the observation that SUSY particles have not been discovered so far, meaning that SUSY must be broken. Since the breaking mechanism is not known, we parameterise it by adding terms which break SUSY explicitly.

2.3 Mass eigenstates

At present, the consensus is that these terms must not introduce quadratic divergences in quantum corrections. In the MSSM, the soft SUSY-breaking terms are given by [28]

$$\begin{aligned}
\mathcal{L}_{\text{soft}} = & -\frac{1}{2}(M_1\tilde{B}\tilde{B} + M_2\tilde{W}\tilde{W} + M_3\tilde{g}\tilde{g} + \text{h.c.}) \\
& -m_1^2 h_1^\dagger h_1 - m_2^2 h_2^\dagger h_2 + (bh_1 h_2 + \text{h.c.}) \\
& -(-\tilde{e}_R^\dagger a_E \tilde{l}_L h_1 - \tilde{d}_R^\dagger a_D \tilde{q}_L h_1 + \tilde{u}_R^\dagger a_U \tilde{q}_L h_2 + \text{h.c.}) \\
& -\tilde{e}_R^\dagger m_E^2 \tilde{e}_R - \tilde{l}_L^\dagger m_L^2 \tilde{l}_L - \tilde{d}_R^\dagger m_D^2 \tilde{d}_R - \tilde{u}_R^\dagger m_U^2 \tilde{u}_R - \tilde{q}_L^\dagger m_Q^2 \tilde{q}_L, \tag{2.18}
\end{aligned}$$

where the gaugino-, Higgs- and sfermion-mass terms are shown in the first, second and last lines, respectively. The third line involves the trilinear scalar interactions. Here again, summations over possible flavour and gauge indices are understood.

The explicit breaking of SUSY, as presented in Eq. (2.18), may appear inelegant. One would prefer to break SUSY spontaneously, so that the action is still invariant under SUSY transformations, but the ground state of the theory is not. A mechanism, which works directly in the MSSM, is unfortunately not known. In present models, spontaneous SUSY breaking has to happen in a hidden sector and is mediated to the visible sector, the MSSM, through a shared interaction. Unfortunately, neither the particle content of the hidden sector nor the mediation with the visible sector are known.

The most popular SUSY-breaking model is called minimal SuperGRAvity (mSUGRA) [29, 30, 31]. In this framework, the hidden and visible sectors communicate through the gravitational interactions. The effective soft terms in Eq. (2.18) are then determined by only five parameters, which are the universal scalar and gaugino masses m_0 and $m_{1/2}$, the universal trilinear coupling A_0 , the sign of the μ -parameter and the ratio of the vacuum expectation values of the Higgs fields $\tan\beta$, discussed in Sec. 2.3.1. At the unification scale, we assume the following relations

$$m_0^2 = m_1^2 = m_2^2 = m_E^2 = m_L^2 = m_D^2 = m_U^2, \tag{2.19}$$

$$m_{1/2} = M_1 = M_2 = M_3, \tag{2.20}$$

$$A_0 y_E = a_E, \quad A_0 y_D = a_D \quad \text{and} \quad A_0 y_U = a_U. \tag{2.21}$$

Then, the parameters at low energy are obtained through their renormalisation-group equations (RGE). In the work presented here, we only consider mSUGRA scenarios, even if several other mediations have been proposed in the literature, e.g. mediations through gauge interactions or the super-Weyl anomaly.

2.3 Mass eigenstates

In order to give masses to the W - and Z -bosons, electroweak symmetry has to be broken. Consequently, all particles with the same spin, electric and colour charge mix, as do the B^0 - and W^0 -bosons in the SM. In the following, we will focus on the ElectroWeak Symmetry Breaking (EWSB) and the resulting mixings which occur in the Higgs, gaugino/Higgsino and sfermion sectors.

2.3.1 Higgs sector

As already mentioned in the previous section, the MSSM contains two Higgs doublets. The scalar Higgs potential is then given by

$$V_{\text{Higgs}} = (|\mu|^2 + m_1^2)|h_1|^2 + (|\mu|^2 + m_2^2)|h_2|^2 - (bh_1h_2 + \text{h.c.}) + \frac{1}{8}(g^2 + g'^2)(|h_1|^2 - |h_2|^2)^2 + \frac{1}{2}g^2|h_1^\dagger h_2|^2, \quad (2.22)$$

where we have included the contributions from both the SUSY scalar potential in Eq. (2.15) and the soft breaking terms in Eq. (2.18). The standard procedure is to use a $SU(2)_L$ transformation to rotate away any vacuum expectation values (vevs) of the charged Higgs fields. We simply get $\langle H_{2,1}^\pm \rangle = 0$ which allows for electric charge conservation in the theory. The next step is to choose the b -parameter real and positive (by redefining the phases of the Higgs fields if necessary). Hence, CP symmetry is not spontaneously broken, and the scalar Higgs mass eigenstates are also CP -eigenstates. EWSB is achieved, if the following conditions are fulfilled:

$$(|\mu|^2 + m_1^2)(|\mu|^2 + m_2^2) < b^2 \quad \text{and} \quad (|\mu|^2 + m_1^2) + (|\mu|^2 + m_2^2) \geq 2b. \quad (2.23)$$

This enforces the neutral components of the Higgs doublets to acquire non-vanishing vevs $\langle H_{1,2}^0 \rangle = v_{1,2}/\sqrt{2}$. Traditionally, the two vevs are parameterised by the SM-like vacuum expectation value v and the angle β defined by

$$v^2 = v_1^2 + v_2^2 \quad \text{and} \quad \tan \beta = \frac{v_2}{v_1}, \quad \beta \in [0, \frac{\pi}{2}[. \quad (2.24)$$

After EWSB, among the eight degrees of freedom present in the two Higgs doublets, three become the massless Nambu-Goldstone bosons $G^{0,\pm}$. The other five become two neutral CP -even (h^0, H^0), one CP -odd A^0 and two charged H^\pm Higgs bosons. They are related to the interaction eigenstates through

$$\begin{pmatrix} H^0 \\ h^0 \end{pmatrix} = \begin{pmatrix} \cos \alpha & \sin \alpha \\ -\sin \alpha & \cos \alpha \end{pmatrix} \begin{pmatrix} \sqrt{2}\text{Re}(H_1^0) - v_1 \\ \sqrt{2}\text{Re}(H_2^0) - v_2 \end{pmatrix}, \quad (2.25)$$

$$\begin{pmatrix} G^0 \\ A^0 \end{pmatrix} = \begin{pmatrix} -\cos \beta & \sin \beta \\ \sin \beta & \cos \beta \end{pmatrix} \begin{pmatrix} \sqrt{2}\text{Im}(H_1^0) \\ \sqrt{2}\text{Im}(H_2^0) \end{pmatrix}, \quad (2.26)$$

$$\begin{pmatrix} G^+ \\ H^+ \end{pmatrix} = \begin{pmatrix} -\cos \beta & \sin \beta \\ \sin \beta & \cos \beta \end{pmatrix} \begin{pmatrix} H_1^{-*} \\ H_2^+ \end{pmatrix}, \quad (2.27)$$

where α is the Higgs mixing angle. At tree level, the Higgs-boson masses are then

$$m_{h^0, H^0}^2 = \frac{1}{2} \left[m_{A^0}^2 + m_Z^2 \mp \sqrt{(m_{A^0}^2 + m_Z^2)^2 - 4m_{A^0}^2 m_Z^2 \cos^2(2\beta)} \right], \quad (2.28)$$

$$m_{A^0}^2 = \frac{2b}{\sin(2\beta)} \quad \text{and} \quad m_{H^\pm}^2 = m_{A^0}^2 + m_W^2, \quad (2.29)$$

where, as in the SM, the W - and Z -boson masses are

$$m_W^2 = \frac{g^2}{4} v^2 \quad \text{and} \quad m_Z^2 = \frac{g^2 + g'^2}{4} v^2. \quad (2.30)$$

2.3 Mass eigenstates

2.3.2 Sfermion sector

In the most general case, the sfermions mass eigenstates are obtained by diagonalising 6×6 matrices, because left- and right-handed sfermions of the three families mix. Assuming that no mixing occurs between sfermions of different flavours reduces the problem into the diagonalisation of three 2×2 matrices. The mass term for sfermions of flavour f can then be written as

$$\mathcal{L} \supset - \begin{pmatrix} \tilde{f}_L^* & \tilde{f}_R^* \end{pmatrix} \begin{pmatrix} m_{LL_f}^2 & m_{LR_f}^2 \\ (m_{LR_f}^2)^* & m_{RR_f}^2 \end{pmatrix} \begin{pmatrix} \tilde{f}_L \\ \tilde{f}_R \end{pmatrix} \quad (2.31)$$

with the following mass matrix entries:

$$m_{LL_f}^2 = m_{\{L,Q\}_f}^2 + (T_f^3 - e_f \sin^2 \theta_W) m_Z^2 \cos 2\beta + m_f^2, \quad (2.32)$$

$$m_{RR_f}^2 = m_{\{E,D,U\}_f}^2 + e_f \sin^2 \theta_W m_Z^2 \cos 2\beta + m_f^2, \quad (2.33)$$

$$m_{LR_f}^2 = m_f A_{\{E,D,U\}_f}^* - m_f \mu (\tan \beta)^{-2T_f^3}. \quad (2.34)$$

We denote m_f , e_f and T_f^3 the mass, electric charge and weak isospin quantum number of the sfermion of flavour f . The diagonalisation of the mass matrix is performed with the unitary matrix $R^{\tilde{f}}$, and the resulting sfermion mass eigenstates are given by

$$\begin{pmatrix} \tilde{f}_1 \\ \tilde{f}_2 \end{pmatrix} = R^{\tilde{f}} \begin{pmatrix} \tilde{f}_L \\ \tilde{f}_R \end{pmatrix}, \quad (2.35)$$

where by convention $m_{\tilde{f}_1} < m_{\tilde{f}_2}$. At tree level, the mass eigenvalues are given by

$$m_{\tilde{f}_{1,2}} = \frac{1}{2} \left[m_{LL_f}^2 + m_{RR_f}^2 \mp \sqrt{(m_{LL_f}^2 - m_{RR_f}^2)^2 + 4|m_{LR_f}^2|^2} \right]. \quad (2.36)$$

2.3.3 Gaugino/Higgsino sector

The electroweak gauginos and the Higgsinos with same electric charge also mix. The resulting neutral and charged mass eigenstates are named the neutralinos and the charginos respectively.

For the neutral eigenstates, the mass term in the Lagrange density $\mathcal{L} = \mathcal{L}_{\text{susy}} + \mathcal{L}_{\text{soft}}$ is given by

$$\mathcal{L} \supset -\frac{1}{2} (\psi^0)^T Y \psi^0 + \text{h.c.} \quad (2.37)$$

It is bilinear in the (two-component) fermionic partners

$$\psi_j^0 = (-i\tilde{B}^0, -i\tilde{W}^0, \tilde{H}_1^0, \tilde{H}_2^0)^T \quad \text{with } j = 1, \dots, 4 \quad (2.38)$$

of the neutral electroweak gauge and Higgs bosons and proportional to the, generally complex and necessarily symmetric, neutralino mass matrix

$$Y = \begin{pmatrix} M_1 & 0 & -m_Z \sin \theta_W \cos \beta & m_Z \sin \theta_W \sin \beta \\ 0 & M_2 & m_Z \cos \theta_W \cos \beta & -m_Z \cos \theta_W \sin \beta \\ -m_Z \sin \theta_W \cos \beta & m_Z \cos \theta_W \cos \beta & 0 & -\mu \\ m_Z \sin \theta_W \sin \beta & -m_Z \cos \theta_W \sin \beta & -\mu & 0 \end{pmatrix}, \quad (2.39)$$

2 Supersymmetry

where θ_W is the electroweak mixing angle. After diagonalisation of the mass matrix Y , one obtains the neutralino mass eigenstates

$$\chi_i^0 = N_{ij}\psi_j^0, \quad i = 1, \dots, 4, \quad (2.40)$$

where N is a unitary matrix satisfying the relation

$$N^*YN^{-1} = \text{diag}(m_{\tilde{\chi}_1^0}, m_{\tilde{\chi}_2^0}, m_{\tilde{\chi}_3^0}, m_{\tilde{\chi}_4^0}). \quad (2.41)$$

In four-component notation, the Majorana-fermionic neutralino mass eigenstates can be written as

$$\tilde{\chi}_i^0 = \begin{pmatrix} \chi_i^0 \\ \bar{\chi}_i^0 \end{pmatrix}. \quad (2.42)$$

At tree level, the application of projection operators leads to relatively compact analytic expressions for the mass eigenvalues $m_{\tilde{\chi}_1^0} < m_{\tilde{\chi}_2^0} < m_{\tilde{\chi}_3^0} < m_{\tilde{\chi}_4^0}$ [32]. As we choose them to be real and non-negative, our unitary matrix N is generally complex [33].

The chargino mass term in the Lagrange density

$$\mathcal{L} \supset -\frac{1}{2} \begin{pmatrix} \psi^+ & \psi^- \end{pmatrix} \begin{pmatrix} 0 & X^T \\ X & 0 \end{pmatrix} \begin{pmatrix} \psi^+ \\ \psi^- \end{pmatrix} + \text{h.c.} \quad (2.43)$$

is bilinear in the (two-component) fermionic partners

$$\psi_j^\pm = (-i\tilde{W}^\pm, \tilde{H}_{2,1}^\pm)^T \quad \text{with} \quad j = 1, 2 \quad (2.44)$$

of the charged electroweak gauge and Higgs bosons and proportional to the, generally complex, chargino mass matrix

$$X = \begin{pmatrix} M_2 & m_W \sqrt{2} \sin \beta \\ m_W \sqrt{2} \cos \beta & \mu \end{pmatrix}. \quad (2.45)$$

Since X is not symmetric, it must be diagonalized by two unitary matrices U and V , which satisfy the relation

$$U^*XV^{-1} = \text{diag}(m_{\tilde{\chi}_1^\pm}, m_{\tilde{\chi}_2^\pm}) \quad (2.46)$$

and define the chargino mass eigenstates

$$\chi_i^+ = V_{ij}\psi_j^+ \quad \text{and} \quad \chi_i^- = U_{ij}\psi_j^-. \quad (2.47)$$

In four-component notation, the Dirac-fermionic chargino mass eigenstates can be written as

$$\tilde{\chi}_i^\pm = \begin{pmatrix} \chi_i^\pm \\ \bar{\chi}_i^\mp \end{pmatrix}. \quad (2.48)$$

As Eq. (2.46) implies

$$VX^\dagger XV^{-1} = \text{diag}(m_{\tilde{\chi}_1^\pm}^2, m_{\tilde{\chi}_2^\pm}^2), \quad (2.49)$$

the hermitian matrix $X^\dagger X$ can be diagonalized using only V , and its eigenvalues

$$m_{\tilde{\chi}_{1,2}^\pm}^2 = \frac{1}{2} \left[|M_2|^2 + |\mu|^2 + 2m_W^2 \mp \sqrt{(|M_2|^2 + |\mu|^2 + 2m_W^2)^2 - 4|\mu M_2^* - m_W^2 s_{2\beta}|^2} \right] \quad (2.50)$$

2.3 Mass eigenstates

are always real. If we take also the mass eigenvalues $m_{\tilde{\chi}_1^\pm} < m_{\tilde{\chi}_2^\pm}$ to be real and non-negative, the rotation matrix

$$V = \begin{pmatrix} \cos \theta_+ & \sin \theta_+ e^{-i\phi_+} \\ -\sin \theta_+ e^{i\phi_+} & \cos \theta_+ \end{pmatrix} \quad (2.51)$$

can still be chosen to have real diagonal elements, but the off-diagonal phase $e^{\mp i\phi_+}$ is needed to rotate away the imaginary part of the off-diagonal matrix element in $X^\dagger X$,

$$\text{Im}[(M_2^* s_\beta + \mu c_\beta) e^{i\phi_+}] = 0. \quad (2.52)$$

The rotation angle $\theta_+ \in [0, \pi]$ is uniquely fixed by the two conditions

$$\tan 2\theta_+ = \frac{2\sqrt{2}m_W(M_2^* s_\beta + \mu c_\beta) e^{i\phi_+}}{|M_2|^2 - |\mu|^2 + 2m_W^2 c_{2\beta}} \quad \text{and} \quad (2.53)$$

$$\sin 2\theta_+ = \frac{-2\sqrt{2}m_W(M_2^* s_\beta + \mu c_\beta) e^{i\phi_+}}{\sqrt{(|M_2|^2 - |\mu|^2 + 2m_W^2 c_{2\beta})^2 + 8m_W^2 [(M_2^* s_\beta + \mu c_\beta) e^{i\phi_+}]^2}}. \quad (2.54)$$

Once V is known, the unitary matrix U can be obtained easily from

$$U = \text{diag}(m_{\tilde{\chi}_1^\pm}^{-1}, m_{\tilde{\chi}_2^\pm}^{-1}) V^* X^T. \quad (2.55)$$

2 *Supersymmetry*

3

Resummation

In this chapter, we present all the formulae needed to apply the threshold and transverse-momentum resummation formalisms to the production of gaugino pairs. To fix the notations, we recall some of the major results of perturbative QCD in Sec. 3.1. Then, we present the formalisms of threshold resummation and transverse-momentum resummation in Sec. 3.3 and Sec. 3.4, respectively. Finally, since both formalisms are defined in conjugate spaces, some subtleties to switch back to the physical spaces are detailed in Sec. 3.5.

3.1 Perturbative QCD

Let us consider the production of a non-coloured system F with mass M and transverse momentum p_T in the collision of two hadrons A and B ,

$$A + B \rightarrow F(M^2, p_T^2) + X \quad (3.1)$$

(see Fig. 3.1). For example, F can be a vector boson, a Higgs boson, a lepton pair or a gaugino pair. At large M^2 , the differential cross section for the production of F can be written in the collinear-factorised form [34]

$$M^2 \frac{d\sigma_{AB}}{dM^2 dp_T^2} \left(\tau = \frac{M^2}{S} \right) = \sum_{ab} \int_0^1 dx_a dx_b dz [x_a f_{a/A}(x_a, \mu^2)] [x_b f_{b/B}(x_b, \mu^2)] \\ \times z \hat{\sigma}_{ab}(z, M^2, M^2/p_T^2, M^2/\mu^2) \delta(\tau - x_a x_b z), \quad (3.2)$$

where $f_{a/A}$ and $f_{b/B}$ are the parton distribution functions (PDF) of parton a, b in hadron A, B . We denote \sqrt{S} the hadronic centre-of-mass energy, $x_{a,b}$ the longitudinal momentum fractions of the two partons and μ the factorisation scale. For the time being, the renormalisation scale is set equal to μ . In Eq. (3.2), the PDFs are convoluted with the hard-scattering function $\hat{\sigma}_{ab}$, which is usually evaluated as a power series in the strong coupling constant $\alpha_s = \alpha_s(\mu^2)$,

$$\hat{\sigma}_{ab}(z, M^2, M^2/p_T^2, M^2/\mu^2) = \sum_{n=0}^{\infty} \left(\frac{\alpha_s}{2\pi} \right)^n \hat{\sigma}_{ab}^{(n)}(z, M^2, M^2/p_T^2, M^2/\mu^2) \\ = \sum_{n=0}^{\infty} a_s^n \hat{\sigma}_{ab}^{(n)}(z, M^2, M^2/p_T^2, M^2/\mu^2). \quad (3.3)$$

3 Resummation

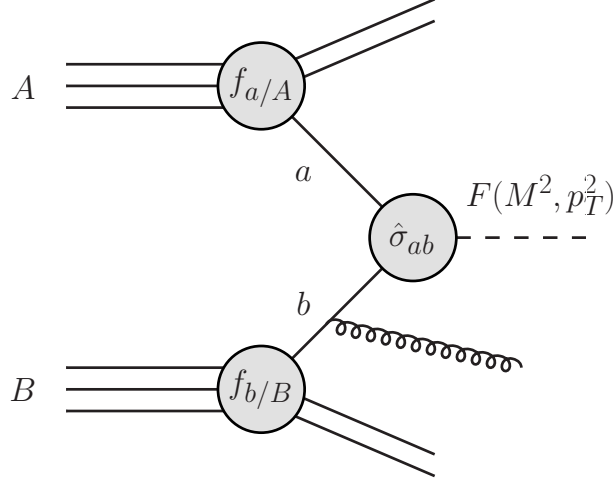


Figure 3.1: Schematic representation of Eq. (3.2) for the production of a colourless system F , balanced by a gluon emission, in the collision of two hadrons A and B .

In the second line, we have taken the opportunity to specify the reduced coupling $a_s(\mu^2)$ employed for the rest of this chapter. Its dependence on the renormalisation scale is determined by the very well-known renormalisation group equation

$$\frac{da_s(\mu^2)}{d\ln\mu^2} = - \sum_{n=0}^{\infty} \beta_n a_s^{n+2}(\mu^2), \quad (3.4)$$

where the minus sign on the right-hand side makes explicit that QCD is an asymptotically free theory [4, 5]. The first expansion coefficients β_0 and β_1 [35] are given by

$$\beta_0 = \frac{11C_A - 2N_f}{6} \quad \text{and} \quad \beta_1 = \frac{17C_A^2 - 5C_A N_f - 3C_F N_f}{6}. \quad (3.5)$$

These coefficients depend on the number of active light flavours N_f and the Casimir operators of $SU(N_c)$ in the fundamental and adjoint representations. For $N_c = 3$, they take the values

$$C_F = \frac{N_c^2 - 1}{2N_c} = \frac{4}{3} \quad \text{and} \quad C_A = N_c = 3. \quad (3.6)$$

Note that the coefficients β_0 and β_1 are independent of the renormalisation scheme unlike the higher coefficients.

At leading order (LO), where no additional partons are produced besides F , the hard scattering function

$$\hat{\sigma}_{ab}^{(0)}(z, M^2, M^2/p_T^2, M^2/\mu^2) = \hat{\sigma}_{ab}^{(0)}(M^2, M^2/\mu^2) \delta(1-z) \delta(p_T^2) \quad (3.7)$$

has its support entirely at $z = 1$ and $p_T^2 = 0$. At higher order in QCD, it develops more complicated structures that we will discuss in the next sections.

In the following, instead of working with τ - and z -dependent cross sections in Eq. (3.2), we will prefer their Mellin moments. We define the Mellin transform of a function $F(x)$ by

$$F(N) = \int_0^1 dx x^{N-1} F(x), \quad (3.8)$$

3.1 Perturbative QCD

where for economy of notation, we denote the transform of $F(x)$ with respect to its variable x by changing its argument to N . After a Mellin transform, the convolution in Eq. (3.2) simplifies to a simple product

$$M^2 \frac{d\sigma_{AB}}{dM^2 dp_T^2}(N-1) = \sum_{ab} f_{a/A}(N, \mu^2) f_{b/B}(N, \mu^2) \hat{\sigma}_{ab}(N, M^2, M^2/p_T^2, M^2/\mu^2). \quad (3.9)$$

We also define the partonic cross section by

$$M^2 \frac{d\sigma_{ab}}{dM^2 dp_T^2}(N-1) = \sum_{cd} \phi_{c/a}(N, \mu^2) \phi_{d/b}(N, \mu^2) \hat{\sigma}_{cd}(N, M^2, M^2/p_T^2, M^2/\mu^2), \quad (3.10)$$

where $\phi_{c/a}(x_c, \mu^2)$ and $\phi_{d/b}(x_d, \mu^2)$ are parton-in-parton distributions of partons c, d in partons a, b , respectively. Like the PDFs, they are defined at fixed longitudinal momentum fraction $x_{c,d}$.

When $p_T \neq 0$, the remaining collinear singularities of $d\sigma_{ab}/dM^2/dp_T^2$ are absorbed in the parton-in-parton distribution functions leaving the hard-scattering function $\hat{\sigma}_{ab}$ infrared safe order by order in perturbation theory. This procedure, called mass factorisation, contains some degrees of freedom. One can actually shift any finite part of the hard-scattering function into the ϕ -distributions. This introduces the factorisation scale dependence into the definition of both the parton-in-parton distributions and the hard-scattering function. In the following, we will stick to the $\overline{\text{MS}}$ factorisation scheme, in which the parton-in-parton distributions are ‘‘pure counterterms’’, i.e. a series of poles in $\varepsilon = 2 - D/2$ in D space-time dimensions (together with the usual constant terms $\ln(4\pi) - \gamma_E$, γ_E being the Euler constant).

The dependence of $\phi_{c/a}$ on the factorisation scale is governed by the so-called Altarelli-Parisi (AP) equation [36]

$$\frac{\partial \phi_{c/a}(N, \mu^2)}{\partial \ln \mu^2} = \sum_b P_{cb}(N, a_s(\mu^2)) \phi_{b/a}(N, \mu^2), \quad (3.11)$$

where the splitting functions $P_{cb}(N, a_s) = \sum_n a_s^n P_{cb}^{(n)}(N)$ are calculable order-by-order in perturbation theory. At LO in a_s , they are given by

$$P_{qq}^{(1)}(N) = C_F \left[\frac{3}{2} + \frac{1}{N(N+1)} - 2 \sum_{k=1}^N \frac{1}{k} \right], \quad (3.12)$$

$$P_{qg}^{(1)}(N) = \frac{1}{2} \left[\frac{2+N+N^2}{N(N+1)(N+2)} \right], \quad (3.13)$$

$$P_{gq}^{(1)}(N) = C_F \left[\frac{2+N+N^2}{N(N^2-1)} \right], \quad (3.14)$$

$$P_{gg}^{(1)}(N) = \beta_0 + 2C_A \left[\frac{1}{N(N-1)} + \frac{1}{(N+1)(N+2)} - \sum_{k=1}^N \frac{1}{k} \right]. \quad (3.15)$$

In order to write the solution of Eq. (3.11) in a compact form, it is convenient to introduce the QCD evolution operator $E_{ab}(N, \mu^2, \mu_0^2)$ defined as the solution of the equation

$$\frac{\partial E_{ab}(N, \mu^2, \mu_0^2)}{\partial \ln \mu^2} = \sum_c P_{ac}(N, a_s(\mu^2)) E_{cb}(N, \mu^2, \mu_0^2). \quad (3.16)$$

3 Resummation

Then the solution of Eq. (3.11), written in terms of the evolution operator, is simply

$$\phi_{c/a}(N, \mu^2) = \sum_b E_{cb}(N, \mu^2, \mu_0^2) \phi_{b/a}(N, \mu_0^2). \quad (3.17)$$

Note that the expression of the evolution operator E_{ab} is in general quite complicated. However, it can be considerably simplified by working in the quark/flavour singlet and non-singlet basis. For instance, by solving the LO approximation of Eq. (3.16)

$$\frac{\partial E_{ab}^{(1)}(N, \mu^2, \mu_0^2)}{\partial \ln \mu^2} = a_s \sum_c P_{ac}^{(1)}(N, a_s(\mu^2)) E_{cb}^{(1)}(N, \mu^2, \mu_0^2), \quad (3.18)$$

one is able to write the LO evolution operator $E_{ab}^{(1)}$ in a closed exponential form [37].

3.2 Resummation philosophy

As can be seen in Eq. (3.2), to compute the differential cross section for the process in Eq. (3.1), we need two different parts. The first part is the knowledge of the PDFs. The PDFs are non-perturbative functions and must be obtained from experiments. Fortunately, they are universal and obey the evolution equations in Eq. (3.11), so that we can reuse the PDFs obtained in an experiment to get predictions for another experiment. The other part is the hard-scattering function $\hat{\sigma}_{ab}$. It is a highly process-dependent function and must be calculated as a power series in a_s . The first coefficient of the series $\hat{\sigma}_{ab}^{(0)}$ is often not too hard to compute for $2 \rightarrow m$ processes, with m small. However, as n grows, the number of Feynman diagrams one must compute to get $\hat{\sigma}_{ab}^{(n)}$ increases factorially. Current calculations reach typically $n = 0$ or 1 and very rarely $n = 2$.

For the evaluation of $\hat{\sigma}_{ab}^{(1)}$, one must consider real-emission contributions and virtual-loop corrections, and one has to deal with different kinds of singularities. The ultraviolet singularities, present in the virtual contributions, are removed by the renormalisation procedure. The infrared singularities are present in both the virtual and real-emission contributions. The cancellation of these singularities is guaranteed by the Bloch-Nordsieck mechanism [38] and the resulting cross section is infrared safe.

Although infrared safe, $\hat{\sigma}_{ab}^{(1)}$ still contains singular distributions at the phase space boundaries, e.g. at $z = 1$ and $p_T = 0$. In such kinematical configurations, the cancellation of the infrared singularities between virtual and real-emission diagrams is constrained by the requirements that the real gluon is either soft or collinear, leaving these (potentially) large terms in the hard-scattering function. Note that because of their infrared origin, those singular structures take the form of logarithmic distributions. That is why the differential cross section $d\sigma_{AB}/dM^2/dp_T^2$ is sometimes called an infrared sensitive quantity. Fortunately, these logarithmic terms have a definite structure. They can therefore be organised and summed to all orders in a_s using resummation formalisms.

We have already mentioned that the factorisation procedure in Eq. (3.10) is not unique and involves some degrees of freedom. Resummation formalisms make heavy use of this property. The starting point is the refactorisation of the cross section in the kinematical regions that give rise to the logarithms. To sketch the resummation procedure, let us take an infrared sensitive quantity $R(M^2, m^2)$, which depends on two scales: the hard scale M and a scale m , which measures the distance from the critical region. One must show, and it is

3.3 Threshold resummation

highly non-trivial, that in the limit $m^2 \ll M^2$, R can be factorised as

$$R(M^2, m^2) = H(M^2/\mu^2)S(m^2/\mu^2), \quad (3.19)$$

where we have separated the two scales M and m by introducing a factorisation scale μ . We see that the functions H and S contain potentially large ratios, depending on the value we assign to μ . Note that this refactorisation does not necessarily hold in the original momentum space, but more often in a ‘‘conjugate’’ space, e.g. Mellin or impact-parameter space.

From the independence of R on μ , we get the evolution equations

$$\frac{d \ln H}{d \ln \mu^2} = \gamma_S(\mu^2) = -\frac{d \ln S}{d \ln \mu^2}. \quad (3.20)$$

Solving the equation for S naturally leads to the following exponentiation

$$S(m^2/\mu^2) = S(1) \exp \left[-\int_{m^2}^{\mu^2} \frac{dq^2}{q^2} \gamma_S(q^2) \right]. \quad (3.21)$$

With the specific choice $\mu = M$, Eq. (3.19) becomes

$$R(M^2, m^2) = H(1)S(1) \exp \left[-\int_{m^2}^{M^2} \frac{dq^2}{q^2} \gamma_S(q^2) \right]. \quad (3.22)$$

We see that the potentially large ratios in the functions H and S are no longer present. They can therefore be computed safely using perturbation theory and the full dependences on the two scales are now in the exponential, sometimes called the Sudakov form factor. Computing the anomalous dimension γ_S to a specific order in a_s resums the large logarithmic terms to a given accuracy.

In the next sections, we present two resummation formalisms. More precisely, Sec. 3.3 is devoted to the threshold resummation [18, 39] which reorganises $z = 1$ singularities. In Sec. 3.4 we present the formalism of transverse-momentum resummation [40, 41] which controls the $p_T = 0$ singularities.

3.3 Threshold resummation

Close to partonic threshold, i.e. when $z = M^2/s$ is close to one, the hard-scattering function reveals potentially large logarithmic structures. The threshold resummation proposes to organise the terms of the form $a_s^n [(1-z)^{-1} \ln^m(1-z)]_+$, with $m \leq 2n-1$, which appear in $\hat{\sigma}_{ab}$. In Mellin space, these terms turn into large logarithms of the Mellin variable N

$$\left(\frac{\ln^m(1-z)}{1-z} \right)_+ \longrightarrow \ln^{m+1} N + \dots \quad (3.23)$$

and it is thus possible, in the $N \rightarrow \infty$ limit, to retain only the leading power in N . In particular, one can neglect parton mixing contributions since they contribute at $\mathcal{O}(1/N)$. This can be seen already at $\mathcal{O}(a_s)$: Taking the large- N limit in Eqs. (3.12)–(3.15), one can see that the AP splitting functions behave as

$$\begin{aligned} P_{qq}^{(1)}(N) &= C_F \left(\frac{3}{2} - 2 \ln \bar{N} \right) + \mathcal{O}\left(\frac{1}{N}\right), & P_{qg}^{(1)}(N) &\sim \frac{1}{2N}, \\ P_{gq}^{(1)}(N) &\sim \frac{C_F}{N} & \text{and} & P_{gg}^{(1)}(N) = \beta_0 - 2C_A \ln \bar{N} + \mathcal{O}\left(\frac{1}{N}\right), \end{aligned} \quad (3.24)$$

3 Resummation

with $\bar{N} = Ne^{\gamma_E}$ and γ_E being the Euler constant.

Consequently, after the integration of Eq. (3.10) over p_T^2 and the removal of the parton-mixing contributions, the partonic cross section becomes

$$M^2 \frac{d\sigma_{ab}}{dM^2}(N-1) = \phi_{a/a}(N, \mu^2) \phi_{b/b}(N, \mu^2) \hat{\sigma}_{ab}(N, M^2, M^2/\mu^2) + \mathcal{O}\left(\frac{1}{N}\right). \quad (3.25)$$

3.3.1 Refactorisation

As mentioned above, this factorisation exhibits singular distributions at $z = 1$. To control them, we follow the work of Sterman [18] and refactorise the partonic cross section as

$$M^2 \frac{d\sigma_{ab}}{dM^2}(N-1) = H_{ab}(M^2, M^2/\mu^2) \times \psi_{a/a}(N, M^2) \psi_{b/b}(N, M^2) S_{ab}(N, M^2/\mu^2) + \mathcal{O}\left(\frac{1}{N}\right). \quad (3.26)$$

The hard function H_{ab} organises infrared-safe coefficients independent of N and can be therefore computed as power series in a_s ,

$$H_{ab}(M^2, M^2/\mu^2) = \sum_{n=0}^{\infty} a_s^n H_{ab}^{(n)}(M^2, M^2/\mu^2). \quad (3.27)$$

The parton-in-parton distributions $\psi_{a/b}$ are defined at measured fraction of energy rather than at usual longitudinal momentum fraction (as in $\phi_{a/b}$). They satisfy the evolution equation

$$\frac{\partial \psi_{a/a}(N, \mu^2)}{\partial \ln \mu^2} = \gamma_a(a_s(\mu^2)) \psi_{a/a}(N, \mu^2), \quad (3.28)$$

where the anomalous dimensions of the field a , $\gamma_a(a_s) = 1/Z_a \partial Z_a / \partial \ln \mu^2 = \sum_n a_s^n \gamma_a^{(n)}$, correspond in the axial gauge [42] to the N -independent (virtual) parts of $P_{aa}(N, a_s)$. Finally, the function S_{ab} describes the large-angle emission of soft gluons and can thus be computed in the eikonal approximation.

To perform mass factorisation, we include Eq. (3.26) in Eq. (3.25) and get

$$\hat{\sigma}_{ab}(N, M^2, M^2/\mu^2) = H_{ab}(M^2, M^2/\mu^2) \frac{\psi_{a/a}(N, M^2) \psi_{b/b}(N, M^2)}{\phi_{a/a}(N, \mu^2) \phi_{b/b}(N, \mu^2)} S_{ab}(N, M^2/\mu^2) + \mathcal{O}\left(\frac{1}{N}\right). \quad (3.29)$$

3.3.2 Exponentiation

Using gauge invariance and renormalisation group arguments, the evolution equations satisfied by $\phi_{a/a}$ and $\psi_{a/a}$ (Eqs. (3.11) and (3.28) respectively) can be solved near threshold, and together with the property of exponentiation of the eikonal function S_{ab} [43], the cross section can be cast in the exponential form

$$\hat{\sigma}_{ab}(N, M^2, M^2/\mu^2) = H_{ab}(M^2, M^2/\mu^2) \exp[G_{ab}(N, M^2, M^2/\mu^2)] + \mathcal{O}\left(\frac{1}{N}\right), \quad (3.30)$$

3.3 Threshold resummation

where the function G_{ab} can be written [39]¹ as

$$G_{ab}(N, M^2, M^2/\mu^2) = \ln \Delta_a(N, M^2, M^2/\mu^2) + \ln \Delta_b(N, M^2, M^2/\mu^2) + \ln \Delta_{ab}^{(s)}(N, M^2). \quad (3.31)$$

The radiation factors Δ 's are given by integrals of the running coupling constant

$$\ln \Delta_a(N, M^2, M^2/\mu^2) = \int_0^1 dz \frac{z^{N-1} - 1}{1-z} \int_{\mu^2}^{(1-z)^2 M^2} \frac{dq^2}{q^2} A_a(a_s(q^2)), \quad (3.32)$$

$$\ln \Delta_{ab}^{(s)}(N, M^2) = \int_0^1 dz \frac{z^{N-1} - 1}{1-z} D_{ab}(a_s((1-z)^2 M^2)). \quad (3.33)$$

The function A_a collects the effects of collinear soft-gluon radiation off the initial-state parton a , and the function D_{ab} collects the process-dependent contributions from large-angle soft-gluon emissions. Both can be expanded as power series in a_s

$$A_a(a_s) = \sum_{n=1}^{\infty} a_s^n A_a^{(n)} \quad \text{and} \quad D_{ab}(a_s) = \sum_{n=1}^{\infty} a_s^n D_{ab}^{(n)}. \quad (3.34)$$

After the integrations in Eqs. (3.32) and (3.33) have been performed, the hard-scattering function in Eq. (3.30) becomes

$$\hat{\sigma}_{ab}(N, M^2, M^2/\mu^2) = \mathcal{H}_{ab}(M^2, M^2/\mu^2) \exp[\mathcal{G}_{ab}(N, M^2, M^2/\mu^2)] + \mathcal{O}\left(\frac{1}{N}\right). \quad (3.35)$$

Here, the perturbative coefficients of the hard function

$$\mathcal{H}_{ab}(M^2, M^2/\mu^2) = \sum_{n=0}^{\infty} a_s^n \mathcal{H}_{ab}^{(n)}(M^2, M^2/\mu^2) \quad (3.36)$$

have been redefined with respect to those in Eq. (3.27) in order to absorb the non-logarithmic terms resulting from the integration, i.e.

$$\mathcal{H}_{ab}^{(0)}(M^2, M^2/\mu^2) = H_{ab}^{(0)}(M^2, M^2/\mu^2), \quad (3.37)$$

$$\mathcal{H}_{ab}^{(1)}(M^2, M^2/\mu^2) = H_{ab}^{(1)}(M^2, M^2/\mu^2) + \frac{\pi^2}{6} (A_a^{(1)} + A_b^{(1)}) H_{ab}^{(0)}(M^2). \quad (3.38)$$

The function \mathcal{G}_{ab} takes the form

$$\mathcal{G}_{ab}(N, M^2, M^2/\mu^2) = L g_{ab}^{(1)}(\lambda) + g_{ab}^{(2)}(\lambda, M^2/\mu^2) + a_s g_{ab}^{(3)}(\lambda, M^2/\mu^2) + \dots \quad (3.39)$$

with $\lambda = a_s \beta_0 L$ and $L = \ln \bar{N}$. The first term in Eq. (3.39) collects the leading logarithmic (LL) large- N contributions $L(a_s L)^n$ and depends on $A_a^{(1)}$ only. The coefficients $A_a^{(2)}$, $A_a^{(1)}$ and $D_{ab}^{(1)}$ determine the function $g_{ab}^{(2)}$ which resums the next-to-leading logarithmic (NLL) terms $(a_s L)^n$. Similarly, the functions $g_{ab}^{(n+1)}$ resum the N^n LL and depend on the coefficients $A_a^{(n+1)}$, $A_a^{(k)}$ and $D_{ab}^{(k)}$ with $1 \leq k \leq n$.

¹We prefer to present the function G_{ab} as in Ref. [39] rather than the one described in Ref. [18]. Of course it has been shown that both formulations are equivalent [44].

3.3.3 NLL approximation

The LL and NLL logarithmic contributions are resummed thanks to the functions

$$2\lambda\beta_0g_{ab}^{(1)}(\lambda) = (A_a^{(1)} + A_b^{(1)})[2\lambda + (1 - 2\lambda)\ln(1 - 2\lambda)], \quad (3.40)$$

$$\begin{aligned} 2\beta_0g_{ab}^{(2)}(\lambda, M^2/\mu^2) &= (A_a^{(1)} + A_b^{(1)})\ln(1 - 2\lambda)\ln\frac{M^2}{\mu^2} \\ &+ (A_a^{(1)} + A_b^{(1)})\frac{\beta_1}{\beta_0^2}\left[2\lambda + \ln(1 - 2\lambda) + \frac{1}{2}\ln^2(1 - 2\lambda)\right] \\ &- (A_a^{(2)} + A_b^{(2)})\frac{1}{\beta_0}\left[2\lambda + \ln(1 - 2\lambda)\right] + D_{ab}^{(1)}\ln(1 - 2\lambda), \end{aligned} \quad (3.41)$$

where the needed coefficients are found to be [39]

$$A_a^{(1)} = 2C_a, \quad A_a^{(2)} = 2C_a\left[\left(\frac{67}{18} - \frac{\pi^2}{6}\right)C_A - \frac{5}{9}n_f\right] \quad \text{and} \quad D_{ab}^{(1)} = 0. \quad (3.42)$$

The colour factors C_a are $C_q = C_F$ and $C_g = C_A$.

The comparison of $\hat{\sigma}_{ab}$ in both Eq. (3.3) and Eq. (3.35) yields

$$\mathcal{H}_{ab}^{(0)}(M^2, M^2/\mu^2) = \hat{\sigma}_{ab}^{(0)}(M^2, M^2/\mu^2), \quad (3.43)$$

$$\begin{aligned} \mathcal{H}_{ab}^{(1)}(M^2, M^2/\mu^2) &= \hat{\sigma}_{ab}^{(0)}(M^2, M^2/\mu^2) \\ &\times \left[\mathcal{A}_0 + (\delta P_{aa}^{(1)} + \delta P_{bb}^{(1)})\ln\frac{M^2}{\mu^2} + \frac{\pi^2}{6}(A_a^{(1)} + A_b^{(1)})\right], \end{aligned} \quad (3.44)$$

where $\delta P_{aa}^{(1)}$ is the coefficient of the $\delta(1-x)$ term in the LO splitting function $P_{aa}^{(1)}(x)$. The coefficient \mathcal{A}_0 represents the IR-finite part of the renormalised virtual correction

$$\begin{aligned} \mathcal{M}^{(1)}\mathcal{M}^{(0)\dagger} + \text{h.c.} &= \\ &a_s\left(\frac{4\pi\mu^2}{M^2}\right)^\varepsilon \frac{\Gamma(1-\varepsilon)}{\Gamma(1-2\varepsilon)}\left(\frac{\mathcal{A}_{-2}}{\varepsilon^2} + \frac{\mathcal{A}_{-1}}{\varepsilon} + \mathcal{A}_0\right)|\mathcal{M}^{(0)}|^2 + \mathcal{O}(\varepsilon), \end{aligned} \quad (3.45)$$

where $\mathcal{M}^{(0)}$ and $\mathcal{M}^{(1)}$ are the Born and one-loop amplitudes of the process $ab \rightarrow F(M^2)$, summed over spins and colours. Eq. (3.45) is obtained using the prescriptions of the $\overline{\text{MS}}$ scheme in $D = 4 - 2\varepsilon$ dimensions.

3.3.4 Improvement of the threshold resummation

Up to this point, we have systematically neglected all terms of $\mathcal{O}(1/N)$. However, since the dominant $1/N$ -terms, i.e. those of the form $a_s^n L^{2n-1}/N$, stem from the universal collinear radiation of initial state partons, they are expected to exponentiate as well. This has been proven to next-to-next-to-leading order for deep-inelastic scattering and Drell-Yan type processes [45] and can be achieved by making the replacement (cf. Eq. (3.55) below)

$$\mathcal{H}_{ab}^{(1)} \rightarrow \mathcal{H}_{ab}^{(1)} + \mathcal{H}_{ab}^{(0)}(A_a^{(1)} + A_b^{(1)})L/N, \quad (3.46)$$

i.e. by including the corresponding subleading terms of the diagonal splitting functions $P_{aa,bb}(N)$ in Eqs. (3.12) and (3.15). Carrying on with this argument, it is even possible to

3.3 Threshold resummation

resum the terms of $\mathcal{O}(1/N)$ coming from the diagonal and non-diagonal splitting functions by identifying the terms [46]

$$\exp\left[-L\frac{A_a^{(1)}+A_b^{(1)}}{\beta_0}\ln(1-2\lambda)\right] \subset \exp\left[Lg_{ab}^{(1)}(\lambda)\right] \quad (3.47)$$

with the LL approximation of the QCD evolution operators E_{ab} defined in Eq. (3.17) and then promoting the LL to the full one-loop approximation $E_{ab}^{(1)}$. The resummed cross section, Eq. (3.35), can then be written in a collinearly improved form as

$$\hat{\sigma}_{ab}(N, M^2, M^2/\mu^2) = \sum_{cd} \tilde{H}_{cd}(M^2, M^2/\mu^2) \exp[\tilde{G}_{cd}(N, M^2, M^2/\mu^2)] \times E_{ca}^{(1)}(N, M^2/\bar{N}^2, \mu^2) E_{db}^{(1)}(N, M^2/\bar{N}^2, \mu^2), \quad (3.48)$$

where the collinearly improved hard coefficient function \tilde{H}_{ab} is expanded as usual as a power series in $a_s(\mu^2)$ and its LO and NLO coefficients read now

$$\tilde{H}_{ab}^{(0)}(M^2, M^2/\mu^2) = \hat{\sigma}_{ab}^{(0)}(M^2, M^2/\mu^2), \quad (3.49)$$

$$\tilde{H}_{ab}^{(1)}(M^2, M^2/\mu^2) = \hat{\sigma}_{ab}^{(0)}(M^2, M^2/\mu^2) \left[\mathcal{A}_0 + \frac{\pi^2}{6}(A_a^{(1)} + A_b^{(1)}) \right]. \quad (3.50)$$

The Sudakov exponential function \tilde{G}_{ab} is expanded in the same way as \mathcal{G}_{ab} in Eq. (3.39) with

$$\begin{aligned} 2\lambda\beta_0\tilde{g}_{ab}^{(1)}(\lambda) &= (A_a^{(1)} + A_b^{(1)}) [2\lambda + \ln(1-2\lambda)], \quad (3.51) \\ 2\beta_0\tilde{g}_{ab}^{(2)}(\lambda, M^2/\mu^2) &= (A_a^{(1)} + A_b^{(1)}) [2\lambda + \ln(1-2\lambda)] \ln \frac{M^2}{\mu^2} \\ &\quad + (A_a^{(1)} + A_b^{(1)}) \frac{\beta_1}{\beta_0^2} [2\lambda + \ln(1-2\lambda) + \frac{1}{2}\ln^2(1-2\lambda)] \\ &\quad - (A_a^{(2)} + A_b^{(2)}) \frac{1}{\beta_0} [2\lambda + \ln(1-2\lambda)] \\ &\quad + (B_a^{(1)} + B_b^{(1)} + D_{ab}^{(1)}) \ln(1-2\lambda). \quad (3.52) \end{aligned}$$

Here the coefficients $B_a^{(1)}$ have been introduced to cancel NLL terms in the one-loop approximation $E_{ab}^{(1)}$ of the evolution operators. They can be directly related to $\delta P_{aa}^{(1)}$ and their values are [47, 48]

$$B_q^{(1)} = -3C_F \quad \text{and} \quad B_g^{(1)} = -2\beta_0. \quad (3.53)$$

3.3.5 Matching procedure

As mentioned above, the large logarithms, which spoil the convergence of the perturbative series and must be resummed to all orders, appear close to production threshold. Conversely, the perturbative cross section should be valid far from this threshold. To obtain a reliable prediction in all kinematic regions, both results must be consistently matched through

$$\hat{\sigma}_{ab} = \hat{\sigma}_{ab}^{(\text{res})} + \hat{\sigma}_{ab}^{(\text{f.o})} - \hat{\sigma}_{ab}^{(\text{exp})}, \quad (3.54)$$

i.e. by subtracting from the sum of the resummed (res) cross section in Eq. (3.48) and the fixed order (f.o) cross section their overlap. The latter can be obtained by expanding (exp)

3 Resummation

the resummed cross section to the same order in a_s as the perturbative result. At $\mathcal{O}(a_s)$, one then obtains

$$\begin{aligned} \hat{\sigma}_{ab}^{(\text{exp})}(N, M^2, M^2/\mu^2) &= \tilde{H}_{ab}^{(0)}(M^2, M^2/\mu^2) + a_s \tilde{H}_{ab}^{(1)}(M^2, M^2/\mu^2) \\ &- a_s \left(2L - \ln \frac{M^2}{\mu^2} \right) \sum_c [\tilde{H}_{ac}^{(0)}(M^2, M^2/\mu^2) P_{cb}^{(1)}(N) + P_{ca}^{(1)}(N) \tilde{H}_{cb}^{(0)}(M^2, M^2/\mu^2)] \\ &- a_s \tilde{H}_{ab}^{(0)}(M^2, M^2/\mu^2) [L^2(A_a^{(1)} + A_b^{(1)}) + L(B_a^{(1)} + B_b^{(1)})]. \end{aligned} \quad (3.55)$$

3.4 Transverse-momentum resummation

The transverse-momentum resummation proposes to organise the large terms of the generic form $a_s^n [p_T^{-2} \ln^m(M^2/p_T^2)]_+$, with $m \leq 2n - 1$. To correctly take into account the kinematical constraints of transverse-momentum conservation, we will follow Collins, Soper and Sterman (CSS) [40]² and work with the Fourier transform \mathcal{W}_{ab} of the partonic cross section defined by

$$M^2 \frac{d\sigma_{ab}}{dM^2 dp_T^2}(N) = \int \frac{d^2\mathbf{b}}{4\pi} e^{i\mathbf{b}\cdot\mathbf{p}_T} \mathcal{W}_{ab}(N+1, M^2, M^2\bar{b}^2, M^2/\mu^2) \quad (3.56)$$

$$= \int_0^\infty db \frac{b}{2} J_0(bp_T) \mathcal{W}_{ab}(N+1, M^2, M^2\bar{b}^2, M^2/\mu^2), \quad (3.57)$$

where b is the impact parameter,³ $\bar{b} = be^{\gamma_E}/2$ and the Bessel function J_0 comes from the angular integration. In impact-parameter space, the $p_T = 0$ singularities give rise to logarithms which get large in the limit $M\bar{b} \rightarrow \infty$

$$\left(\frac{1}{p_T^2} \ln^m \frac{M^2}{p_T^2} \right)_+ \longrightarrow \ln^{m+1} M^2 \bar{b}^2 + \dots \quad (3.58)$$

3.4.1 Refactorisation

In their paper, CSS refactorise the cross section and absorb the remaining collinear singularities in the parton-in-parton distributions $\mathcal{P}_{c/a}(x, k_T^2, M^2/k_T^2)$. These distributions are defined at longitudinal momentum fraction x and at fixed parton transverse-momentum k_T . The resulting factorisation takes the form

$$\begin{aligned} \mathcal{W}_{ab}(N, M^2, M^2\bar{b}^2, M^2/\mu^2) &= \sum_{cd} H_{cd}(M^2, M^2/\mu^2) \\ &\times \mathcal{P}_{c/a}(N, b^2, M^2\bar{b}^2) \mathcal{P}_{d/b}(N, b^2, M^2\bar{b}^2) S_{cd}(N, M^2\bar{b}^2) + \mathcal{O}\left(\frac{1}{M^2\bar{b}^2}\right), \end{aligned} \quad (3.59)$$

where S_{cd} is a pure eikonal function that describes coherent soft-gluon emission at fixed transverse momentum. The function H_{cd} is a short-distance function which absorbs the hard gluon corrections independent of b and can therefore be computed as a power series in a_s

$$H_{cd}(M^2, M^2/\mu^2) = \sum_{n=0}^{\infty} a_s^n H_{cd}^{(n)}(M^2, M^2/\mu^2). \quad (3.60)$$

²The CSS formalism was first developed for the production of back-to-back jets in e^+e^- annihilation [49, 50] because of a debate whether Drell-Yan like processes (like Eq. (3.1)) factorise.

³Here, b describes the minimal distance of the two incident particles in the limit of no interaction.

3.4 Transverse-momentum resummation

Here we use same notations as in the previous section to show that both resummation formalisms are very similar. However, one must keep in mind that the functions H_{cd} and S_{cd} in Eq. (3.60) are not exactly the same as those in Eq. (3.26).

3.4.2 Exponentiation

By solving the evolution equations of $\mathcal{P}_{c/a}$ and using the eikonal exponentiation of S_{cd} , one obtains the equation

$$\begin{aligned} \mathcal{W}_{ab}(N, M^2, M^2 \bar{b}^2, M^2/\mu^2) &= \sum_{cd} H_{cd}(M^2, M^2/\mu^2) \\ &\times \mathcal{P}_{c/a}(N, b^2, 1) \mathcal{P}_{d/b}(N, b^2, 1) \exp[G_{cd}(M^2, M^2 \bar{b}^2, M^2/\mu^2)]. \end{aligned} \quad (3.61)$$

The Sudakov exponent G_{cd} has the integral representation

$$\begin{aligned} G_{cd}(M^2, M^2 \bar{b}^2, M^2/\mu^2) &= \\ &= -\frac{1}{2} \int_{1/\bar{b}^2}^{M^2} \frac{dq^2}{q^2} \left[A_c(a_s(q^2)) \ln \frac{M^2}{q^2} + B_c(a_s(q^2)) \right] + (c \leftrightarrow d) \end{aligned} \quad (3.62)$$

and the $\mathcal{P}_{b/a}$ -distributions can be related to the usual k_T -integrated parton-in-parton distribution functions $\phi_{b/a}$ by

$$\mathcal{P}_{b/a}(N, b^2, 1) = \sum_c C_{bc}(N, a_s(1/\bar{b}^2)) \phi_{c/a}(N, 1/\bar{b}^2). \quad (3.63)$$

We now apply the mass-factorisation procedure and get the resummed formula

$$\begin{aligned} \hat{\sigma}_{ab}(N, M^2, M^2/p_T^2, M^2/\mu^2) &= \\ &= \int_0^\infty db \frac{b}{2} J_0(bp_T) \sum_{cdef} H_{cd}(M^2, M^2/\mu^2) \exp[G_{cd}(M^2, M^2 \bar{b}^2, M^2/\mu^2)] \\ &\times C_{ce}(N, a_s(1/\bar{b}^2)) C_{df}(N, a_s(1/\bar{b}^2)) E_{ea}(N, 1/\bar{b}^2, \mu^2) E_{fb}(N, 1/\bar{b}^2, \mu^2) \end{aligned} \quad (3.64)$$

where we have used Eq. (3.17) to evolve the parton distribution $\phi_{c/a}$ from the factorisation scale μ to the natural scale of the process $1/\bar{b}$.

As for the threshold resummation, the needed functions A_a , B_a and C_{ab} can be calculated perturbatively in powers of a_s ,

$$A_a(a_s) = \sum_{n=1}^{\infty} a_s^n A_a^{(n)}, \quad B_a(a_s) = \sum_{n=1}^{\infty} a_s^n B_a^{(n)}, \quad (3.65)$$

$$\text{and } C_{ab}(N, a_s) = \delta_{ab} + \sum_{n=1}^{\infty} a_s^n C_{ab}^{(n)}(N). \quad (3.66)$$

The resummation of the logarithms is completely achieved by computing the four functions H_{ab} , A_a , B_a and C_{ab} at a given order in a_s . The knowledge of the coefficients $H_{ab}^{(0)}$, $A_a^{(1)}$ leads to the resummation of the LL contributions. Analogously, the coefficients $H_{ab}^{(1)}$, $A_a^{(2)}$, $B_a^{(1)}$ and $C_{ab}^{(1)}$ give the NLL terms, $H_{ab}^{(2)}$, $A_a^{(3)}$, $B_a^{(2)}$ and $C_{ab}^{(2)}$ give the NNLL terms, and so forth.

3.4.3 NLL approximation

By performing the integral in Eq. (3.62), the exponent G_{ab} can be expanded as

$$G_{ab}(M^2, M^2 \bar{b}^2, M^2/\mu^2) = L g_{ab}^{(1)}(\lambda) + g_{ab}^{(2)}(\lambda, M^2/\mu^2) + \dots \quad (3.67)$$

with $\lambda = a_s \beta_0 L$ and $L = \ln M^2 \bar{b}^2$. Again, the first term of the expansion collects the LL contributions and the second term collects the NLL contributions present in G_{ab} . The two functions $g_{ab}^{(1,2)}$ have the following explicit expressions

$$\begin{aligned} 2\lambda \beta_0 g_{ab}^{(1)}(\lambda) &= (A_a^{(1)} + A_b^{(1)}) [\lambda + \ln(1 - \lambda)], \\ 2\beta_0 g_{ab}^{(2)}(\lambda, M^2/\mu^2) &= (A_a^{(1)} + A_b^{(1)}) \left[\frac{\lambda}{1 - \lambda} + \ln(1 - \lambda) \right] \ln \frac{M^2}{\mu^2} \\ &\quad + (A_a^{(1)} + A_b^{(1)}) \frac{\beta_1}{\beta_0^2} \left[\frac{\lambda + \ln(1 - \lambda)}{1 - \lambda} + \frac{1}{2} \ln^2(1 - \lambda) \right] \\ &\quad - (A_a^{(2)} + A_b^{(2)}) \frac{1}{\beta_0} \left[\frac{\lambda}{1 - \lambda} + \ln(1 - \lambda) \right] \\ &\quad + (B_a^{(1)} + B_b^{(1)}) \ln(1 - \lambda), \end{aligned} \quad (3.68)$$

where the coefficients $A_a^{(1)}$, $A_a^{(2)}$ and $B_a^{(1)}$ are known [47, 48] and are actually the same as for the threshold resummation in Eq. (3.42) and Eq. (3.53).

As was shown in Ref. [51], there is actually some freedom in how one assigns the individual contributions to $H_{ab}^{(1)}$, $C_{ab}^{(1)}$ and $B_{a,b}^{(2)}$. A choice for one coefficient uniquely determines the others. For instance, in the original CSS formulation, the function H_{ab} is fixed to

$$H_{ab}(M^2, M^2/\mu^2) = \hat{\sigma}_{ab}^{(0)}(M^2, M^2/\mu^2). \quad (3.70)$$

With this specific choice, the coefficients $B_a^{(2)}$ and $C_{ab}^{(1)}$ are given by [52, 53]

$$C_{ab}^{(1)}(N) = \delta_{ab} \left[C_a \frac{\pi^2}{6} + \frac{1}{2} \mathcal{A}_0 \right] - P_{ab}^{(1),\varepsilon}(N), \quad (3.71)$$

$$B_a^{(2)} = -2\delta P_{aa}^{(2)} + \beta_0 \left[\frac{2\pi^2}{3} C_a + \mathcal{A}_0 \right], \quad (3.72)$$

where $P_{ab}^{(1),\varepsilon}$ is the $\mathcal{O}(\varepsilon)$ term in the AP splitting kernel, $\delta P_{aa}^{(2)}$ is the coefficient of the $\delta(1-x)$ term in the two-loop AP splitting function, and \mathcal{A}_0 is the finite part of the one-loop virtual contributions defined in Eq. (3.45). We see that with this choice of resummation scheme, even the Sudakov exponent depends on hard contributions coming from the one-loop amplitude. That is why, in the following we will prefer a more “physical” choice for which the full \mathcal{A}_0 -dependence of the coefficients $B_a^{(2)}$ and $C_{ab}^{(1)}$ is absorbed in the short-distance function H_{ab}

$$H_{ab}(M^2, M^2/\mu^2) = \hat{\sigma}_{ab}^{(0)}(M^2, M^2/\mu^2) [1 + a_s \mathcal{A}_0] + \mathcal{O}(a_s^2). \quad (3.73)$$

Given this choice, the needed coefficient $C_{ab}^{(1)}$ to achieve NLL accuracy becomes

$$C_{ab}^{(1)}(N) = C_a \frac{\pi^2}{6} \delta_{ab} - P_{ab}^{(1),\varepsilon}(N), \quad (3.74)$$

3.4 Transverse-momentum resummation

where

$$\begin{aligned} P_{qq}^{(1),\varepsilon}(N) &= \frac{-C_F}{N(N+1)}, & P_{qg}^{(1),\varepsilon}(N) &= \frac{-1}{(N+1)(N+2)}, \\ P_{gq}^{(1),\varepsilon}(N) &= \frac{-C_F}{N+1}, & P_{gg}^{(1),\varepsilon}(N) &= 0. \end{aligned} \quad (3.75)$$

3.4.4 Improvements of the resummation formalism

In the implementation of Eq. (3.64), the resummation of the large logarithmic contributions $L = \ln M^2 \bar{b}^2$, affects not only the small- p_T region ($M\bar{b} \rightarrow \infty$) but also the region of large p_T ($M\bar{b} \rightarrow 0$) where resummation is not justified. This problem can be solved by implementing the following change [41]

$$\bar{b}^2 \rightarrow \tilde{b}^2 \quad \text{with} \quad \tilde{b}^2 = \bar{b}^2 + \frac{1}{M^2}. \quad (3.76)$$

Note that this replacement is legitimate to arbitrary logarithmic accuracy because in the small- p_T region, $\ln(M^2 \tilde{b}^2) = L + \mathcal{O}(1/M^2/\bar{b}^2)$. However, at large p_T , the resummed cross section has a far better behaviour. Furthermore, this change allows us to recover the corresponding fixed-order total cross section upon integration over p_T [41].

In Eq. (3.64), the variable b is integrated from 0 to ∞ . When $b \gtrsim 1/\Lambda_{QCD}$, the resummation formalism is no longer reliable because of complicated long-distance effects which cannot be computed perturbatively. Nevertheless, due to their long-distance nature, these Non-Perturbative (NP) effects are assumed to be universal and can be measured in experiments. Practically, these effects are introduced thanks to the replacement

$$G_{cd} \rightarrow G_{cd} + \ln F_{cd}^{\text{NP}}(N, M^2, b^2). \quad (3.77)$$

Global fits of experimental Drell-Yan data allow for different forms of the NP function F_{ab}^{NP} , whose explicit expressions⁴ can be found in Refs. [54, 55, 56, 57].

3.4.5 Matching procedure

Although resummation is needed at small p_T , it is not justified in the large p_T -region, where the usual perturbative calculation is fully reliable. A consistent description of the whole phase space requires a matching between the two results that avoids double counting. Therefore, we adopt the following matching procedure

$$\hat{\sigma}_{ab} = \hat{\sigma}_{ab}^{(\text{res})} + \hat{\sigma}_{ab}^{(\text{f.o})} - \hat{\sigma}_{ab}^{(\text{exp})}, \quad (3.78)$$

where $\hat{\sigma}_{ab}^{(\text{res})}$ is the resummed hard-scattering function given in Eq. (3.64) and $\hat{\sigma}_{ab}^{(\text{f.o})}$ is the fixed-order perturbative result at a given order in a_s . Finally, $\hat{\sigma}_{ab}^{(\text{exp})}$ denotes the expansion of the resummed result to the same order in a_s as $\hat{\sigma}_{ab}^{(\text{f.o})}$.

⁴The expressions of the function F_{ab}^{NP} are usually written in x -space rather than in Mellin space as presented here.

3 Resummation

The perturbative expansion of the resummed component is easily obtained by expanding Eq. (3.64) to the desired accuracy. At order $\mathcal{O}(a_s)$, we find

$$\begin{aligned} \hat{\sigma}_{ab}^{(\text{exp})}(N, M^2, M^2/p_T^2, M^2/\mu^2) &= H_{ab}^{(0)}(M^2, M^2/\mu^2) + a_s H_{ab}^{(1)}(M^2, M^2/\mu^2) \\ &- a_s \left(\mathcal{J} - \ln \frac{M^2}{\mu^2} \right) \sum_c [H_{ac}^{(0)}(M^2, M^2/\mu^2) P_{cb}^{(1)}(N) + P_{ca}^{(1)}(N) H_{cb}^{(0)}(M^2, M^2/\mu^2)] \\ &+ a_s \sum_c [H_{ac}^{(0)}(M^2, M^2/\mu^2) C_{cb}^{(1)}(N) + C_{ca}^{(1)}(N) H_{cb}^{(0)}(M^2, M^2/\mu^2)] \\ &- a_s H_{ab}^{(0)}(M^2, M^2/\mu^2) \left[\frac{\mathcal{J}^2}{4} (A_a^{(1)} + A_b^{(1)}) + \frac{\mathcal{J}}{2} (B_a^{(1)} + B_b^{(1)}) \right], \end{aligned} \quad (3.79)$$

where the full dependence on p_T is embodied in the Bessel integral

$$\mathcal{J} = \int_0^\infty db \frac{b}{2} J_0(bp_T) \ln(M^2 \tilde{b}^2). \quad (3.80)$$

3.5 Inverse transforms

After the resummation has been performed in N - and/or b -space, we have to switch back to the physical x - and/or p_T -space in order to achieve phenomenological studies. Special attention has to be paid to the singularities in the resummed exponents (when $\lambda = 1$ or $1/2$ in Eqs. (3.40), (3.41), (3.68) and (3.69)). They are related to the presence of the Landau pole in the perturbative running of a_s and prescriptions for both the Mellin and Fourier inverse transforms are needed.

For the Fourier inverse transform of Eq. (3.64) we follow Ref. [58] and deform the integration contour of the b -integral in the complex plane. We define then two integration branches

$$b = (\cos \varphi \pm i \sin \varphi)t, \quad t \in [0, \infty[\quad (3.81)$$

where φ has to be chosen in the range $]0, \pi/2[$. The Bessel function J_0 in Eq. (3.64) is then replaced by the sum of the two auxiliary functions

$$h_1(z, \nu) = -\frac{1}{2\pi} \int_{-i\nu\pi}^{-\pi+i\nu\pi} d\theta e^{-iz \sin \theta}, \quad (3.82)$$

$$h_2(z, \nu) = -\frac{1}{2\pi} \int_{\pi+i\nu\pi}^{-i\nu\pi} d\theta e^{-iz \sin \theta}. \quad (3.83)$$

The functions $h_{1,2}$ are finite for any value of z , and their sum, independent of ν , is always equal to $J_0(z)$. Since they distinguish positive and negative phases in the complex b -plane, they can be associated with only one of the two branches.

For the inverse Mellin transform,

$$F(x) = \int_{\mathcal{C}_N} \frac{dN}{2\pi i} \tau^{-N} F(N), \quad (3.84)$$

we choose an integration contour (\mathcal{C}_N) inspired by the minimal prescription [59] and the principal value resummation [60], where one again defines two branches

$$\mathcal{C}_N: \quad N = C + z e^{\pm i\phi}, \quad z \in [0, \infty[. \quad (3.85)$$

3.5 Inverse transforms

The parameter C must be chosen in such a way that the poles in the Mellin moments of the PDFs, which are related to the small- x (Regge) singularity, lie to the left and the Landau pole to the right of the integration contour. While formally the angle ϕ can be chosen in the range $[\pi/2, \pi[$, it is advantageous to take $\phi > \pi/2$ to improve the convergence of the inverse Mellin transform.

3 Resummation

4

Gaugino-pair production: Fixed-order calculations

In this chapter, we present our perturbative calculations for gaugino-pair production at hadron colliders, while we dedicate the next chapter to the results using resummation techniques.

In Sec. 4.1, we present an exploratory study of gaugino-pair production in polarised hadron collisions, focusing on the correlation of beam polarisation and gaugino/Higgsino mixing in the general MSSM. Analytical and numerical results for the LO cross section and spin asymmetries are then given for several hadron colliders. In Sec. 4.2, we present our NLO SUSY-QCD calculations, focusing on the squark mixing, the ultraviolet renormalisation procedure and the dipole subtraction method employed for the cancellation of the infrared divergences among virtual and real contributions.

The results presented here have been published in Refs. [61, 62].

4.1 LO cross section and spin asymmetries

Unpolarised cross sections for gaugino pairs have already been calculated in Refs. [63, 64, 65, 66]. Here, we generalise these results by including the effects of both initial-state polarisations and mixing of the left- and right-handed squarks. We start by fixing the notations for the different couplings we need in order to then compute analytically the partonic cross sections for the pair production of gauginos and Higgsinos.

4.1.1 Coupling definitions

For the electroweak interactions, we define the square of the weak coupling constant $g^2 = e^2/\sin^2\theta_W$ in terms of the electromagnetic fine structure constant $\alpha = e^2/(4\pi)$ and the squared sine of the weak mixing angle $\sin^2\theta_W$. The couplings of the neutralinos and charginos $\tilde{\chi}_i^{0,\pm}$ to the electroweak gauge bosons γ , W and Z are then given by

$$L_{\gamma\tilde{\chi}_i^+\tilde{\chi}_j^+} = -e\delta_{ij}, \quad R_{\gamma\tilde{\chi}_i^+\tilde{\chi}_j^+} = L_{\gamma\tilde{\chi}_i^+\tilde{\chi}_j^+}, \quad (4.1)$$

$$L_{W\tilde{\chi}_i^0\tilde{\chi}_j^+} = g \left[-\frac{1}{\sqrt{2}}N_{i4}V_{j2}^* + N_{i2}V_{j1}^* \right], \quad R_{W\tilde{\chi}_i^0\tilde{\chi}_j^+} = g \left[\frac{1}{\sqrt{2}}N_{i3}^*U_{j2} + N_{i2}^*U_{j1} \right], \quad (4.2)$$

4 Gaugino-pair production: Fixed-order calculations

$$L_{Z\tilde{\chi}_i^0\tilde{\chi}_j^0} = \frac{g}{2\cos\theta_W} \left[-N_{i3}N_{j3}^* + N_{i4}N_{j4}^* \right], \quad R_{Z\tilde{\chi}_i^0\tilde{\chi}_j^0} = -L_{Z\tilde{\chi}_i^0\tilde{\chi}_j^0}, \quad (4.3)$$

$$L_{Z\tilde{\chi}_i^+\tilde{\chi}_j^+} = \frac{g}{\cos\theta_W} \left[-V_{i1}V_{j1}^* - \frac{1}{2}V_{i2}V_{j2}^* + \delta_{ij}\sin^2\theta_W \right] \quad \text{and}$$

$$R_{Z\tilde{\chi}_i^+\tilde{\chi}_j^+} = \frac{g}{\cos\theta_W} \left[-U_{i1}^*U_{j1} - \frac{1}{2}U_{i2}^*U_{j2} + \delta_{ij}\sin^2\theta_W \right], \quad (4.4)$$

where the matrices N , U and V relate to the gaugino/Higgsino mixing (see Sec. 2.3.3).

The coupling strengths of the left- and right-handed quarks to electroweak gauge bosons are proportional to

$$L_{\gamma qq'} = -e e_q \delta_{qq'}, \quad R_{\gamma qq'} = L_{\gamma qq'}, \quad (4.5)$$

$$L_{Z qq'} = -\frac{g}{\cos\theta_W} (T_q^3 - e_q \sin^2\theta_W) \delta_{qq'}, \quad R_{Z qq'} = \frac{g}{\cos\theta_W} e_q \sin^2\theta_W \delta_{qq'}, \quad (4.6)$$

$$L_{Wud} = -\frac{g}{\sqrt{2}} \quad \text{and} \quad R_{Wud} = 0, \quad (4.7)$$

where the weak isospin quantum number is $T_q^3 = \pm 1/2$ for left-handed up- and down-type quarks, and their fractional electromagnetic charges are denoted by e_q .¹ To simplify the notations, we have suppressed the generation indices, i.e. the subscript ud stands for any pair ud , cs and tb .

The SUSY counterparts of these interactions correspond to the gaugino-squark-quark couplings, which are given by

$$L_{\tilde{\chi}_i^0\tilde{d}_{jd}} = -g\sqrt{2} \left[(e_d - T_d^3) \tan\theta_W N_{i1}^* + T_d^3 N_{i2}^* \right] R_{j1}^{\tilde{d}} - y_d N_{i3}^* R_{j2}^{\tilde{d}},$$

$$R_{\tilde{\chi}_i^0\tilde{d}_{jd}} = -g\sqrt{2} \left[-e_d \tan\theta_W N_{i1} \right] R_{j2}^{\tilde{d}} - y_d N_{i3} R_{j1}^{\tilde{d}}, \quad (4.8)$$

$$L_{\tilde{\chi}_i^0\tilde{u}_{ju}} = -g\sqrt{2} \left[(e_u - T_u^3) \tan\theta_W N_{i1}^* + T_u^3 N_{i2}^* \right] R_{j1}^{\tilde{u}} - y_u N_{i4}^* R_{j2}^{\tilde{u}},$$

$$R_{\tilde{\chi}_i^0\tilde{u}_{ju}} = -g\sqrt{2} \left[-e_u \tan\theta_W N_{i1} \right] R_{j2}^{\tilde{u}} - y_u N_{i4} R_{j1}^{\tilde{u}}, \quad (4.9)$$

$$L_{\tilde{\chi}_i^+\tilde{u}_{jd}} = -gV_{i1}^* R_{j1}^{\tilde{u}} + y_u V_{i2}^* R_{j2}^{\tilde{u}},$$

$$R_{\tilde{\chi}_i^+\tilde{u}_{jd}} = y_d U_{i2} R_{j1}^{\tilde{u}}, \quad (4.10)$$

$$L_{\tilde{\chi}_i^+\tilde{d}_{ju}} = -gU_{i1}^* R_{j1}^{\tilde{d}} + y_d U_{i2}^* R_{j2}^{\tilde{d}},$$

$$R_{\tilde{\chi}_i^+\tilde{d}_{ju}} = y_u V_{i2} R_{j1}^{\tilde{d}}, \quad (4.11)$$

where $R_{ij}^{\tilde{u},\tilde{d}}$ are the elements of rotation matrices diagonalising the up- and down-type squark mass matrices presented in Sec. 2.3.2. These general expressions can be simplified by neglecting the Yukawa couplings

$$y_u = \frac{gm_u}{\sqrt{2}m_W \sin\beta} \quad \text{and} \quad y_d = \frac{gm_d}{\sqrt{2}m_W \cos\beta}, \quad (4.12)$$

except for the one of the top quark, whose mass is not small compared to m_W . All other couplings vanish due to electromagnetic charge conservation.

¹Here, we are neglecting the non-diagonal entries of the CKM matrix.

4.1 LO cross section and spin asymmetries

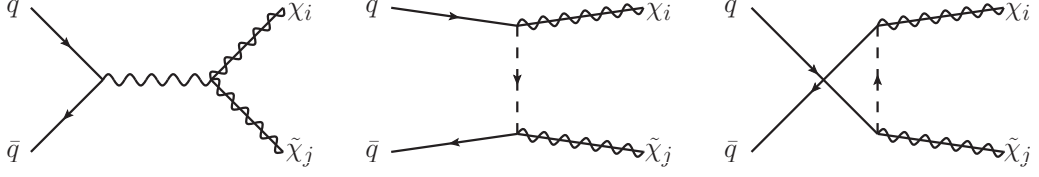


Figure 4.1: Tree-level Feynman diagrams for the production of gaugino pairs.

4.1.2 Polarised partonic cross section

The process

$$q(h_a, p_a)\bar{q}'(h_b, p_b) \rightarrow \tilde{\chi}_i^{0,+}(p_1)\tilde{\chi}_j^{0,-}(p_2) \quad (4.13)$$

is induced by initial quarks q and antiquarks \bar{q}' with definite helicities $h_{a,b}$ and momenta $p_{a,b}$ and is mediated by s -channel electroweak gauge-boson and t - and u -channel squark exchanges (see Fig. 4.1). Using a Fierz transformation, its cross section can be expressed generically as

$$\begin{aligned} \frac{d\sigma_{q\bar{q}'}^{h_a, h_b}}{dt} = \frac{s^{-2}f}{48\pi} \bigg\{ & (1-h_a)(1+h_b) [|Q_{LL}^u|^2 u_{\tilde{\chi}_i} u_{\tilde{\chi}_j} + |Q_{LL}^t|^2 t_{\tilde{\chi}_i} t_{\tilde{\chi}_j} + 2\text{Re}[Q_{LL}^{u*} Q_{LL}^t] m_{\tilde{\chi}_i} m_{\tilde{\chi}_j} s] \\ & + (1+h_a)(1-h_b) [|Q_{RR}^u|^2 u_{\tilde{\chi}_i} u_{\tilde{\chi}_j} + |Q_{RR}^t|^2 t_{\tilde{\chi}_i} t_{\tilde{\chi}_j} + 2\text{Re}[Q_{RR}^{u*} Q_{RR}^t] m_{\tilde{\chi}_i} m_{\tilde{\chi}_j} s] \\ & + (1-h_a)(1-h_b) [|Q_{LR}^u|^2 u_{\tilde{\chi}_i} u_{\tilde{\chi}_j} + |Q_{LR}^t|^2 t_{\tilde{\chi}_i} t_{\tilde{\chi}_j} - 2\text{Re}[Q_{LR}^{u*} Q_{LR}^t] (ut - m_{\tilde{\chi}_i}^2 m_{\tilde{\chi}_j}^2)] \\ & + (1+h_a)(1+h_b) [|Q_{RL}^u|^2 u_{\tilde{\chi}_i} u_{\tilde{\chi}_j} + |Q_{RL}^t|^2 t_{\tilde{\chi}_i} t_{\tilde{\chi}_j} - 2\text{Re}[Q_{RL}^{u*} Q_{RL}^t] (ut - m_{\tilde{\chi}_i}^2 m_{\tilde{\chi}_j}^2)] \bigg\}, \quad (4.14) \end{aligned}$$

i.e. in terms of generalised charges $Q_{IJ}^{t,u}$, the conventional Mandelstam variables

$$s = (p_a + p_b)^2, \quad t = (p_a - p_1)^2 \quad \text{and} \quad u = (p_a - p_2)^2, \quad (4.15)$$

the gaugino and squark masses $m_{\tilde{\chi}_{i,j}^{0,\pm}}$ and $m_{\tilde{q}_k}$, and the masses of the neutral and charged electroweak gauge bosons m_W and m_Z . Propagators and scalar products of momenta appear as mass-subtracted Mandelstam variables,

$$s_\gamma = s, \quad s_W = s - m_W^2, \quad s_Z = s - m_Z^2, \quad (4.16)$$

$$t_{\tilde{q}_k} = t - m_{\tilde{q}_k}^2, \quad u_{\tilde{q}_k} = u - m_{\tilde{q}_k}^2, \quad (4.17)$$

$$t_{\tilde{\chi}_i} = t - m_{\tilde{\chi}_i}^2, \quad u_{\tilde{\chi}_i} = u - m_{\tilde{\chi}_i}^2. \quad (4.18)$$

The Majorana nature of the neutralinos is taken into account thanks to the symmetry factor $f = 1/(1 + \delta_{\tilde{\chi}_i \tilde{\chi}_j})$.

Unpolarised cross sections, averaged over initial spins, can easily be derived from the expression

$$d\sigma = \frac{d\sigma^{1,1} + d\sigma^{1,-1} + d\sigma^{-1,1} + d\sigma^{-1,-1}}{4}, \quad (4.19)$$

while single- and double-polarised cross sections, including the same average factor for initial spins, are given by

$$d\Delta\sigma_L = \frac{d\sigma^{1,1} \pm d\sigma^{1,-1} \mp d\sigma^{-1,1} - d\sigma^{-1,-1}}{4} \quad \text{and} \quad (4.20)$$

$$d\Delta\sigma_{LL} = \frac{d\sigma^{1,1} - d\sigma^{1,-1} - d\sigma^{-1,1} + d\sigma^{-1,-1}}{4}, \quad (4.21)$$

4 Gaugino-pair production: Fixed-order calculations

where the upper (lower) signs refer to polarised (anti-)quarks. The partonic single- and double-spin asymmetries then become

$$\hat{A}_L = \frac{d\Delta\sigma_L}{d\sigma} \quad \text{and} \quad \hat{A}_{LL} = \frac{d\Delta\sigma_{LL}}{d\sigma}. \quad (4.22)$$

The generalised charges are given by

$$Q_{LL}^u = \sum_{V=\gamma,W,Z} \frac{L_{Vqq'} L_V \tilde{\chi}_i \tilde{\chi}_j}{s_V} - \sum_{\tilde{q}_k} \frac{L_{\tilde{\chi}_i \tilde{q}_k q'}^* L_{\tilde{\chi}_j \tilde{q}_k q}}{2u_{\tilde{q}_k}}, \quad (4.23)$$

$$Q_{LL}^t = \sum_{V=\gamma,W,Z} \frac{L_{Vqq'} R_V \tilde{\chi}_i \tilde{\chi}_j}{s_V} + \sum_{\tilde{q}_k} \frac{L_{\tilde{\chi}_i \tilde{q}_k q} L_{\tilde{\chi}_j \tilde{q}_k q'}^*}{2t_{\tilde{q}_k}}, \quad (4.24)$$

$$Q_{RR}^u = \sum_{V=\gamma,W,Z} \frac{R_{Vqq'} R_V \tilde{\chi}_i \tilde{\chi}_j}{s_V} - \sum_{\tilde{q}_k} \frac{R_{\tilde{\chi}_i \tilde{q}_k q'}^* R_{\tilde{\chi}_j \tilde{q}_k q}}{2u_{\tilde{q}_k}}, \quad (4.25)$$

$$Q_{RR}^t = \sum_{V=\gamma,W,Z} \frac{R_{Vqq'} L_V \tilde{\chi}_i \tilde{\chi}_j}{s_V} + \sum_{\tilde{q}_k} \frac{R_{\tilde{\chi}_i \tilde{q}_k q} R_{\tilde{\chi}_j \tilde{q}_k q'}^*}{2t_{\tilde{q}_k}}, \quad (4.26)$$

$$Q_{LR}^u = - \sum_{\tilde{q}_k} \frac{R_{\tilde{\chi}_i \tilde{q}_k q'}^* L_{\tilde{\chi}_j \tilde{q}_k q}}{2u_{\tilde{q}_k}}, \quad (4.27)$$

$$Q_{LR}^t = + \sum_{\tilde{q}_k} \frac{L_{\tilde{\chi}_i \tilde{q}_k q} R_{\tilde{\chi}_j \tilde{q}_k q'}^*}{2t_{\tilde{q}_k}}, \quad (4.28)$$

$$Q_{RL}^u = - \sum_{\tilde{q}_k} \frac{L_{\tilde{\chi}_i \tilde{q}_k q}^* R_{\tilde{\chi}_j \tilde{q}_k q}}{2u_{\tilde{q}_k}}, \quad (4.29)$$

$$Q_{RL}^t = + \sum_{\tilde{q}_k} \frac{R_{\tilde{\chi}_i \tilde{q}_k q} L_{\tilde{\chi}_j \tilde{q}_k q'}^*}{2t_{\tilde{q}_k}}. \quad (4.30)$$

After accounting for our harmonisation of generalised charge definitions, which are now similar for all gaugino channels, our results agree with those published in Ref. [67]. The cross section for chargino-pair production in e^+e^- -collisions can be deduced by changing all the (s)quark masses and coupling to the (s)lepton ones and multiplying the cross section by the colour factor $N_c = 3$. Neglecting all Yukawa couplings, we can then reproduce the calculations of Ref. [65]. In the case of non-mixing squarks with neglected Yukawa couplings, we agree with the results of Ref. [66] and Ref. [68], provided we correct a sign in their Eq. (2) as described in the Erratum. Note that for $\tilde{\chi}_i^+ \tilde{\chi}_j^-$ -production, there is no interference between t - and u -channel diagrams due to (electromagnetic) charge conservation.

4.1.3 Numerical results

We now present numerical predictions for the cross sections and single- and double-spin asymmetries of gaugino-pair production at the polarised pp collider RHIC [69] and possible polarisation upgrades of the $p\bar{p}$ and pp colliders Tevatron [70] and LHC [71]. Thanks to the QCD factorisation theorem, total unpolarised hadronic cross sections

$$\sigma_{AB} = \int_{(m_{\tilde{\chi}_i} + m_{\tilde{\chi}_j})^2/S}^1 d\tau \int_{-1/2 \ln \tau}^{1/2 \ln \tau} dy \int_{t_{\min}}^{t_{\max}} dt f_{a/A}(x_a, \mu_F) f_{b/B}(x_b, \mu_F) \frac{d\sigma_{ab}}{dt} \quad (4.31)$$

4.1 LO cross section and spin asymmetries

can be calculated by convolving the relevant partonic cross sections $d\sigma/dt$, computed in Sec. 4.1.2, with universal parton densities $f_{a/A}$ and $f_{b/B}$ of partons a, b in the hadrons A, B , which depend on the longitudinal momentum fractions of the two partons $x_{a,b} = \sqrt{\tau}e^{\pm y}$ and on the unphysical factorisation scale μ_F . Polarised cross sections are computed similarly by replacing either one or both of the unpolarised parton densities $f_{a,b}(x_{a,b}, \mu_F)$ with their polarised equivalents $\Delta f_{a,b}(x_{a,b}, \mu_F)$ and the unpolarised partonic cross section $d\sigma$, given in Eq. (4.19), with its single- or double-polarised equivalent given in Eqs. (4.20) and (4.21). The hadronic centre-of-mass energy is denoted by \sqrt{S} , and the Mandelstam variable t is integrated over the range

$$t_{\min, \max} = \frac{-(s - m_{\tilde{\chi}_i}^2 - m_{\tilde{\chi}_j}^2) \mp \sqrt{(s - m_{\tilde{\chi}_i}^2 - m_{\tilde{\chi}_j}^2)^2 - 4m_{\tilde{\chi}_i}^2 m_{\tilde{\chi}_j}^2}}{2}. \quad (4.32)$$

Efforts over the past three decades have produced extensive data sets for polarised deep-inelastic scattering (DIS), resulting in a good knowledge in particular of the polarised valence-quark (non-singlet) distributions. For consistency with our leading order (LO) QCD calculation in the collinear approximation, where all squared quark masses (except for the top-quark mass) $m_q^2 \ll s$, we employ related sets of unpolarised (GRV [72]) and polarised (GRSV [73]) LO parton densities. We estimate the theoretical uncertainty due to the less well known polarised parton densities by showing our numerical predictions for both the GRSV2000 LO standard (STD) and valence (VAL) parameterizations, which treat the polarised sea-quarks in a flavour-symmetric or flavour-asymmetric way. The polarised gluon density could not be constrained very well in the fits to the DIS data, but it fortunately does not enter directly in our analysis.

Results from semi-inclusive DIS with an identified hadron in the final state have the promise to put individual constraints on the various quark flavour distributions in the nucleon. In addition, precise asymmetry measurements from RHIC are expected to put significant constraints on the polarised gluon distribution. A first step in this direction has been undertaken very recently by including semi-inclusive DIS data from the SMC, HERMES and COMPASS experiments and π^0 and jet production data from the PHENIX and STAR collaborations in a global analysis [74].

If not stated otherwise, we set the factorisation scale μ_F to the average mass of the final state SUSY particles. The bottom- and top-quark densities in the proton are small and absent in the GRV and GRSV parameterizations, as is the charm-quark density. We therefore consider for squark exchanges only the SUSY-partners of the light quark flavours without mixing and all degenerate in mass. The corresponding uncertainty is estimated by giving predictions for two different squark masses, one at the mass limit set by the D0 collaboration at 325 GeV [75] and one for a typical SUSY-breaking scale of 1 TeV.

Gaugino masses and mixings

We wish to study the correlations of beam polarisations and the gaugino/Higgsino fractions of charginos and neutralinos without referring to a particular SUSY-breaking model. Furthermore, we wish to keep the physical gaugino masses as constant as possible, since the absolute cross sections depend strongly on them through trivial phase space effects. We start therefore by fixing the lightest chargino mass $m_{\tilde{\chi}_1^\pm}$ to either 80 GeV (for our RHIC predictions) or 151 GeV (for our Tevatron and LHC predictions). The relatively strong limit of 151 GeV has recently been obtained by the CDF collaboration at Run II of the Tevatron

4 Gaugino-pair production: Fixed-order calculations

and holds for a constrained MSSM with light non-mixing sleptons [76]. On the other hand, charginos with a mass as low as 80 GeV may still be allowed, if they are gaugino-like, their mass difference with the lightest neutralino is very small, and if the sneutrinos are light [77, 78]. The second-lightest neutralino usually stays close in mass to the lightest chargino (see below) and must be heavier than 62.4 GeV, while the lightest neutralino can be half as heavy and is constrained to masses above 32.5–46 GeV, depending again on the sfermion masses [79]. The associated production of the second-lightest neutralino with the lightest chargino is usually experimentally easily identifiable through the gold-plated tri-lepton decay. It has been pointed out that the electroweak precision fits improve when including heavy sfermions as proposed by split-SUSY scenarios, but light gauginos or Higgsinos with masses close to the current exclusion limits [80].

In the MSSM, the gaugino masses and mixing depend on the *a priori* unknown SUSY-breaking parameters M_1 , M_2 , μ , and on $\tan\beta$ (see Sec. 2.3.3). Taking $\tan\beta = 10$ and assuming Bino and Wino mass unification at the GUT scale, so that $M_1 = \frac{5}{3}\tan^2\theta_W M_2 \simeq 0.5M_2$ at the electroweak scale, we can compute the Higgsino mass parameter μ from Eq. (2.50),

$$\mu = \frac{m_W^2 M_2 s_{2\beta} \pm m_{\tilde{\chi}_1^\pm} \sqrt{(m_{\tilde{\chi}_1^\pm}^2 - M_2^2 - m_W^2)^2 - m_W^4 c_{2\beta}^2}}{M_2^2 - m_{\tilde{\chi}_1^\pm}^2}, \quad (4.33)$$

as a function of the only remaining parameter M_2 , once the lightest chargino mass $m_{\tilde{\chi}_1^\pm}$ is fixed. Since the one-loop contribution to the anomalous magnetic moment $a_\mu = (g_\mu - 2)/2$ of the muon induced by gauginos and sleptons of common mass M_{SUSY} is approximately given by [81]

$$a_\mu^{\text{SUSY},1\text{-loop}} = 13 \times 10^{-10} \left(\frac{100 \text{ GeV}}{M_{\text{SUSY}}} \right)^2 \tan\beta \text{sgn}(\mu), \quad (4.34)$$

negative values of μ would increase, not decrease, the disagreement between the recent BNL measurement and the theoretical SM value of a_μ [79]. The region $\mu < 0$ is therefore disfavoured, and we take $\mu > 0$ unless noted otherwise.

As the off-diagonal matrix elements of the gaugino mass matrices depend on $\sin\beta$ and $\cos\beta$ (see Sec. 2.3.3), one might be tempted to fix M_2 , e.g. to $2m_{\tilde{\chi}_1^\pm}$, and study rather the variation of the chargino/neutralino masses and gaugino/Higgsino fractions with $\tan\beta$. However, this parameter can often be constrained from the Higgs sector alone [82], at least if it is large [83]; otherwise measurements from the sfermion or neutralino sector may still be necessary [84]. Furthermore, $\sin\beta$ and $\cos\beta$ vary significantly only for low $\tan\beta = 2 - 10$. In this range, the gaugino fraction of the lightest negative chargino decreases, e.g., from 40% to 20% in the optimal case of $M_2 = 2m_{\tilde{\chi}_1^\pm} = 160$ GeV.

In Fig. 4.2 we show the physical masses of the two charginos and the four neutralinos as a function of M_2 for $m_{\tilde{\chi}_1^\pm} = 80$ GeV (left) and 151 GeV (right). The lightest chargino mass (short-dashed line) is, of course, constant in both cases. As mentioned above, the mass of the second-lightest neutralino stays close to it, except around $M_2 = 190$ GeV (320 GeV), where an avoided crossing with $m_{\tilde{\chi}_3^0}$ occurs, which is typical of Hermitian matrices depending continuously on a single parameter. At this point, these two neutralino eigenstates change character, as can clearly be seen from the gaugino fractions plotted in Fig. 4.3. While for small values of $M_2 \ll |\mu|$ the lighter neutralinos, diagonalised by the matrix N , are gaugino-like, they become Higgsino-like for large values of $M_2 \gg |\mu|$. Furthermore, in this region the mass difference between the lightest neutralino and chargino becomes small (see Fig. 4.2). It can also be seen from this figure that the heavier chargino and the heaviest neutralino

4.1 LO cross section and spin asymmetries

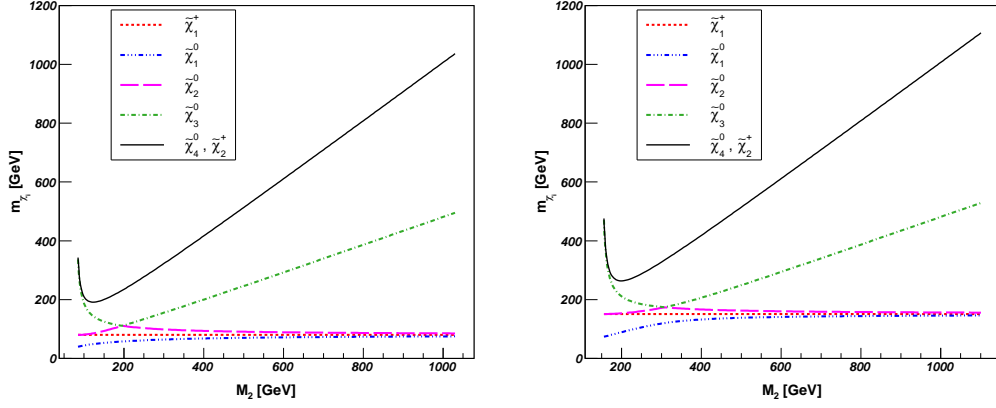


Figure 4.2: Neutralino and chargino masses as a function of the SUSY-breaking parameter M_2 for a fixed lightest chargino mass of $m_{\tilde{\chi}_1^\pm} = 80$ GeV (left) and 151 GeV (right). We choose $\tan\beta = 10$, $\mu > 0$ using Eq. (4.33), and fix $M_1 = \frac{5}{3} \tan^2 \theta_W M_2$.

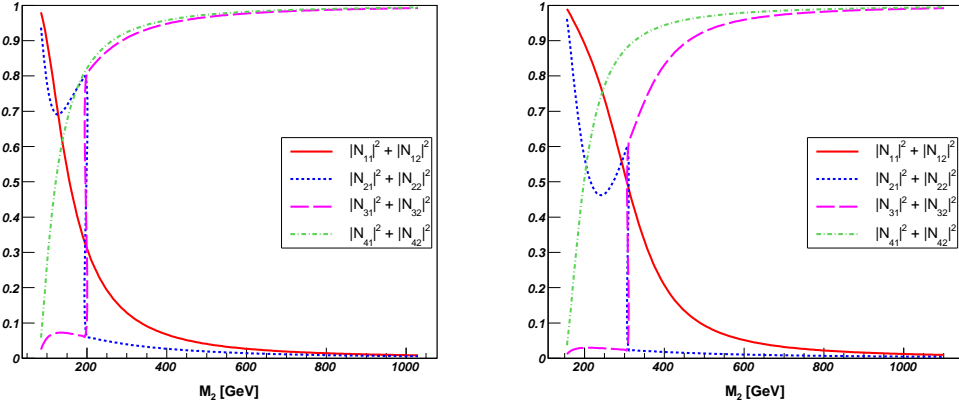


Figure 4.3: Gaugino and Higgsino fractions of the four neutralinos as a function of the SUSY-breaking parameter M_2 for a fixed lightest chargino mass of $m_{\tilde{\chi}_1^\pm} = 80$ GeV (left) and 151 GeV (right). We choose $\tan\beta = 10$, $\mu > 0$ using Eq. (4.33), and fix $M_1 = \frac{5}{3} \tan^2 \theta_W M_2$.

4 Gaugino-pair production: Fixed-order calculations

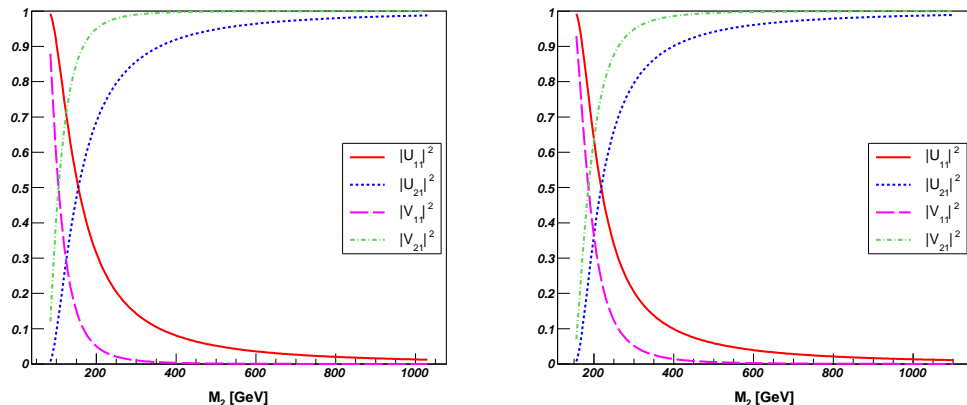


Figure 4.4: Gaugino and Higgsino fractions for charginos as a function of the SUSY-breaking parameter M_2 for a fixed lightest chargino mass of $m_{\tilde{\chi}_1^\pm} = 80$ GeV (left) and 151 GeV (right). We choose $\tan\beta = 10$, $\mu > 0$ using Eq. (4.33), and fix $M_1 = \frac{5}{3} \tan^2 \theta_W M_2$.

are mass-degenerate for all values of M_2 and that their mass grows linearly with M_2 , when $M_2 \gg |\mu|$. The gaugino fractions of the negative and positive charginos, diagonalised by the matrices U and V , are shown in Fig. 4.4. They behave similarly to those of the lightest and heaviest neutralinos. We will frequently refer to these well-known variations of the neutralino/chargino masses and gaugino/Higgsino fractions in the subsequent sections when discussing the behaviour of cross sections and asymmetries.

RHIC cross sections and asymmetries

RHIC is scheduled to operate in the years 2009 through 2012 in its polarised pp mode at an increased centre-of-mass energy of $\sqrt{s} = 500$ GeV and with a large integrated luminosity of 266 pb^{-1} during each of the ten-week physics runs [69]. It has been demonstrated that polarisation loss during RHIC beam acceleration and storage can be kept small, so that a polarisation degree of about 45% has already been and 65%–70% may ultimately be reached [85]. Recently, the STAR experiment have shown the first results on the measurement of W -boson production in polarized pp collisions [86]. It is therefore interesting to investigate the influence of proton beam polarisation on production cross sections and longitudinal spin asymmetries for SUSY particle production at the existing polarised pp collider RHIC.

In the upper left part of Fig. 4.5, we show the total unpolarised cross section for the pair production of the lightest chargino of mass 80 GeV (short-dashed line) and the one for its associated production with the second-lightest neutralino (dot-dashed line) at the pp collider RHIC, expected to produce a total integrated luminosity of about 1 fb^{-1} during the next two years [69]. Both cross sections exceed 1 fb (short-dashed horizontal line, corresponding to one produced event) in most of the M_2 range shown and depend little on the squark mass, indicating that s -channel gauge-boson exchanges dominate. From Eqs. (4.8–4.11) and (4.23–4.30) we learn indeed that, in the absence of heavy bottom- and top-quarks, squark exchanges contribute only to $Q_{LL}^{t,u}$ for chargino pairs and in addition to Q_{LR}^u and Q_{RL}^t for the associated channel. For the latter, we sum both charge conjugate processes, even though it might be interesting to identify the chargino charge, given that the dependence of its gaugino fraction on M_2 is slightly different for the two charges (see Fig. 4.4). The pair

4.1 LO cross section and spin asymmetries

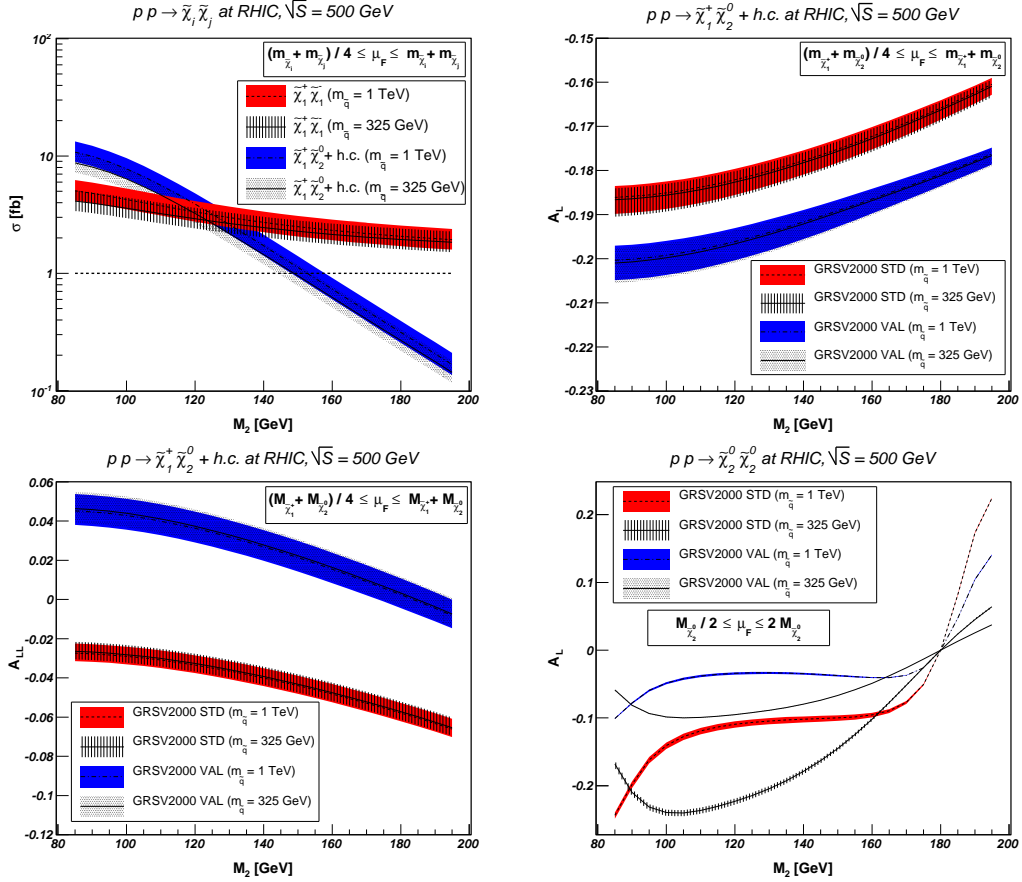


Figure 4.5: Unpolarised gaugino-pair production cross sections (top left), single- (top right) and double-spin asymmetries (bottom left) for chargino-neutralino associated production, and single-spin asymmetry for neutralino-pair production (bottom right) with $m_{\tilde{\chi}_2^0} \simeq m_{\tilde{\chi}_1^\pm} = 80$ GeV in pp collisions at RHIC and $\sqrt{S} = 500$ GeV using LO GRV [72] and GRSV [73] parton densities. We choose $\tan\beta = 10$, $\mu > 0$ using Eq. (4.33), and fix $M_1 = \frac{5}{3} \tan^2 \theta_W M_2$.

4 Gaugino-pair production: Fixed-order calculations

production of the second-lightest neutralino (not shown) does receive squark contributions from all generalised charges, but the corresponding cross section lies below 10^{-2} fb and will therefore be invisible at RHIC. As our cross sections are computed at LO, they depend to some extent on the factorisation scale μ_F . Since this scale is unphysical and unknown, we vary it in the traditional way by a factor of two around the average final state mass, representing the large perturbative scale in the partonic cross section (shaded bands).

Among the bosons exchanged in the s -channel, the W -boson is most sensitive to the polarisation of the initial quarks and antiquarks, and consequently the single-spin asymmetry for the associated channel, shown in the upper right part of Fig. 4.5, reaches large values of around -20% . Note that polarisation of the proton beam(s) will not be perfect, so that all calculated single-spin (double-spin) asymmetries should be multiplied by the degree of beam polarisation $P_{A,B} \simeq 0.7$ (squared).

As the mass of the neutralino increases and the gaugino fractions of the chargino and neutralino fall up to $M_2 \leq 200$ GeV, the cross section and the absolute value of the asymmetry decrease, too. For these values of M_2 , the conditions of the LEP chargino mass limit still apply. The uncertainty in the scale variation is with 0.5% considerably smaller than the variation in the asymmetry of 2%, while the uncertainty coming from the polarised parton densities is with 1.5% of almost comparable size. Single-spin asymmetry measurements for associated chargino-neutralino production at the only existing polarised hadron collider RHIC could therefore be used to determine the gaugino and Higgsino components of charginos and neutralinos, provided the polarised quark and antiquark densities at momentum fractions of $x_{a,b} \simeq 2 \times 80 \text{ GeV} / 500 \text{ GeV} = 0.32$ are slightly better constrained. For the double-spin asymmetry (lower left part of Fig. 4.5), the parton density uncertainty exceeds the variation and leads to a sign change of the relatively small asymmetry ($+6\%/-6\%$), so that in this case no useful information on the gaugino/Higgsino mixing can be extracted.

The single-spin asymmetry for neutralino pairs (lower right part of Fig. 4.5) reaches similar size as those for the associated channel, since the left- and right-handed couplings of the Z -boson exchanged in the s -channel are also different. Although the corresponding cross section is unfortunately too small at RHIC, the variation of the asymmetry would, however, be quite dramatic: A_L changes its sign from -20% to $+20\%$ for $M_2 \leq 200$ GeV.

For chargino pairs, massless photons can be exchanged in the s -channel which leads to single- and double-spin asymmetries that vary very little with M_2 (as can be seen in Fig. 4.6) and that can therefore not be used to extract information on gaugino/Higgsino mixing. In addition, these asymmetries depend strongly on the polarised parton densities.

Tevatron cross sections and asymmetries

The $p\bar{p}$ collider Tevatron will continue running in 2011 and possibly until 2014, and the future accelerator program at Fermilab is currently less clear than ever. The feasibility of polarising the proton beam has been demonstrated many years ago [70]. It would require replacing some of the dipoles with higher-field magnets to gain space to install the six required Siberian snakes at a very moderate cost [87] and would represent an interesting possibility for QCD studies as well as new physics searches. Given the recent impressive achievements at RHIC, the degree of polarisation should be comparable, i.e. about 65%–70%. Polarisation of the antiproton beam is, however, much more challenging.

In the upper left part of Fig. 4.7, we show the total unpolarised cross sections for gaugino production with $m_{\tilde{\chi}_1^\pm} = 151$ GeV at the Tevatron, which is currently running at $\sqrt{S} = 1.96$

4.1 LO cross section and spin asymmetries

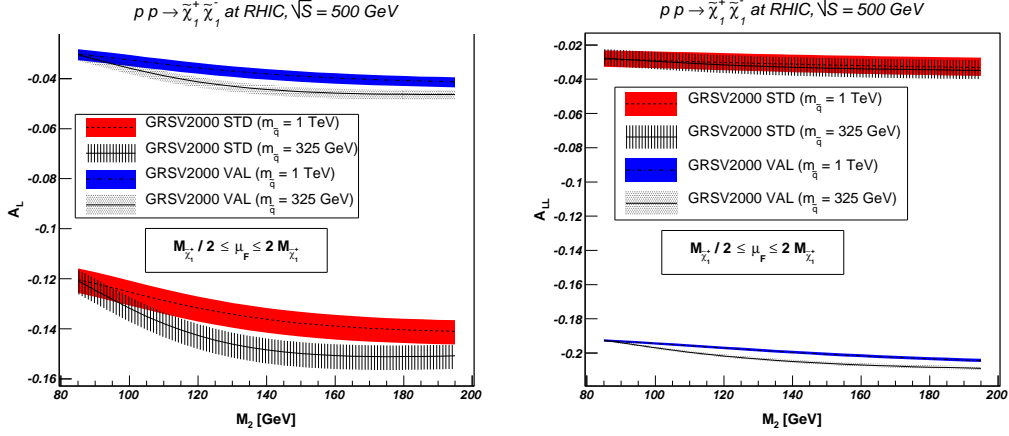


Figure 4.6: Single- (left) and double-spin asymmetries (right) for chargino-pair production with $m_{\tilde{\chi}_1^\pm} = 80$ GeV in pp collisions at RHIC and $\sqrt{S} = 500$ GeV using LO GRV [72] and GRSV [73] parton densities. We choose $\tan\beta = 10$, $\mu > 0$ using Eq. (4.33), and fix $M_1 = \frac{5}{3} \tan^2 \theta_W M_2$.

TeV and expected to produce a total integrated luminosity of 10 fb^{-1} recorded per experiment up to 2011. Therefore, besides the pair production of the lightest chargino (short-dashed line) and its associated production with the second-lightest neutralino (dot-dashed line), also pair production of the latter might be visible (long-dashed line), at least for low values of $M_2 \leq 300$ GeV, where the gaugino component is still large (see Figs. 4.3 and 4.4) and the cross section exceeds 1 fb (short-dashed horizontal line). The influence of squark exchanges and the dependence on the squark mass are clearly visible in this channel, whereas they are again much smaller (but slightly larger than at RHIC) for the other two channels. The factorisation scale dependence (shaded bands) remains modest (10%–13%) at the Tevatron.

The single-spin asymmetry for chargino-pair production (upper right part of Fig. 4.7) at a possible proton beam polarisation upgrade of the Tevatron [70] could be very large and reach -40% . Since the physical mass has been fixed at 151 GeV and the unpolarised cross section stays almost constant, the reduction in absolute value by about 6% for any given curve is directly related to the reduction of the gaugino fraction, as M_2 increases. The parton density (and factorisation scale) uncertainties are (much) smaller than this variation, i.e. 2% (or 1%), so that significant information could be extracted from this asymmetry. On the other hand, the double-spin asymmetry (not shown), although large with about -20% , is almost insensitive to the gaugino fraction and would furthermore require polarisation of the antiproton beam, which is a technical challenge.

In contrast to our results for RHIC, the associated channel (lower part of Fig. 4.7) is not very interesting at the Tevatron. While the single- and double-spin asymmetries may be large (about -10% and $+15\%$, respectively), they are almost constant and would not yield new information on the gaugino fractions.

The single- and double-spin asymmetries (see Fig. 4.8) for the pair production of the second lightest neutralino are most sensitive to its gaugino component and (relatively modest) mass variation, in particular for the low values of $M_2 \leq 300$ GeV, where the cross section should be visible. Here, A_L changes sign from -50% to almost $+30\%$ and the theoretical

4 Gaugino-pair production: Fixed-order calculations

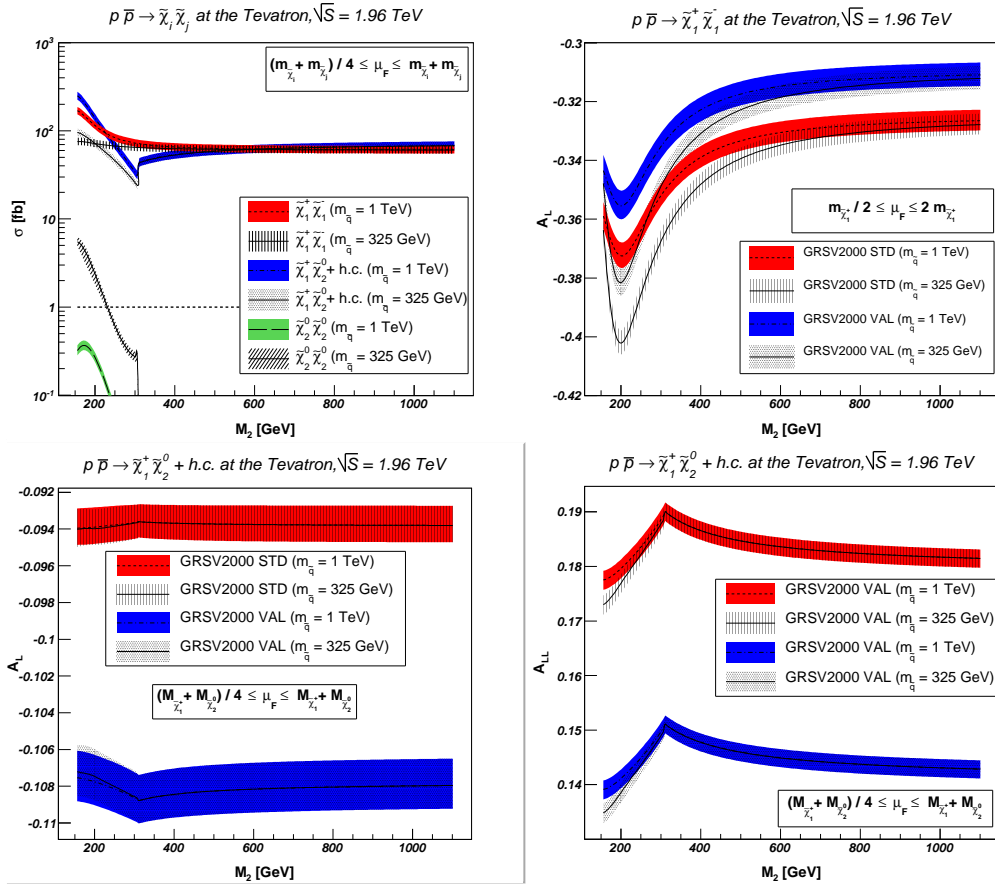


Figure 4.7: Unpolarised gaugino-pair production cross sections (top left), single-spin asymmetries for chargino-pair (top right) and chargino-neutralino production (bottom left), and double-spin asymmetries for chargino-neutralino production (bottom right) with $m_{\tilde{\chi}_2^0} \simeq m_{\tilde{\chi}_1^\pm} = 151$ GeV in $p\bar{p}$ collisions at the Tevatron and $\sqrt{S} = 1.96$ TeV using LO GRV [72] and GRSV [73] parton densities. We choose $\tan\beta = 10$, $\mu > 0$ using Eq. (4.33), and fix $M_1 = \frac{5}{3} \tan^2 \theta_W M_2$.

4.1 LO cross section and spin asymmetries

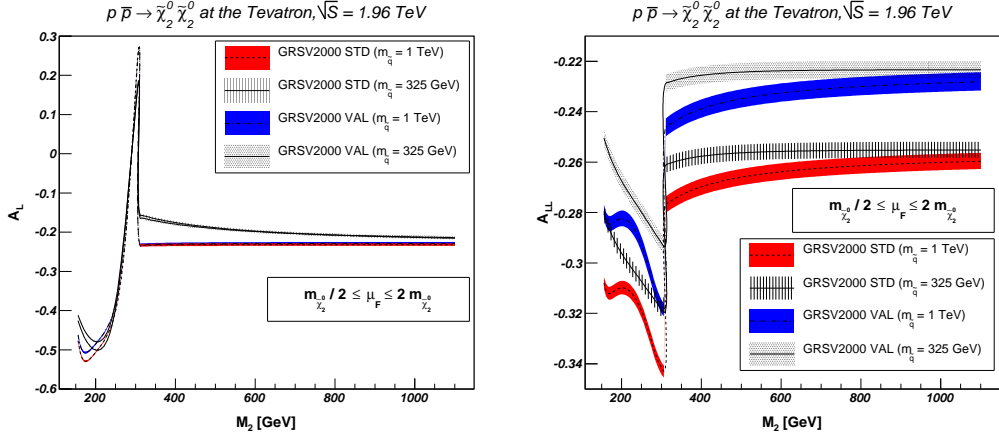


Figure 4.8: Single- (left) and double-spin asymmetries for neutralino-pair production (right) with $m_{\tilde{\chi}_2^0} \simeq m_{\tilde{\chi}_1^\pm} = 151$ GeV in $p\bar{p}$ collisions at the Tevatron and $\sqrt{S} = 1.96$ TeV using LO GRV [72] and GRSV [73] parton densities. We choose $\tan\beta = 10$, $\mu > 0$ using Eq. (4.33), and fix $M_1 = \frac{5}{3} \tan^2 \theta_W M_2$.

uncertainties are extremely small. In the same region, the absolute value of A_{LL} increases by about 5% and can almost reach -35% for the standard GRSV parameterization of the polarised parton densities. The parton density uncertainty remains modest with about 3%. For large $M_2 \geq 300$ GeV, both asymmetries are constant in this channel.

LHC cross sections and asymmetries

As the LHC is now running, different upgrade scenarios are emerging, concerning foremost higher luminosity and beam energy [88], but also beam polarisation [71]. It is interesting to remember that a detailed study has been performed some time ago for the SSC, resulting in a design that had reserved 52 lattice locations for the future installation of Siberian snakes [87]. Since this is currently not the case at the LHC, its polarisation upgrade would require replacing some of the dipoles with higher-field magnets to create these locations, just as in the case of the Tevatron. The number of resonances to be crossed during acceleration would be considerably larger due to the higher energy of the LHC, requiring longer tuning before ultimately reaching polarisations of up to 65%–70%.

For pp collisions of 14 TeV centre-of-mass energy at the LHC, we show the unpolarised total cross sections for a chargino of mass 151 GeV in the upper left part of Fig. 4.9. With the high luminosity originally expected at the LHC, pair production of the lightest chargino (short-dashed line), its associated production with the second-lightest neutralino (dot-dashed line), and pair production of the latter (long-dashed line) should all be well visible. Whereas the cross sections for the first two channels are again almost constant and fairly independent of the squark mass, at least for the Higgsino-like region of $M_2 \geq 300$ GeV, the neutralino-pair production cross section is again quite sensitive to squark exchanges in the gaugino-like region below that value and stays almost constant above. The factorisation scale dependence is very small at the LHC and included in the line width of the upper left part of Fig. 4.9. Note, however, that with 100 fb^{-1} of data, the mass of the lightest chargino will only be measured with an uncertainty of $\pm 11\%$ [89]. This induces a very visible uncertainty (shaded bands) in the total cross sections (lower left part of Fig. 4.9).

4 Gaugino-pair production: Fixed-order calculations

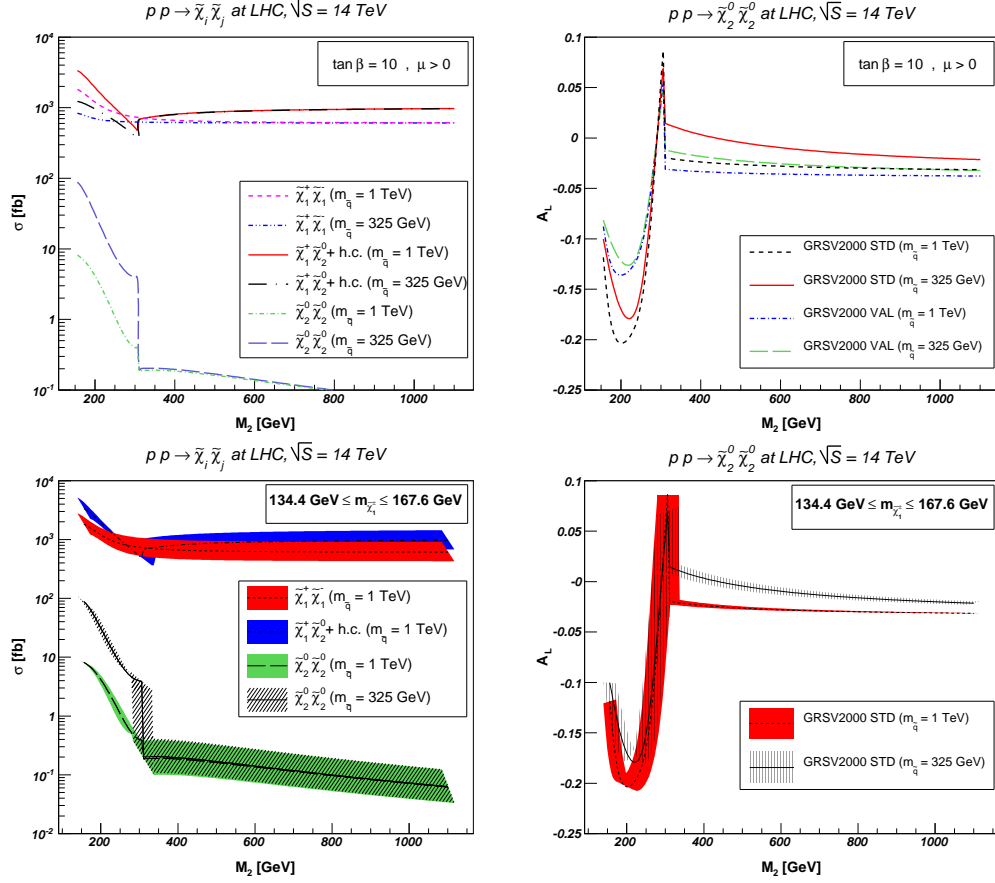


Figure 4.9: Unpolarised gaugino-pair production cross sections (left) and single-spin asymmetries for neutralino-pair production (right) with $m_{\tilde{\chi}_2^0} \simeq m_{\tilde{\chi}_1^\pm} = 151 \text{ GeV}$ in pp collisions at the LHC and $\sqrt{S} = 14 \text{ TeV}$ using LO GRV [72] and GRSV [73] parton densities. The shaded bands (bottom) show the uncertainty induced by the error on the chargino mass as determined with 100 fb^{-1} of data [89]. We choose $\tan\beta = 10$, $\mu > 0$ using Eq. (4.33), and fix $M_1 = \frac{5}{3} \tan^2 \theta_W M_2$.

4.1 LO cross section and spin asymmetries

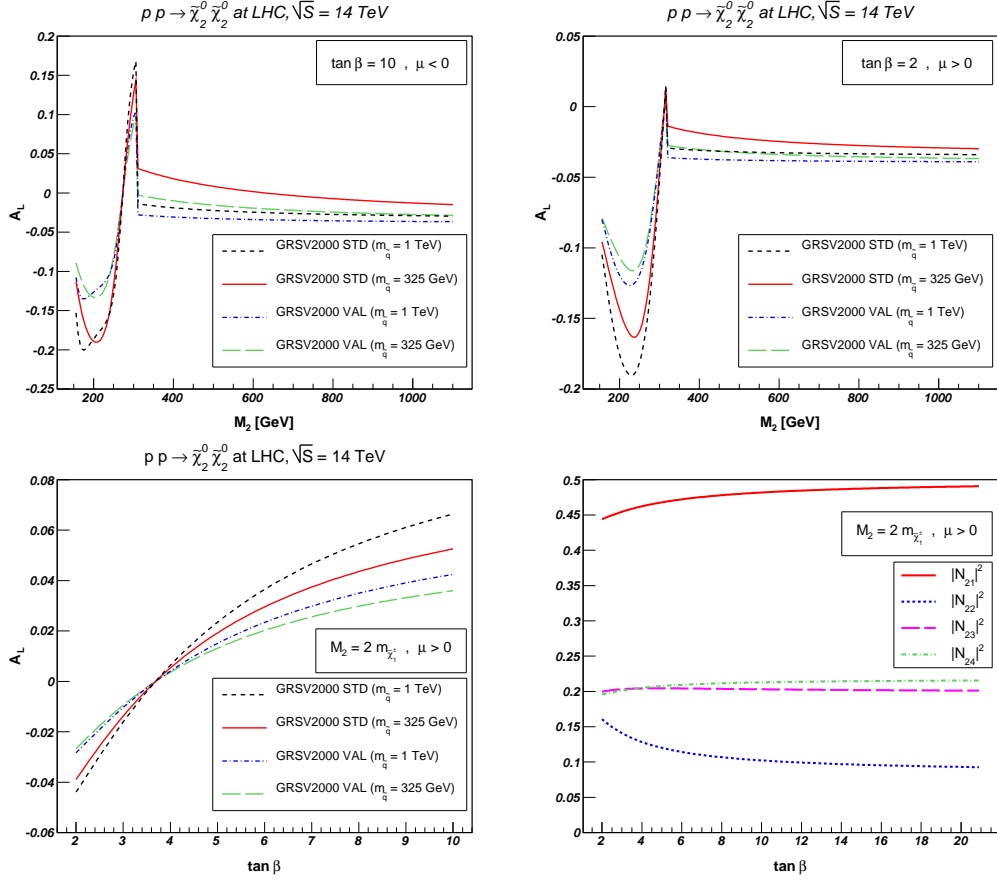


Figure 4.10: Single-spin asymmetries for neutralino-pair production with $\tan\beta = 10$ and $\mu < 0$ (top left), $\tan\beta = 2$ and $\mu > 0$ (top right), and $M_2 = 2m_{\tilde{\chi}_1^\pm}$ with $\mu > 0$ as a function of $\tan\beta$ (bottom left) in pp collisions at the LHC and $\sqrt{s} = 14$ TeV. For the third scenario, we show also the gaugino and Higgsino fractions of the second-lightest neutralino (bottom right). We fix μ using Eq. (4.33) and $M_1 = \frac{5}{3} \tan^2 \theta_W M_2$.

For a possible polarisation upgrade of the LHC [71], we show the single-spin asymmetry for neutralino-pair production in the right parts of Fig. 4.9, again with the scale (line width, top) and chargino mass (shaded bands, bottom) uncertainty. At $M_2 \geq 300$ GeV, where the gaugino fraction is small, the asymmetry is not very interesting, as it is almost constant and smaller than 5%. In the gaugino-like region at $M_2 \leq 300$ GeV, it changes sign from -20% to almost $+10\%$, a variation, that is considerably larger than the parton density uncertainty of at most 7%, the squark mass dependence of at most 2%, the almost invisible scale dependence, and also the chargino mass uncertainty of 3% to 10%. At a polarised LHC, a measurement of the single-spin asymmetry for neutralino-pair production would therefore yield interesting information about its gaugino fraction.

While the cross sections vary very little when changing the sign of μ or varying $\tan\beta$, it is interesting to study further the single-spin asymmetries for neutralino pairs in these alternative scenarios. When comparing the asymmetry for $\mu < 0$, shown in the upper left part of Fig. 4.10, to the one for $\mu > 0$, shown in the upper right part of Fig. 4.9, one notices an even steeper rise in the former to more than $+15\%$, as M_2 approaches the critical value

4 Gaugino-pair production: Fixed-order calculations

of $2m_{\tilde{\chi}_1^\pm}$, the neutralino changes its character from gaugino to Higgsino, and the sign and (smaller) absolute value of the Higgsino mass parameter μ become of particular importance.

A similar effect is observed when comparing for $\mu > 0$ the asymmetry with a lower value of $\tan\beta = 2$ in the upper right part of Fig. 4.10 to the one for the standard value of $\tan\beta = 10$ in the upper right part of Fig. 4.9. In this case, the asymmetry rises less (barely above zero) towards $M_2 = 2m_{\tilde{\chi}_1^\pm}$, where the gaugino/Higgsino decomposition is flipped, the ratio of the two Higgs vacuum expectation values $\tan\beta$ is particularly important, and the absolute value of the Higgsino mass parameter μ is effectively larger than in the standard scenario.

The dependence on $\tan\beta$ at the critical point $M_2 = 2m_{\tilde{\chi}_1^\pm}$ can be seen more clearly in the lower left part of Fig. 4.10, and indeed the asymmetry decreases from large to small $\tan\beta$ from distinctively positive values to values at or below zero for all choices of squark masses (1 TeV or 325 GeV) and parton density functions (standard or valence GRSV parameterizations). This decrease is correlated with a similar decrease in the Bino fraction $|N_{21}|^2$ and with an increase in the Wino fraction $|N_{22}|^2$ of the second-lightest neutralino, while the Higgsino fractions $|N_{23}|^2$ and $|N_{24}|^2$ stay almost constant, as can be seen in the lower right part of Fig. 4.10.

The double-spin asymmetry for neutralino pairs, as well as the one for chargino pairs and the associated channel, are always smaller than 4% and 2%, respectively. Furthermore, they vary by less than 2% and are therefore not shown here. The single-spin asymmetry for chargino pairs (not shown) can reach a slightly larger value of -12% , but again it varies by less than 3% as a function of M_2 , which is almost of the same size as the parton density uncertainty (2%). The situation for the single-spin asymmetry of the associated channel (not shown, either) is similar with a maximum of -10% , a variation with M_2 of about 1% and a parton density uncertainty of less than 1%.

4.2 SUSY-QCD corrections

SUSY-QCD corrections for gaugino-pair production have been first calculated in Ref. [68]. Here, we generalise these results by including the squark mixing effects and present in detail the renormalisation scheme and the subtraction method we have chosen.

4.2.1 Virtual corrections

At NLO of SUSY-QCD, $\mathcal{O}(\alpha_s)$, the cross section for gaugino pair production receives contributions from the interference of the virtual one-loop diagrams shown in Figs. 4.11–4.13 with the tree-level diagrams shown in Fig. 4.1 on the one hand and from real gluon (Fig. 4.14) and (anti-)quark emission diagrams on the other hand, where the latter are obtained by crossing the final-state gluon in Fig. 4.14 with the initial-state antiquark (Fig. 4.15) or quark (not shown). All diagrams have been evaluated analytically with self-written FORM programs and cross-checked independently with self-written MATHEMATICA programs.

The virtual self-energy diagrams for left- and right-handed quarks $q_{L,R} = P_{L,R}q = \frac{1}{2}(1 \mp$

4.2 SUSY-QCD corrections

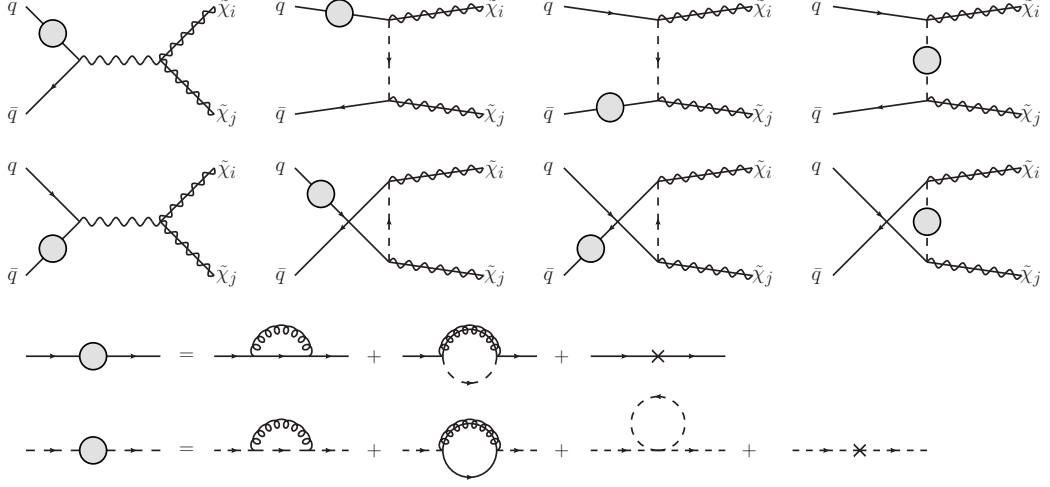


Figure 4.11: Self-energy insertions (top) and contributions (bottom) to the production of gaugino pairs.

$\gamma_5)q$ (Fig. 4.11, third line),

$$\Sigma_{L,R}^{(g)}(p) = -\frac{g_s^2 C_F}{16\pi^2} [(D-2)\not{p}B_1(p, m_q, 0) + Dm_q B_0(p, m_q, 0)] P_{L,R}, \quad (4.35)$$

$$\Sigma_L^{(\bar{g})}(p) = -\frac{g_s^2 C_F}{8\pi^2} \sum_{i=1}^2 \left[\not{p}B_1(p, m_{\bar{g}}, m_{\bar{q}_i}) R_{i1}^{\bar{q}^*} R_{i1}^{\bar{q}} + m_{\bar{g}} B_0(p, m_{\bar{g}}, m_{\bar{q}_i}) R_{i2}^{\bar{q}^*} R_{i1}^{\bar{q}} \right] P_L, \quad (4.36)$$

$$\Sigma_R^{(\bar{g})}(p) = -\frac{g_s^2 C_F}{8\pi^2} \sum_{i=1}^2 \left[\not{p}B_1(p, m_{\bar{g}}, m_{\bar{q}_i}) R_{i2}^{\bar{q}^*} R_{i2}^{\bar{q}} + m_{\bar{g}} B_0(p, m_{\bar{g}}, m_{\bar{q}_i}) R_{i1}^{\bar{q}^*} R_{i2}^{\bar{q}} \right] P_R, \quad (4.37)$$

expanded as usual into vector (V) and scalar (S) parts $\Sigma(p) = [\Sigma_L^V(p^2)\not{p} + \Sigma_L^S(p^2)]P_L + (L \leftrightarrow R)$, as well as those for squarks (Fig. 4.11, fourth line),

$$\begin{aligned} \Sigma_{ij}^{(g)}(p^2) = & -\frac{g_s^2 C_F}{16\pi^2} \left[p^2 (B_0(p, m_{\bar{q}_i}, 0) - 2B_1(p, m_{\bar{q}_i}, 0) + B_{21}(p, m_{\bar{q}_i}, 0)) \right. \\ & \left. + DB_{22}(p, m_{\bar{q}_i}, 0) \right] \delta_{ij}, \end{aligned} \quad (4.38)$$

$$\begin{aligned} \Sigma_{ij}^{(\bar{g})}(p^2) = & -\frac{g_s^2 C_F}{4\pi^2} \left\{ \left[p^2 (B_1(p, m_q, m_{\bar{g}}) + B_{21}(p, m_q, m_{\bar{g}})) + DB_{22}(p, m_q, m_{\bar{g}}) \right] \delta_{ij} \right. \\ & \left. - m_q m_{\bar{g}} B_0(p, m_q, m_{\bar{g}}) (R_{i1}^{\bar{q}} R_{j2}^{\bar{q}^*} + R_{i2}^{\bar{q}} R_{j1}^{\bar{q}^*}) \right\} \quad \text{and} \end{aligned} \quad (4.39)$$

$$\Sigma_{ij}^{(\tilde{q})}(p^2) = \frac{g_s^2 C_F}{16\pi^2} \sum_{k=1}^2 S_{ki}^{\tilde{q}} S_{kj}^{\tilde{q}^*} A_0(m_{\tilde{q}_k}) \quad \text{with} \quad S_{ki} = R_{k1}^{\tilde{q}^*} R_{i1}^{\tilde{q}} - R_{k2}^{\tilde{q}^*} R_{i2}^{\tilde{q}}, \quad (4.40)$$

contain ultraviolet (UV) divergences in the scalar integrals $B_{0,1,\dots}(p, m_1, m_2)$ [90], which exhibit themselves as $1/\epsilon$ poles in $D = 4 - 2\epsilon$ dimensions.² They must therefore be absorbed through a suitable renormalisation procedure into the fundamental wave functions,

²As it is customary, we absorb a factor of $(2\pi\mu_R)^{4-D}$ in the definition of the scalar integrals, where μ_R is the renormalisation scale.

4 Gaugino-pair production: Fixed-order calculations

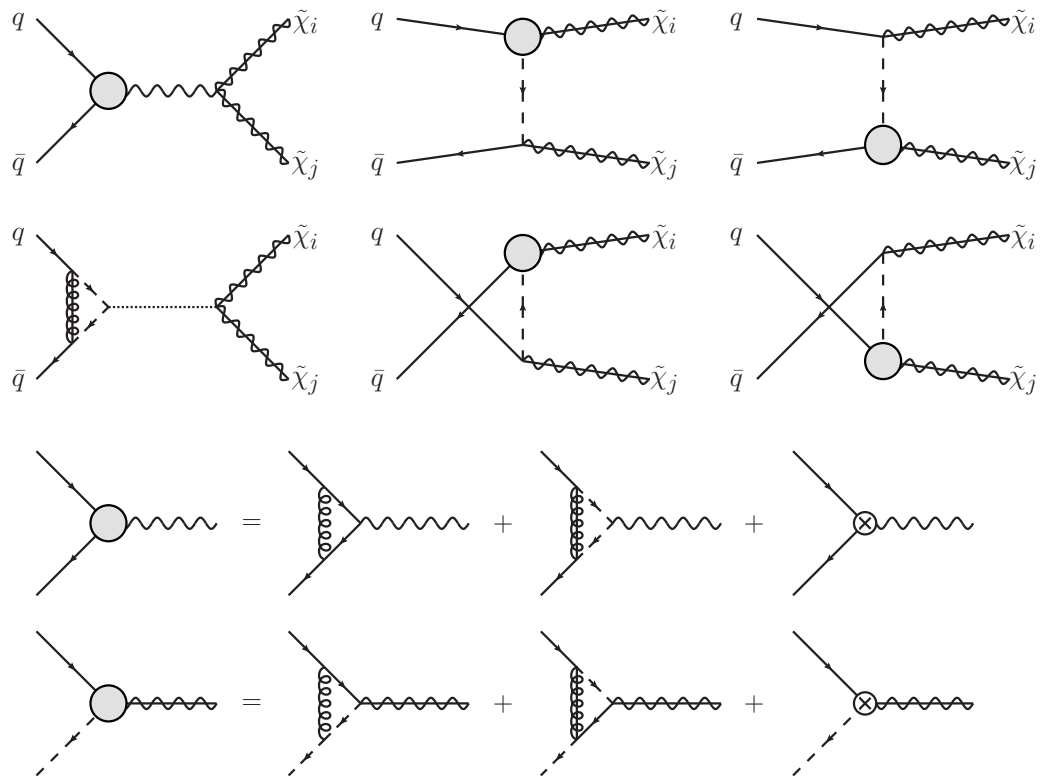


Figure 4.12: Vertex correction insertions (top) and contributions (bottom) to the production of gaugino pairs.

4.2 SUSY-QCD corrections

mass parameters, and coupling constants of the SUSY-QCD Lagrangian

$$\mathcal{L} = \left[\bar{q}_L^0 i \not{\partial} q_L^0 - \bar{q}_R^0 m_q^0 q_L^0 + (L \leftrightarrow R) \right] + \left[\sum_{i=1}^2 (\partial_\mu \tilde{q}_i^0)^\dagger (\partial^\mu \tilde{q}_i^0) - \tilde{q}_i^{0\dagger} (m_{\tilde{q}}^2)_{ii}^0 \tilde{q}_i^0 \right] + \dots \quad (4.41)$$

The two components of the unrenormalised squark field \tilde{q}^0 correspond originally to the left- and right-handed chiralities of the unrenormalised SM quark field q^0 , but mix due to the fact that soft SUSY-breaking and Higgs terms render the 2×2 -dimensional mass matrix $(m_{\tilde{q}}^2)^0$ non-diagonal (see Sec. 2.3.2). In Eq. (4.41) we have diagonalized this mass matrix with the squark rotation matrix $R^{\tilde{q}^0}$, so that the components $i = 1(2)$ of the squark field correspond to the squark mass eigenvalues $m_{\tilde{q}_i}^0$. The squark self-energies in Eqs. (4.38)–(4.40) thus also carry indices $i, j = 1, 2$ corresponding to the (outgoing and incoming) squark mass eigenstates. Multiplicative renormalisation is achieved perturbatively by expanding the renormalisation constants,

$$q_{L,R}^0 = \left(1 + \frac{1}{2} \delta Z_q \right) q_{L,R}, \quad m_q^0 = m_q + \delta m_q, \quad (4.42)$$

$$\tilde{q}_i^0 = \left(\delta_{ij} + \frac{1}{2} \delta Z_{\tilde{q},ij} \right) \tilde{q}_j, \quad (m_{\tilde{q}}^2)_{ij}^0 = (m_{\tilde{q}}^2)_{ij} + (\delta m_{\tilde{q}}^2)_{ij}, \quad (4.43)$$

with the usual factor of $1/2$ for the (s)quark wave functions. The renormalised self-energies are then

$$\begin{aligned} \hat{\Sigma}(p) = & \left[\Sigma_L^V(p^2) + \frac{1}{2} (\delta Z_q + \delta Z_q^\dagger) \right] \not{p} P_L \\ & + \left[\Sigma_L^S(p^2) - \frac{1}{2} (m_q \delta Z_q + \delta Z_q^\dagger m_q) - \delta m_q \right] P_L + (L \leftrightarrow R) \end{aligned} \quad (4.44)$$

for quarks and

$$\begin{aligned} \hat{\Sigma}_{ij}(p^2) = & \Sigma_{ij}(p^2) + \frac{1}{2} (\delta Z_{\tilde{q},ij} + \delta Z_{\tilde{q},ji}^*) p^2 \\ & - \frac{1}{2} \sum_{k=1}^2 [(m_{\tilde{q}}^2)_{ik} \delta Z_{\tilde{q},kj} + \delta Z_{\tilde{q},ki}^* (m_{\tilde{q}}^2)_{kj}] - (\delta m_{\tilde{q}}^2)_{ij} \end{aligned} \quad (4.45)$$

for squarks.

We choose to renormalise the wave functions in the $\overline{\text{MS}}$ -scheme, so that the definition of the quark fields corresponds to the one employed in the parton densities in the external hadrons. In this scheme, the quark wave function counterterm

$$\delta Z_q = \delta Z_q^{(g)} + \delta Z_q^{(\tilde{g})} \quad (4.46)$$

with

$$\delta Z_q^{(g)} = \delta Z_q^{(\tilde{g})} = -\frac{g_s^2 C_F}{16\pi^2} \Delta \quad \text{and} \quad \Delta = \frac{1}{\epsilon} - \gamma_E + \ln 4\pi, \quad (4.47)$$

defined as the UV-divergent plus universal finite parts of the on-shell counterterm $-\Sigma_{L,R}^V(m_q^2) - m_q^2 [\Sigma_{L,R}^{V'}(m_q^2) + \Sigma_{R,L}^{V'}(m_q^2)] - m_q [\Sigma_{L,R}^{S'}(m_q^2) + \Sigma_{R,L}^{S'}(m_q^2)]$ [91], is hermitian ($\delta Z_q = \delta Z_q^\dagger$) and the same for left- and right-handed quarks. The superscripts g and \tilde{g} label the gluon and gluino exchange contributions, respectively, and γ_E is the Euler constant. The squark wave function counterterms

$$\delta Z_{\tilde{q},ij} = \delta Z_{\tilde{q},ij}^{(g)} + \delta Z_{\tilde{q},ij}^{(\tilde{g})} + \delta Z_{\tilde{q},ij}^{(\tilde{q})}, \quad (4.48)$$

4 Gaugino-pair production: Fixed-order calculations

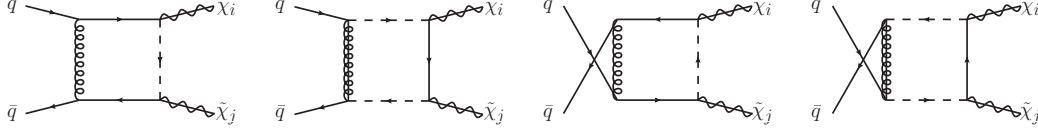


Figure 4.13: Box diagrams contributing to the production of gaugino pairs at NLO.

with

$$\delta Z_{\tilde{q},ii}^{(g)} = -\delta Z_{\tilde{q},ii}^{(\tilde{g})} = \frac{g_s^2 C_F}{8\pi^2} \Delta \quad \text{and} \quad \delta Z_{\tilde{q},ii}^{(\tilde{q})} = 0 \quad (4.49)$$

for $i = j$ and

$$\delta Z_{\tilde{q},ij}^{(g)} = 0, \quad (4.50)$$

$$\delta Z_{\tilde{q},ij}^{(\tilde{g})} = \frac{g_s^2 C_F}{4\pi^2} \frac{2\Delta}{m_{\tilde{q}_i}^2 - m_{\tilde{q}_j}^2} \left[m_q m_{\tilde{g}} (R_{i1}^{\tilde{q}} R_{j2}^{\tilde{q}*} + R_{i2}^{\tilde{q}} R_{j1}^{\tilde{q}*}) \right] \quad \text{and} \quad (4.51)$$

$$\delta Z_{\tilde{q},ij}^{(\tilde{q})} = \frac{g_s^2 C_F}{16\pi^2} \frac{2\Delta}{m_{\tilde{q}_i}^2 - m_{\tilde{q}_j}^2} \sum_{k=1}^2 m_{\tilde{q}_k}^2 S_{ki} S_{kj}^* \quad (4.52)$$

for $i \neq j$, defined similarly as the UV-divergent plus universal finite parts of the on-shell counterterms $-\text{Re}\Sigma'_{ii}(m_{\tilde{q}_i}^2)$ for $i = j$ and $2\text{Re}\Sigma_{ij}(m_{\tilde{q}_i}^2)/(m_{\tilde{q}_i}^2 - m_{\tilde{q}_j}^2)$ for $i \neq j$ [91], enter only through the renormalisation of the squark mixing matrix,

$$R^{\tilde{q}0} = R^{\tilde{q}} + \delta R^{\tilde{q}} \quad \text{with} \quad \delta R_{ij}^{\tilde{q}} = \frac{1}{4} \sum_{k=1}^2 (\delta Z_{\tilde{q},ik} - \delta Z_{\tilde{q},ki}^*) R_{kj}^{\tilde{q}} = \frac{1}{2} \sum_{k=1}^2 \delta Z_{\tilde{q},ik} R_{kj}^{\tilde{q}}, \quad (4.53)$$

since in the $\overline{\text{MS}}$ -scheme the gluon and gluino contributions for $i = j$ in Eq. (4.49) cancel each other. In the last step of Eq. (4.53), we have made use of the fact that in the $\overline{\text{MS}}$ -scheme the squark wave-function renormalisation constants are anti-hermitian matrices ($\delta Z_{\tilde{q},ij} = -\delta Z_{\tilde{q},ji}^*$). The (s)quark masses are renormalised in the on-shell scheme to make them correspond to the physical masses. The quark mass counterterm is then defined by $m_q \Sigma^V(m_q^2) + \Sigma^S(m_q^2)$ [91] with the result

$$\delta m_q = \delta m_q^{(g)} + \delta m_q^{(\tilde{g})} \quad (4.54)$$

and

$$\delta m_q^{(g)} = -\frac{g_s^2 C_F}{16\pi^2} m_q \left[(D-2)B_1(m_q, m_q, 0) + DB_0(m_q, m_q, 0) \right], \quad (4.55)$$

$$\delta m_q^{(\tilde{g})} = -\frac{g_s^2 C_F}{16\pi^2} \sum_{i=1}^2 \left[m_q B_1(m_q, m_{\tilde{g}}, m_{\tilde{q}_i}) + 2m_{\tilde{g}} B_0(m_q, m_{\tilde{g}}, m_{\tilde{q}_i}) \text{Re}(R_{i2}^{\tilde{q}*} R_{i1}^{\tilde{q}}) \right]. \quad (4.56)$$

For our numerical results, we will set the masses of external quarks to zero in accordance with the collinear factorisation of quarks in hadrons. The squark mass counterterm is defined by $\text{Re}[\Sigma_{ii}(m_{\tilde{q}_i}^2)]$. The result is

$$\delta m_{\tilde{q}_i}^2 = \delta m_{\tilde{q}_i}^{2(g)} + \delta m_{\tilde{q}_i}^{2(\tilde{g})} + \delta m_{\tilde{q}_i}^{2(\tilde{q})} \quad (4.57)$$

4.2 SUSY-QCD corrections

with

$$\delta m_{\tilde{q}_i}^{2(g)} = \frac{g_s^2 C_F}{8\pi^2} m_{\tilde{q}_i}^2 \left[B_1(m_{\tilde{q}_i}, m_{\tilde{q}_i}, 0) - B_0(m_{\tilde{q}_i}, m_{\tilde{q}_i}, 0) \right], \quad (4.58)$$

$$\delta m_{\tilde{q}_i}^{2(\hat{g})} = -\frac{g_s^2 C_F}{4\pi^2} \left[m_{\tilde{q}_i}^2 B_1(m_{\tilde{q}_i}, m_q, m_{\tilde{g}}) + m_q^2 B_0(m_{\tilde{q}_i}, m_q, m_{\tilde{g}}) + A_0(m_{\tilde{g}}) \right. \\ \left. - 2m_q m_{\tilde{g}} B_0(m_{\tilde{q}_i}, m_q, m_{\tilde{g}}) \text{Re}(R_{i1}^{\tilde{q}} R_{i2}^{\tilde{q}*}) \right] \quad \text{and} \quad (4.59)$$

$$\delta m_{\tilde{q}_i}^{2(\tilde{q})} = \frac{g_s^2 C_F}{16\pi^2} \sum_{j=1}^2 |S_{ji}|^2 A_0(m_{\tilde{q}_j}). \quad (4.60)$$

Supersymmetric Ward identities link the quark-quark-gauge boson and quark-squark-gaugino vertices to the weak gauge-boson and gaugino self-energies. As the latter do not receive strong corrections at NLO, the former require no further renormalisation beyond the one for the (s)quark wave functions discussed above. However, the artificial breaking of supersymmetry by the mismatch of two gaugino and $(D-2)$ transverse vector degrees of freedom must be compensated by a finite counterterm $\hat{g} = g[1 - \alpha_s C_F / (8\pi)]$, effectively shifting the quark-squark-gaugino scalar coupling constant \hat{g} with respect to the weak gauge coupling constant g [92, 93].

4.2.2 Real corrections

Apart from the (now UV-finite) virtual corrections $d\sigma_{ab}^{(V)}$ to the LO cross section $d\sigma_{ab}^{(0)}$ described above, the NLO cross section

$$d\sigma_{ab}^{(1)}(p_a, p_b) = \int_{2+1} \left[\left(d\sigma_{ab}^{(R)}(p_a, p_b) \right)_{\varepsilon=0} - \left(\sum_{\text{dipoles}} d\sigma_{ab}^{(0)}(p_a, p_b) \otimes dV_{\text{dipole}} \right)_{\varepsilon=0} \right] \\ + \int_2 \left[d\sigma_{ab}^{(V)}(p_a, p_b) + d\sigma_{ab}^{(0)}(p_a, p_b) \otimes \mathbf{I} \right]_{\varepsilon=0} \\ + \sum_{a'} \int_0^1 dx \int_2 \left[d\sigma_{a'b}^{(0)}(xp_a, p_b) \otimes (\mathbf{P} + \mathbf{K})^{a',a}(x) + d\sigma_{aa'}^{(0)}(p_a, xp_b) \otimes (\mathbf{P} + \mathbf{K})^{a',b}(x) \right]_{\varepsilon=0} \quad (4.61)$$

also receives contributions $d\sigma_{ab}^{(R)}$ from real gluon (Fig. 4.14), quark (Fig. 4.15) and antiquark (not shown) emission diagrams, where the emitted parton carries four-momentum p_3 . In the Catani-Seymour dipole formalism [94], the real contributions are rendered infrared (IR) finite by subtracting from them their soft and collinear limits ($p_{a,b} \cdot p_3 \rightarrow 0$)

$$d\sigma_{ab}^{(0)}(p_a, p_b) \otimes dV_{\text{dipole}} = \sum_i \left[\mathcal{D}^{a3,b}(p_1, p_2, p_3; p_a, p_b) F_J^{(2)}(\tilde{p}_1, \tilde{p}_2; \tilde{p}_{a3}, p_b) + (a \leftrightarrow b) \right] \quad (4.62)$$

before integration over the three-particle final-state phase space. They can then be evaluated in four dimensions (i.e. with $\varepsilon = 0$). In the case at hand of two initial-state partons and no coloured final state particles at LO, the only dipole contribution comes from an initial state emitter and an initial state spectator, e.g.

$$\mathcal{D}^{a3,b}(p_1, p_2, p_3; p_a, p_b) = -\frac{1}{2p_a \cdot p_3} \frac{1}{x_{3,ab}} {}_{2,ab} \langle \tilde{1}, \tilde{2}; \tilde{a3}, b | \frac{\mathbf{T}_b \cdot \mathbf{T}_{a3}}{\mathbf{T}_{a3}^2} \mathbf{V}^{a3,b} | \tilde{1}, \tilde{2}; \tilde{a3}, b \rangle_{2,ab} \quad (4.63)$$

4 Gaugino-pair production: Fixed-order calculations

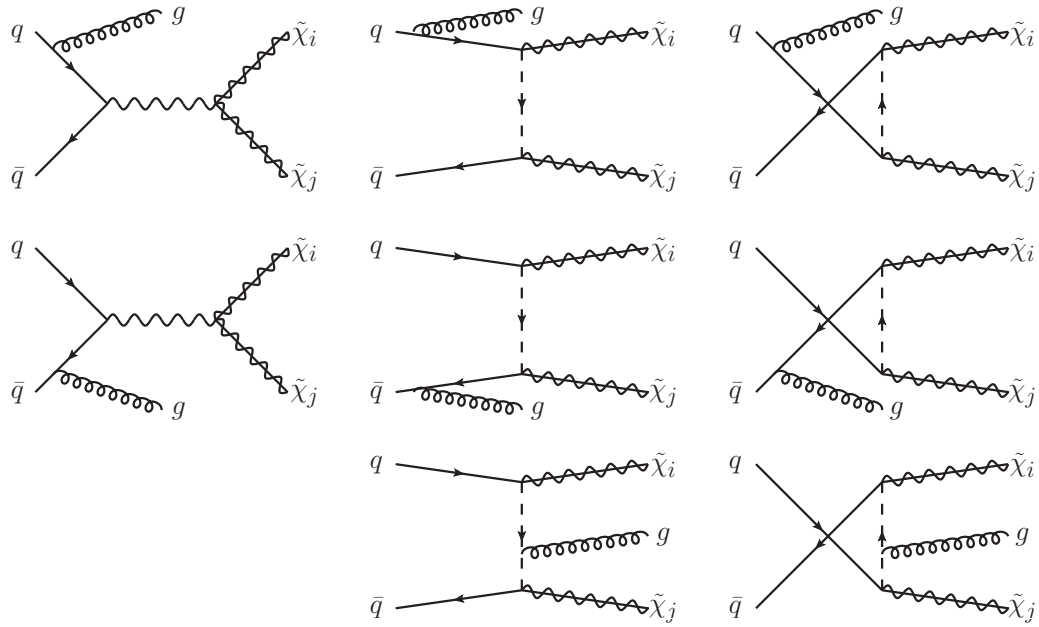


Figure 4.14: Gluon emission diagrams contributing to the production of gaugino pairs at NLO.

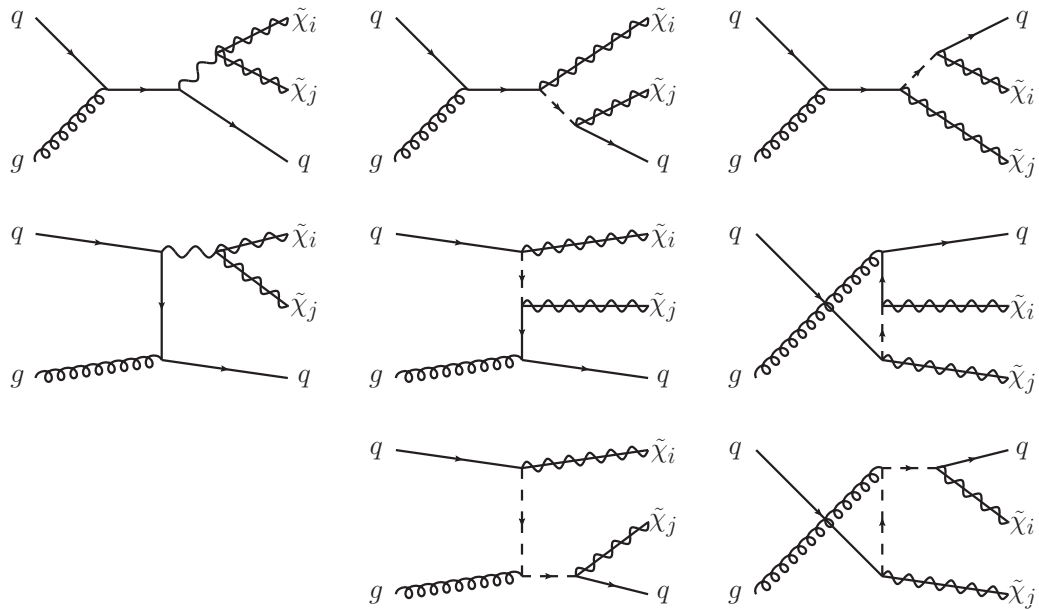


Figure 4.15: Quark emission diagrams contributing to the production of gaugino pairs at NLO.

4.2 SUSY-QCD corrections

(see Eq. (5.136) of Ref. [94]). The colour charges $\mathbf{T}_{a3,b}$ and splitting functions $\mathbf{V}^{a3,b}$ (Eqs. (5.145)-(5.148) of Ref. [94]) act on Born-like squared matrix elements, which are written here in terms of vectors $|\tilde{1}, \tilde{2}; \tilde{a3}, b\rangle_{2,ab}$ in colour and helicity space. These matrix elements involve an initial-state parton $\tilde{a3}$ with momentum parallel to p_a ,

$$\tilde{p}_{a3}^\mu = x_{3,ab} p_a^\mu \quad \text{where} \quad x_{3,ab} = \frac{p_a \cdot p_b - p_3 \cdot p_a - p_3 \cdot p_b}{p_a \cdot p_b}, \quad (4.64)$$

and rescaled four-momenta of the final-state gauginos

$$\tilde{p}_{1,2}^\mu = p_{1,2}^\mu - \frac{2p_{1,2} \cdot (K + \tilde{K})}{(K + \tilde{K})^2} (K + \tilde{K})^\mu + \frac{2p_{1,2} \cdot K}{K^2} \tilde{K}^\mu, \quad (4.65)$$

where $K^\mu = p_a^\mu + p_b^\mu - p_3^\mu$ and $\tilde{K}^\mu = \tilde{p}_{a3}^\mu + p_b^\mu$. The phase space function $F_J^{(2)}(\tilde{p}_1, \tilde{p}_2; \tilde{p}_{a3}, p_b)$ tends to zero with $p_a \cdot p_3$ and ensures therefore that the LO cross section is IR-finite. To compensate for the subtracted auxiliary dipole term $d\sigma_{ab}^{(0)}(p_a, p_b) \otimes dV_{\text{dipole}}$, the latter must be integrated analytically over the full phase space of the emitted parton,

$$\mathbf{I} = \sum_{\text{dipoles}} \int_1 dV_{\text{dipole}}, \quad (4.66)$$

and added to the virtual cross section. The integrated dipole term is defined explicitly in Eq. (10.15) of Ref. [94]; it contains all the simple and double poles in ϵ necessary to cancel the IR singularities in $d\sigma_{ab}^{(V)}$. The insertion operators

$$\mathbf{P}^{a',a}(p_1, \dots, p_m, p_b; x p_a, x; \mu_F^2) = \frac{\alpha_s}{2\pi} P^{a'a}(x) \frac{1}{\mathbf{T}_{a'}^2} \left[\sum_i \mathbf{T}_i \cdot \mathbf{T}_{a'} \ln \frac{\mu_F^2}{2x p_a \cdot p_i} + \mathbf{T}_b \cdot \mathbf{T}_{a'} \ln \frac{\mu_F^2}{2x p_a \cdot p_b} \right] \quad (4.67)$$

are directly related to the regularized Altarelli-Parisi splitting distributions at $\mathcal{O}(\alpha_s)$,³

$$P^{qq}(x) = C_F \left[\frac{1+x^2}{(1-x)_+} + \frac{3}{2} \delta(1-x) \right], \quad (4.68)$$

$$P^{qg}(x) = T_R \left[x^2 + (1-x)^2 \right], \quad (4.69)$$

$$P^{gq}(x) = C_F \left[\frac{1+(1-x)^2}{x} \right] \quad \text{and} \quad (4.70)$$

$$P^{gg}(x) = 2C_A \left[\frac{1}{(1-x)_+} + \frac{1-x}{x} - 1 + x(1-x) \right] + \beta_0 \delta(1-x), \quad (4.71)$$

where $\beta_0 = 11C_A/6 - 2N_f T_R/3$ and $\beta_1 = (17C_A^2 - 5C_A N_f - 3C_F N_f)/6$ are the one- and two-loop coefficients of the QCD beta-function, $C_F = 4/3$, $T_R = 1/2$, $C_A = 3$, and N_f is the number of quark flavours. They cancel the dependence of the hadronic cross section on the factorisation scale μ_F up to NLO accuracy. The insertion operators

$$\mathbf{K}^{a',a}(x) = \frac{\alpha_s}{2\pi} \left\{ \bar{K}^{a'a}(x) - K_{\text{FS}}^{a'a}(x) + \delta^{a'a} \sum_i \mathbf{T}_i \cdot \mathbf{T}_a \frac{\gamma_i^{(1)}}{\mathbf{T}_i^2} \left[\frac{1}{(1-x)_+} + \delta(1-x) \right] \right\} - \frac{\alpha_s}{2\pi} \mathbf{T}_b \cdot \mathbf{T}_{a'} \frac{1}{\mathbf{T}_{a'}^2} \tilde{K}^{a'a}(x) \quad (4.72)$$

³Note that these distributions are simply the inverse Mellin transform of those previously defined in Eqs. (3.12)–(3.15).

4 Gaugino-pair production: Fixed-order calculations

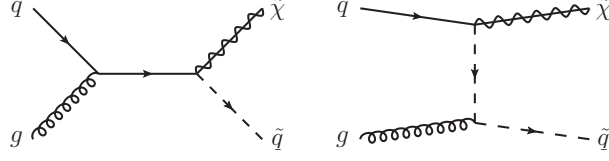


Figure 4.16: Associated production of a gaugino and a virtual squark, decaying subsequently into a gaugino and a quark.

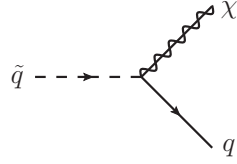


Figure 4.17: Tree-level diagram for a squark decaying into a gaugino and a quark.

with $\gamma_q^{(1)} = 3C_F/2$ and $\gamma_g^{(1)} = \beta_0$,

$$\begin{aligned} \overline{K}^{qq}(x) = \overline{K}^{\tilde{q}\tilde{q}}(x) = C_F \left[\left(\frac{2}{1-x} \ln \frac{1-x}{x} \right)_+ - (1+x) \ln \frac{1-x}{x} + (1-x) \right] \\ - \delta(1-x)(5 - \pi^2)C_F, \end{aligned} \quad (4.73)$$

$$\overline{K}^{qg}(x) = \overline{K}^{\tilde{q}g}(x) = P^{qg}(x) \ln \frac{1-x}{x} + T_R 2x(1-x), \quad (4.74)$$

$$\overline{K}^{gq}(x) = \overline{K}^{g\tilde{q}}(x) = P^{gq}(x) \ln \frac{1-x}{x} + C_F x, \quad (4.75)$$

$$\begin{aligned} \overline{K}^{gg}(x) = 2C_A \left[\left(\frac{1}{1-x} \ln \frac{1-x}{x} \right)_+ + \left(\frac{1-x}{x} - 1 + x(1-x) \right) \ln \frac{1-x}{x} \right] \\ - \delta(1-x) \left[\left(\frac{50}{9} - \pi^2 \right) C_A - \frac{16}{9} T_R N_f \right], \end{aligned} \quad (4.76)$$

$$\overline{K}^{\tilde{q}q}(x) = \overline{K}^{q\tilde{q}}(x) = 0, \quad (4.77)$$

and

$$\tilde{K}^{ab}(x) = P_{\text{reg}}^{ab}(x) \ln(1-x) + \delta^{ab} \mathbf{T}_a^2 \left[\left(\frac{2}{1-x} \ln(1-x) \right)_+ - \frac{\pi^2}{3} \delta(1-x) \right] \quad (4.78)$$

depend on the factorisation scheme through the term $K_{\text{FS}}^{aa'}(x)$, which vanishes in the $\overline{\text{MS}}$ -scheme, and also on the regular parts of the Altarelli-Parisi splitting distributions given by $P_{\text{reg}}^{ab}(x) = P^{ab}(x)$, if $a \neq b$, and otherwise by

$$P_{\text{reg}}^{qq}(x) = -C_F(1+x) \quad \text{and} \quad P_{\text{reg}}^{gg}(x) = 2C_A \left[\frac{1-x}{x} - 1 + x(1-x) \right]. \quad (4.79)$$

The last line in Eq. (4.61) contains therefore the finite remainders that are left after the factorisation of collinear initial-state singularities into the parton densities in the $\overline{\text{MS}}$ -scheme at the factorisation scale μ_F . As guaranteed by the Kinoshita-Lee-Nauenberg and factorisation theorems, the total NLO cross section is then not only UV-, but also IR-finite.

4.2 SUSY-QCD corrections

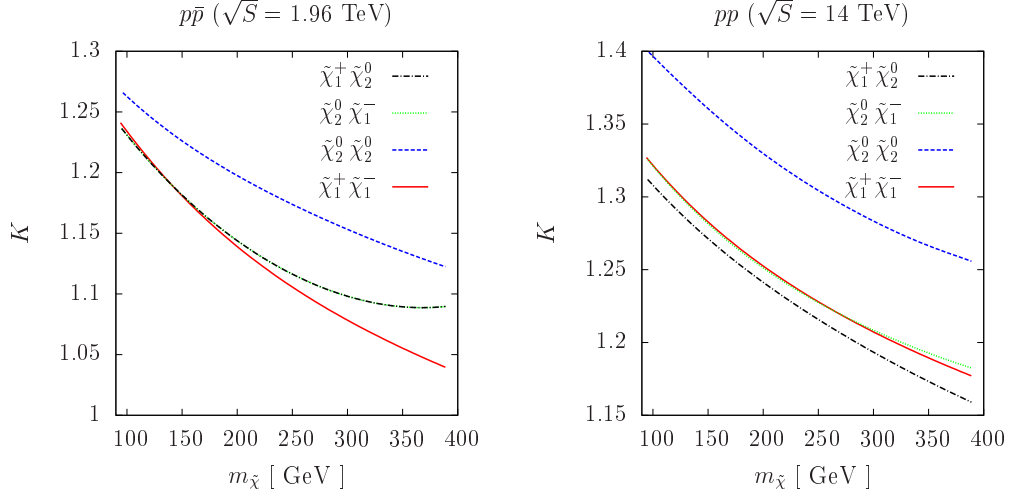


Figure 4.18: K-factors for gaugino-pair production at the Tevatron (left) and the LHC (right) using LO CTEQ6L1 and NLO CTEQ6.6M parton densities [96].

Finally, one subtlety must still be addressed: in Fig. 4.15, the centre and right diagrams of lines one and three proceed through a squark propagator, which can become on-shell if $m_{\tilde{q}} \geq m_{\tilde{\chi}}$ and $s \geq (m_{\tilde{q}} + m_{\tilde{\chi}})^2$. The singularity associated with the pole of the on-shell squark propagator is regularized by a small finite width $\Gamma_{\tilde{q}} \sim 10^{-2} m_{\tilde{q}}$ (the exact value has little influence numerically) [92, 95]. To avoid double counting, the resonance contribution

$$d\sigma_{qg}^{(\tilde{q})} = d\sigma(qg \rightarrow \tilde{\chi}\tilde{q}) \times \text{BR}(\tilde{q} \rightarrow \tilde{\chi}q) \quad (4.80)$$

must be subtracted from the gaugino pair production process using the narrow-width approximation, as it is identified experimentally as the associated production of a gaugino and a squark (Fig. 4.16), followed by the decay of the squark into a gaugino and a quark (Fig. 4.17).

4.2.3 Numerical results

Here we now present numerical results showing the impact of the SUSY-QCD corrections to the total cross section for the gaugino-pair production. In Figs. 4.18 and 4.19, we show the NLO K-factors, defined by

$$K = \frac{\sigma^{\text{NLO}}}{\sigma^{\text{LO}}}, \quad (4.81)$$

as a function of the average gaugino mass $m_{\tilde{\chi}} = (m_{\tilde{\chi}_i} + m_{\tilde{\chi}_j})/2$ and the universal trilinear coupling A_0 , respectively. This is for the Snowmass slope SPS1a, whose mSUGRA parameters are [97]

$$m_0 = -A_0 = 0.4m_{1/2}, \quad \tan\beta = 10 \quad \text{and} \quad \mu > 0. \quad (4.82)$$

The low-scale SUSY parameters are obtained with the computer code SuSpect2.41 [98]. The QCD corrections are found to be large and positive at both the Tevatron (up to 25%) and the LHC (up to 40%), increasing the mass range of neutralino and chargino that can be covered by the two colliders.

4 Gaugino-pair production: Fixed-order calculations

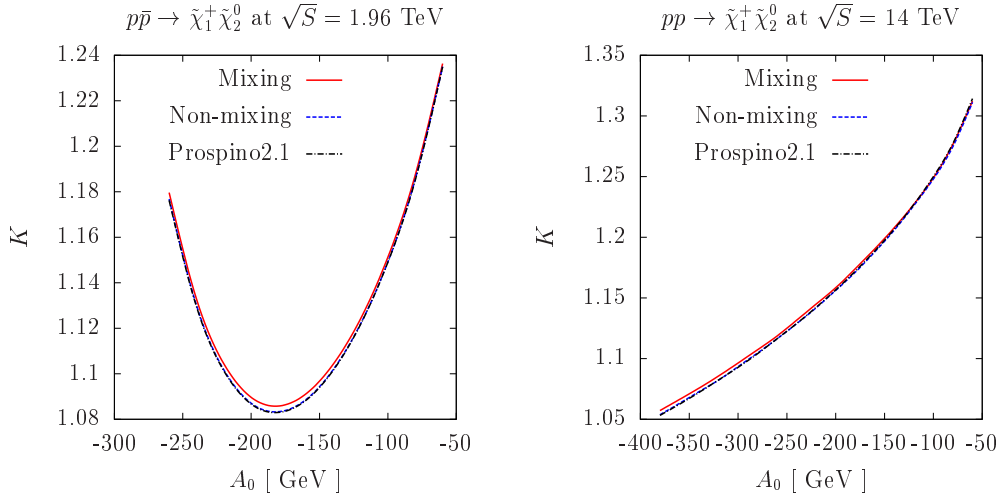


Figure 4.19: K-factor for the associated production of a chargino and a neutralino at the Tevatron (left) and the LHC (right) using LO CTEQ6L1 and NLO CTEQ6.6M parton densities [96].

In Fig. 4.19,⁴ we compare our predictions to those obtained with the computer code Prospino2.1 [68]. Since in the latter squark-mixing effects are neglected, we also show our predictions without squark mixing for comparison. The predictions without mixing (dashed) are in very good agreement with the those of Prospino2.1 (dot-dashed), whereas the results with mixing are slightly shifted in the large- $|A_0|$ region. This is expected, because the squark mass splitting is proportional to A_0 (see Eq. (2.34)).

A careful analysis of factorisation and renormalisation scale dependences as well as PDF uncertainties will be presented in Sec. 5.4.

⁴To produce these figures, we had to correct a bug in the mass factorisation in Prospino2.1.

5

Gaugino-pair production: Resummed calculations

We now turn to our numerical analysis of transverse-momentum and threshold resummation effects on the production of various gaugino pairs at the Tevatron $p\bar{p}$ -collider ($\sqrt{S} = 1.96$ TeV) and the LHC pp -collider ($\sqrt{S} = 7, 10$ and 14 TeV). For the masses and widths of the electroweak gauge bosons, we use the current values of $m_Z = 91.1876$ GeV and $m_W = 80.403$ GeV. The squared sine of the electroweak mixing angle

$$\sin^2 \theta_W = 1 - \frac{m_W^2}{m_Z^2} \quad (5.1)$$

and the electromagnetic fine structure constant

$$\alpha = \frac{\sqrt{2}G_F m_W^2 \sin^2 \theta_W}{\pi} \quad (5.2)$$

can be calculated in the improved Born approximation using the world average value of $G_F = 1.16637 \cdot 10^{-5}$ GeV $^{-2}$ for Fermi's coupling constant [99]. The CKM-matrix is assumed to be diagonal, and the top quark mass is taken to be 173.1 GeV [100]. The strong coupling constant is evaluated in the one-loop and two-loop approximation for LO and NLO/NLL+NLO results, respectively, with a value of $\Lambda_{\overline{\text{MS}}}^{n_f=5}$ corresponding to the employed LO (CTEQ6L1) and NLO (CTEQ6.6M) parton densities [96].

In Sec. 5.1, we present our choices for the different benchmark points in the MSSM parameter space. Then, we study the transverse-momentum and invariant-mass spectra of the gaugino pairs at current hadron colliders in Sec. 5.2 and 5.3, respectively. Finally, the total cross sections and the effects of the threshold enhanced contributions are studied in Sec. 5.4. The results presented here have been published in Refs. [62, 101].

5.1 Benchmark points

The running electroweak couplings as well as the physical masses of the SUSY particles and their mixing angles are computed with the computer program SPheno 2.2.3 [102], which includes a consistent calculation of the Higgs boson masses and all one-loop and the dominant two-loop radiative corrections in the renormalisation group equations linking the restricted set of SUSY-breaking parameters at the gauge coupling unification scale to the complete

5 Gaugino-pair production: Resummed calculations

Scenario	SPS1a'	LM0	LM1	LM7	LM9	SU2	SU3
m_0 [GeV]	70	200	60	3000	1450	3550	100
$m_{1/2}$ [GeV]	250	160	250	230	175	300	300
A_0 [GeV]	-300	-400	0	0	0	0	-300
$\tan\beta$	10	10	10	10	50	10	6
$\text{sgn}(\mu)$	+	+	+	+	+	+	+
$m_{\tilde{\chi}_1^0}$ [GeV]	98	61	96	94	70	124	118
$m_{\tilde{\chi}_1^\pm, \tilde{\chi}_2^0}$ [GeV]	184	113	178	176	128	229	223
$m_{\tilde{\chi}_3^0}$ [GeV]	400	313	346	337	263	355	465
$m_{\tilde{\chi}_2^\pm, \tilde{\chi}_4^0}$ [GeV]	415	329	366	359	284	384	481
$m_{\tilde{q}}$ [GeV]	550	420	550	3000	1480	3560	650
$m_{\tilde{g}}$ [GeV]	604	409	603	636	487	809	715

Table 5.1: Names, mSUGRA parameters and physical SUSY particle masses of the benchmark points used in our numerical studies.

set of observable SUSY masses and mixing angles at the electroweak scale. We choose the widely used minimal supergravity (mSUGRA) point SPS1a' [93] as the benchmark for most of our numerical studies. This point has an intermediate value of $\tan\beta = 10$ and $\mu > 0$ (favored by the rare decay $b \rightarrow s\gamma$ and the measured anomalous magnetic moment of the muon), a light gaugino mass parameter of $m_{1/2} = 250$ GeV, and a slightly lower scalar mass parameter $m_0 = 70$ GeV and trilinear coupling $A_0 = -300$ GeV than the original point SPS1a [97] in order to render it compatible with low-energy precision data, high-energy mass bounds, and the observed cold dark matter relic density. It is also similar to the post-WMAP point B' ($m_0 = 60$ GeV and $A_0 = 0$) [103], which has been adopted by the CMS collaboration as their first low-mass point (LM1) [104]. In the SPS1a' scenario, the $\tilde{\chi}_1^0$ is the LSP with a mass of 98 GeV, the gauginos producing the trilepton signal have masses of $m_{\tilde{\chi}_1^\pm} \simeq m_{\tilde{\chi}_2^0} = 184$ GeV, and the heavier gauginos, which decay mostly into the lighter gauginos, W and Z bosons as well as the lightest Higgs boson, have masses of $m_{\tilde{\chi}_3^0} = 400$ GeV and $m_{\tilde{\chi}_2^\pm} \simeq m_{\tilde{\chi}_4^0} = 415$ GeV. The average squark and gluino masses are $m_{\tilde{q}} \simeq 550$ GeV and $m_{\tilde{g}} = 604$ GeV.

Apart from the low-mass point LM1, we will also study the points LM7 and LM9, since all three points have been found by the CMS collaboration to lead to visible three-lepton signals. For LM7, the direct $\tilde{\chi}_1^\pm \tilde{\chi}_2^0$ production cross section exceeds even 70% of the total SUSY particle production cross section [104]. The ATLAS collaboration have studied the direct production of gauginos at the points SU2 and SU3 with or without a jet veto (denoted JV, i.e. no jet in the event with transverse momentum $p_T > 20$ GeV) in order to suppress the background from top quark pair production [105]. We also present results for the common CMS/ATLAS low-mass point LM0/SU4 with the objective of high cross sections and thus early discovery at the LHC. A summary of all scenarios considered here is presented in Tab. 5.1. Note that none of these points falls into (but most of them lie relatively close to) the regions excluded by the Tevatron collaborations CDF and D0, which assume, however, a lower value of $\tan\beta = 3$ and always $A_0 = 0$ [14].

5.2 Transverse-momentum distribution

For an efficient suppression of the SM background from vector-boson and top-quark production and a precise determination of the underlying SUSY-breaking model and masses, an accurate theoretical calculation of the signal (and background) cross section is imperative. As the lightest SUSY particle (LSP) escapes undetected, the key distribution for SUSY discovery and measurements is the missing transverse-energy (\cancel{E}_T) spectrum, which is typically restricted by a cut of 20 GeV at the Tevatron and 30 GeV at the LHC. While the SUSY particle pair is produced with zero transverse momentum (p_T) in the Born approximation, the possible radiation of gluons from the quark-antiquark initial state or the splitting of gluons into quark-antiquark pairs at $\mathcal{O}(\alpha_s)$ in the strong coupling constant induces transverse momenta extending to quite substantial values and must therefore be taken into account. In addition, the perturbative calculation diverges at small p_T , indicating the need for a resummation of soft-gluon radiation to all orders. Only after a consistent matching of the perturbative and resummed calculations an accurate description of the (missing) transverse energy spectrum and precise measurements of the SUSY particle masses can be achieved.

In the following, we report on the first precision analysis of the transverse-momentum spectrum of gaugino pairs produced at the Tevatron and the LHC with centre-of-mass energies of 1.96 and 10 or 14 TeV, respectively. We briefly recall in the next section our implementation of the resummation formalism and present then numerical results for the production of various gaugino pairs at two typical MSSM benchmark points. We also discuss the impact of the computed precise transverse-momentum spectrum on the determination of SUSY mass parameters and investigate in detail the remaining theoretical uncertainties coming from scale and parton-density function variations and non-perturbative effects.

5.2.1 Transverse-momentum resummation

In the Born approximation, the production of neutralinos and charginos at hadron colliders

$$p\bar{p}, pp \rightarrow q\bar{q}' + X \rightarrow \tilde{\chi}_i \tilde{\chi}_j + X \quad (5.3)$$

is induced by the quarks q and antiquarks \bar{q}' in the initial (anti-)protons and is mediated by s -channel electroweak gauge-boson and t - and u -channel squark exchanges. Its partonic cross section $\hat{\sigma}_{ab}^{(0)}$ can be expressed in terms of the gaugino and squark masses $m_{\tilde{\chi}_{i,j}^{0,\pm}}$ and $m_{\tilde{q}}$, the masses of the electroweak gauge bosons, the Mandelstam variables s , t and u , and generalized charges (see Eqs. (4.14)–(4.30)).

As shown in Sec. 4.2, at leading order (LO) in the strong coupling constant, $\mathcal{O}(\alpha_s)$, virtual loop and real parton emission corrections must be taken into account. The latter induce transverse momenta of the gaugino pair, that extend typically to values of the order of the gaugino mass. In the small- p_T region, where the bulk of the events is produced, the convergence of the perturbative expansion is spoiled due to the presence of large logarithms $a_s^n/p_T^2 \ln^m(M^2/p_T^2)$ with $m \leq 2n - 1$ and $a_s = \alpha_s/(2\pi)$. These must be resummed to all orders in impact parameter (b) space in order to correctly implement transverse-momentum

conservation. In Mellin N -space, the resummed component is deduced from Eq. (3.64),

$$\begin{aligned} \hat{\sigma}_{ab}^{(\text{res})}(N, M^2, M^2/p_T^2, M^2/\mu^2) = & \\ & \int_0^\infty db \frac{b}{2} J_0(bp_T) \sum_{cdef} H_{cd}(M^2, M^2/\mu^2) \exp[G_{cd}(M^2, M^2\bar{b}^2, M^2/\mu^2)] \\ & \times C_{ce}(N, a_s(1/\bar{b}^2)) C_{df}(N, a_s(1/\bar{b}^2)) E_{ea}(N, 1/\bar{b}^2, \mu^2) E_{fb}(N, 1/\bar{b}^2, \mu^2). \end{aligned} \quad (5.4)$$

Here, b describes the minimal distance of the two incident particles in the limit of no interaction and is the conjugate variable of the transverse momentum p_T , $J_0(x)$ is the 0^{th} -order Bessel function and M is the invariant mass of the gaugino pair. The b -independent function H_{ab} (see Eq. (3.73)),

$$H_{ab}(M^2, M^2/\mu^2) = \hat{\sigma}_{ab}^{(0)}(M^2, M^2/\mu^2)[1 + a_s \mathcal{A}_0] + \mathcal{O}(a_s^2) \quad (5.5)$$

includes the IR-finite part of the renormalised virtual corrections as defined in Eq. (3.45) and the exponential form factor

$$G_{ab}(M^2, M^2\bar{b}^2, M^2/\mu^2) = L g_{ab}^{(1)}(a_s \beta_0 L) + g_{ab}^{(2)}(a_s \beta_0 L, M^2/\mu^2) + \dots, \quad (5.6)$$

resums the divergent leading and next-to-leading contributions in the logarithm $L = \ln(M^2\bar{b}^2)$ through the functions $g_{ab}^{(1,2)}$. Unphysical logarithmic divergences at $b \rightarrow 0$ are regularized by replacing L with $\ln(M^2\bar{b}^2 + 1)$. The C_{ab} function are then given by Eq. (3.74) and, up to NLL accuracy, the evolution from the factorisation scale μ to the low scale $1/\bar{b}$ is achieved through the one-loop approximation $E_{ab}^{(1)}$ defined in Eq. (3.18).

To obtain a valid hadronic cross section at all values of p_T , the $\mathcal{O}(\alpha_s)$ (LO) and resummed (res) partonic cross sections are matched by subtracting from their sum the perturbatively expanded (exp) resummed cross section,

$$\hat{\sigma} = \hat{\sigma}^{(\text{LO})} + \hat{\sigma}^{(\text{res})} - \hat{\sigma}^{(\text{exp})}, \quad (5.7)$$

and by performing numerically the necessary inverse Mellin and Fourier transforms (as described in Sec. 3.5), kinematic integrations, and parton density convolutions.

5.2.2 Numerical results

In this section, we present the transverse-momentum distributions of the gaugino pairs for the minimal supergravity benchmark points LM0 and SPS1a', defined in Tab. 5.1. In the latter, the lightest chargino and second-lightest neutralino decay almost exclusively to three charged leptons and missing transverse energy albeit through real sleptons, which may be experimentally reconstructed through endpoints in kinematic distributions [93].

In Fig. 5.1, we show the corresponding transverse-momentum spectra of chargino-neutralino pairs produced at run II of the Tevatron (top) and the initial run of the LHC (bottom) with centre-of-mass energies of $\sqrt{S} = 1.96$ and 10 TeV, respectively. As expected, the $\mathcal{O}(\alpha_s)$ predictions (dashed curves) diverge at low p_T , but become finite after matching them to the resummed predictions at next-to-leading logarithmic (NLL) accuracy (full curves). In this region, the perturbative expansions of the resummed predictions (dots) coincide with those at $\mathcal{O}(\alpha_s)$, while at large p_T they coincide with the resummed ones. Through resummation, the perturbative predictions are considerably enhanced even at values of p_T , which are of the order of the experimental \cancel{E}_T cuts. It is therefore important

5.2 Transverse-momentum distribution

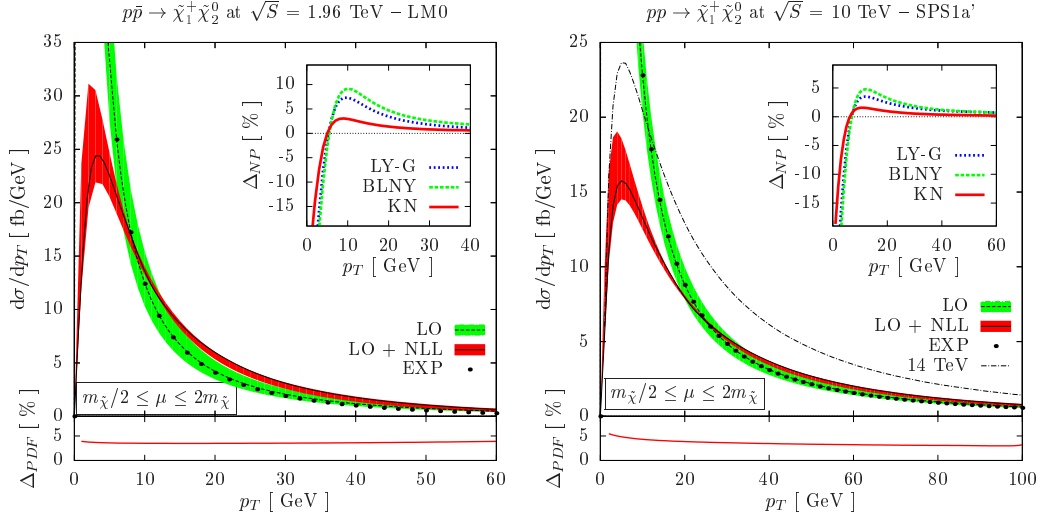


Figure 5.1: Transverse-momentum spectra of chargino-neutralino pairs at the Tevatron (left) and the LHC (right). The $\mathcal{O}(\alpha_s)$ calculation (green/dashed) is matched to the resummed calculation (red/full) by subtracting its fixed-order expansion (dotted). The scale uncertainty is shown as a shaded band, the PDF (below) and non-perturbative (insert) uncertainties as separate graphs, and the matched result for the LHC design energy of $\sqrt{S} = 14$ TeV as a dot-dashed line (bottom).

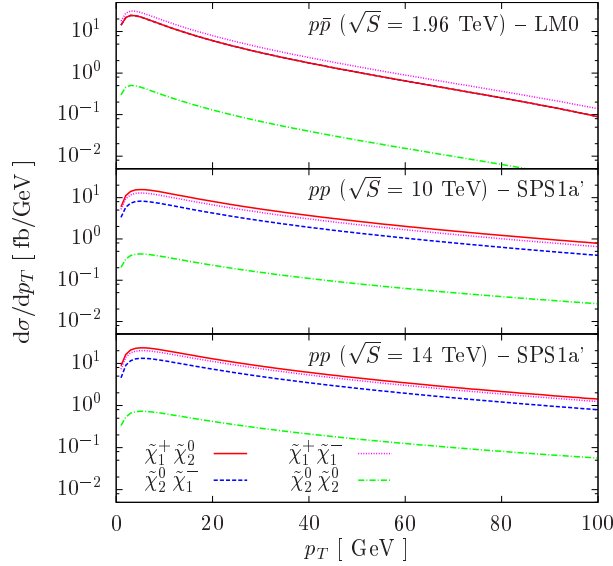


Figure 5.2: Transverse-momentum spectra at NLL accuracy for the associated production of charginos and neutralinos (full and dashed) as well as chargino (dotted) and neutralino (dot-dashed) pairs (dotted) in three different collider modes.

5 Gaugino-pair production: Resummed calculations

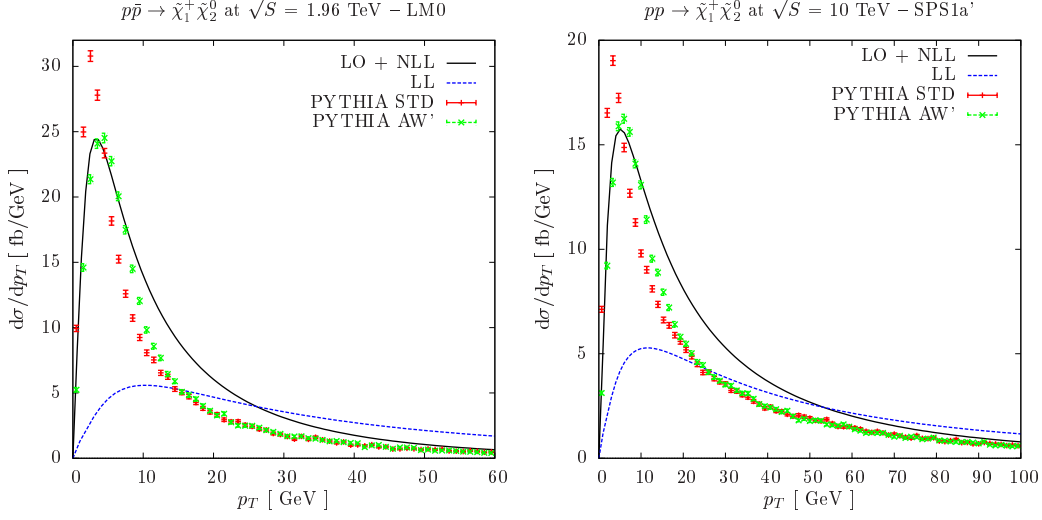


Figure 5.3: Transverse-momentum spectra at LO+NLL (full), LL (dashed), and generated by the PYTHIA parton shower with default (bars) and tuned (crosses) parameters at the Tevatron.

to clearly distinguish the effects induced by QCD radiation and by the unobserved LSPs and neutrinos. By construction, the matched LO+NLL prediction allows to reproduce the correct $\mathcal{O}(\alpha_s)$ correction (K) factor of the total perturbative cross section after integration over p_T , e.g. of 1.26 at the Tevatron. For comparison, we also show the matched LO+NLL p_T -spectrum (dot-dashed curve) for the 14 TeV design energy of the LHC, which extends to considerably larger values of p_T than at 10 TeV. The theoretical predictions are influenced by three main sources of uncertainty: scale variations, evaluated in the canonical range of $\mu_{F,R}/\bar{m} = 0.5 - 2$ (shaded bands), variations of the parton densities, evaluated through

$$\Delta_{\text{PDF}} = \sqrt{\sum_{i=1}^{22} (d\sigma_i^+ - d\sigma_i^-)^2} / (2d\sigma) \quad (5.8)$$

along the 22 eigenvector directions defined by the CTEQ collaboration (lower curves), and three choices of non-perturbative (NP) form factors, evaluated through

$$\Delta_{\text{NP}} = \frac{d\sigma^{\text{NP}} - d\sigma}{d\sigma} \quad (5.9)$$

(insets) [54, 56, 57]. For $p_T > 5$ GeV, all theoretical uncertainties are smaller than 5% for the LO+NLL predictions. In particular, the 5% PDF uncertainty is similar to the one obtained for weak boson production [96].

In Fig. 5.2, the matched p_T -spectra for chargino (dotted) and neutralino (dot-dashed) pairs are compared to those of the tri-lepton channel (full/dashed) discussed above. While positive and negative charginos are produced with equal rates in $p\bar{p}$ collisions at the Tevatron, their rates differ slightly in pp collisions at the LHC. The cross sections for neutralino pair production are about one order of magnitude smaller, as the second-lightest neutralino couples to the s -channel Z^0 -boson only through its relatively small Higgsino component.

In experimental analyses, QCD radiation in hadronic collisions is usually simulated with tree-level matrix elements and parton showers based on an exponential Sudakov form factor, which resums the leading logarithms (LL) and some next-to-leading logarithms. In Fig.

5.3 Invariant-mass distribution

5.3, we compare therefore our matched LO+NLL prediction (full curve) with our resummed prediction at LL order (dashed curve) and the default (bars) and tuned (crosses) predictions of the PYTHIA6.4 Monte Carlo (MC) generator [106, 107]. While the default MC prediction is clearly improved beyond the LL approximation and approaches the LO+NLL result, it peaks at too small values of p_T . Tuning the intrinsic p_T of the partons in the proton to 2.1 GeV for Z^0 -bosons (CDF tune AW) and 4 GeV for gaugino pairs (our tune AW') improves the description of the peak, but still underestimates the intermediate p_T -region and the mean value of p_T (14 GeV for PYTHIA6.4, 15 GeV for our tune AW', and 18 GeV for our LO+NLL prediction). This has, of course, a direct impact on the determination of the gaugino (and slepton) masses through variables derived from the transverse momenta of the observed leptons $p_{T,i}$ and \cancel{E}_T , such as the effective mass $M_{\text{eff}} = \sum_i p_{T,i} + \cancel{E}_T$ [108] or the stransverse mass [109]. Let us mention that the contribution of unmeasured (low- p_T or forward) or mismeasured hadronic energy to the “fake” \cancel{E}_T is under close scrutiny both at the Tevatron and at the LHC. The ATLAS trilepton analysis, e.g., does not identify jets with $p_T < 10$ GeV, and an optional cut on jets with $p_T > 20$ GeV reduces the significance considerably. As the two LSPs are often back-to-back, the \cancel{E}_T in the trilepton analysis is required to be relatively small (> 30 GeV). It can then be affected by an error of up to 10% (Aad *et al.* [105]).

5.3 Invariant-mass distribution

In this section, we present our results for the invariant-mass distributions of the gaugino pairs at the Tevatron and the LHC within the mSUGRA model. A similar study has been previously performed for the trilepton channel $\tilde{\chi}_1^\pm \tilde{\chi}_2^0$ in Ref. [95]. In this work, we extend and improve this published result in several respects. First, we include not only the QCD, but the full SUSY-QCD virtual loop contributions in the hard coefficient function of the resummed cross section, which therefore reproduces, when expanded, the correct NLO SUSY-QCD cross section in the threshold region. Second, we resum not only the diagonal, but the full matrix contributions coming from the anomalous dimension, thereby including all universal subleading terms and full singlet mixing. For the Tevatron, we consider not only the production of $\tilde{\chi}_1^\pm \tilde{\chi}_2^0$, but also of $\tilde{\chi}_2^0 \tilde{\chi}_2^0$ and $\tilde{\chi}_1^+ \tilde{\chi}_1^-$ pairs. In particular, the latter can have significantly larger cross sections than trilepton production due to the s -channel exchange of massless photons. For the LHC, we concentrate on predictions for its initial centre-of-mass energy $\sqrt{S} = 7$ TeV and include also the production of heavy gaugino ($\tilde{\chi}_2^\pm, \tilde{\chi}_{3,4}^0$) combinations, where threshold effects and direct gaugino pair production (as opposed to the production from squark and gluino cascade decays) will be more important. However, we will also show cross sections for $\sqrt{S} = 14$ TeV for comparison.

5.3.1 Threshold resummation

Starting at NLO, i.e. at $\mathcal{O}(\alpha_s)$, the cancellation of soft parton emission among virtual and real corrections is restricted by the phase space boundary of the latter. This leads to logarithmic contributions $a_s [\ln(1-z)/(1-z)]_+$ with $a_s = \alpha_s/(2\pi)$ which may become large close to partonic threshold i.e. z close to one. Threshold resummation reorganises and resums these contributions to all orders in a_s in Mellin (N) space in order to correctly implement

energy conservation.¹ Hence, the resummed component can be obtained from Eq. (3.35),

$$\hat{\sigma}_{ab}^{(\text{res})}(N, M^2, M^2/\mu^2) = \mathcal{H}_{ab}(M^2, M^2/\mu^2) \exp[\mathcal{G}_{ab}(N, M^2, M^2/\mu^2)], \quad (5.10)$$

where the N -independent function \mathcal{H}_{ab} (see Eq. (3.44)),

$$\begin{aligned} \mathcal{H}_{ab}(M^2, M^2/\mu^2) &= \hat{\sigma}_{ab}^{(0)}(M^2, M^2/\mu^2) \\ &+ a_s \hat{\sigma}_{ab}^{(0)}(M^2, M^2/\mu^2) \left[\mathcal{A}_0 + (\delta P_{aa}^{(1)} + \delta P_{bb}^{(1)}) \ln \frac{M^2}{\mu^2} + \frac{\pi^2}{6} (A_a^{(1)} + A_b^{(1)}) \right]. \end{aligned} \quad (5.11)$$

The coefficient function $\mathcal{H}^{(1)}$, given by the second line of Eq. (5.11), agrees with the one presented in Eq. (115) of Ref. [95] except for the last three terms. While their last term corresponds to the flavour-diagonal collinear improvement already discussed in Sec. 3.3.4, the two other terms represent leading and next-to-leading logarithms and should therefore not be present. Furthermore, the two terms in $(\ln 4\pi\mu_R^2/M^2 - \gamma_E)$ should be squared individually, not together, and the virtual correction $\mathcal{M}_V^{\text{QCD}}$ defined in Eq. (116) of Ref. [95] should include the complete SUSY-QCD contributions and not only their UV-singular parts.

The exponential form factor

$$\mathcal{G}_{ab}(N, M^2/\mu^2) = L g_{ab}^{(1)}(a_s \beta_0 L) + g_{ab}^{(2)}(a_s \beta_0 L) + \dots \quad (5.12)$$

resums the leading and next-to-leading contributions in the logarithm $L = \ln(Ne^{\gamma_E})$ through the functions $g_{ab}^{(1,2)}$. Furthermore, by following the procedure described in Sec. 3.3.4, the dominant $\mathcal{O}(1/N)$ terms are also resummed.

The matching with the fixed-order calculation is achieved from Eq. (3.54),

$$\hat{\sigma}_{ab} = \hat{\sigma}_{ab}^{(\text{res})} + \hat{\sigma}_{ab}^{(\text{f.o})} - \hat{\sigma}_{ab}^{(\text{exp})}, \quad (5.13)$$

where again $\hat{\sigma}_{ab}^{(\text{exp})}$ is the truncation of the resummed cross section to the same perturbative order as $\hat{\sigma}_{ab}^{(\text{f.o})}$. At $\mathcal{O}(\alpha_s)$, it is given by Eq. (3.55).

In the following, when we present spectra in the invariant mass M of the gaugino pair, we identify the unphysical scales $\mu_F = \mu_R = \mu$ with M . The remaining theoretical uncertainty is estimated by varying the common scale μ about these central values by a factor of two up and down.

5.3.2 Numerical results

In Ref. [95], the cross section for the associated production of $\tilde{\chi}_1^\pm$ and $\tilde{\chi}_2^0$ has been computed as a function of $\tan\beta$ and $m_{1/2}$ for $m_0 = 200$ and 1000 GeV and assuming $A_0 = 0$ and $\mu > 0$. Unfortunately, the exact version of the renormalisation group program SPheno used there could not be determined, and we were not able to reproduce the physical SUSY particle mass spectra of Ref. [95]. Since we also do not completely agree analytically with the coefficient function $\mathcal{H}_{ab}^{(1)}(M^2, \mu^2)$ of Ref. [95] (see above), we must refrain from a direct comparison of our numerical results.

In Fig. 5.4 we present invariant mass spectra $M^3 d\sigma/dM$ for the production of various combinations of $\tilde{\chi}_1^\pm$ and $\tilde{\chi}_2^0$ with $m_{\tilde{\chi}_1^\pm} \simeq m_{\tilde{\chi}_2^0} = 184$ GeV in the SPS1a' scenario at the

¹In fact, it is the Laplace transform which correctly implement energy conservation. However, close to threshold, Mellin and Laplace transforms are basically equivalent.

5.3 Invariant-mass distribution

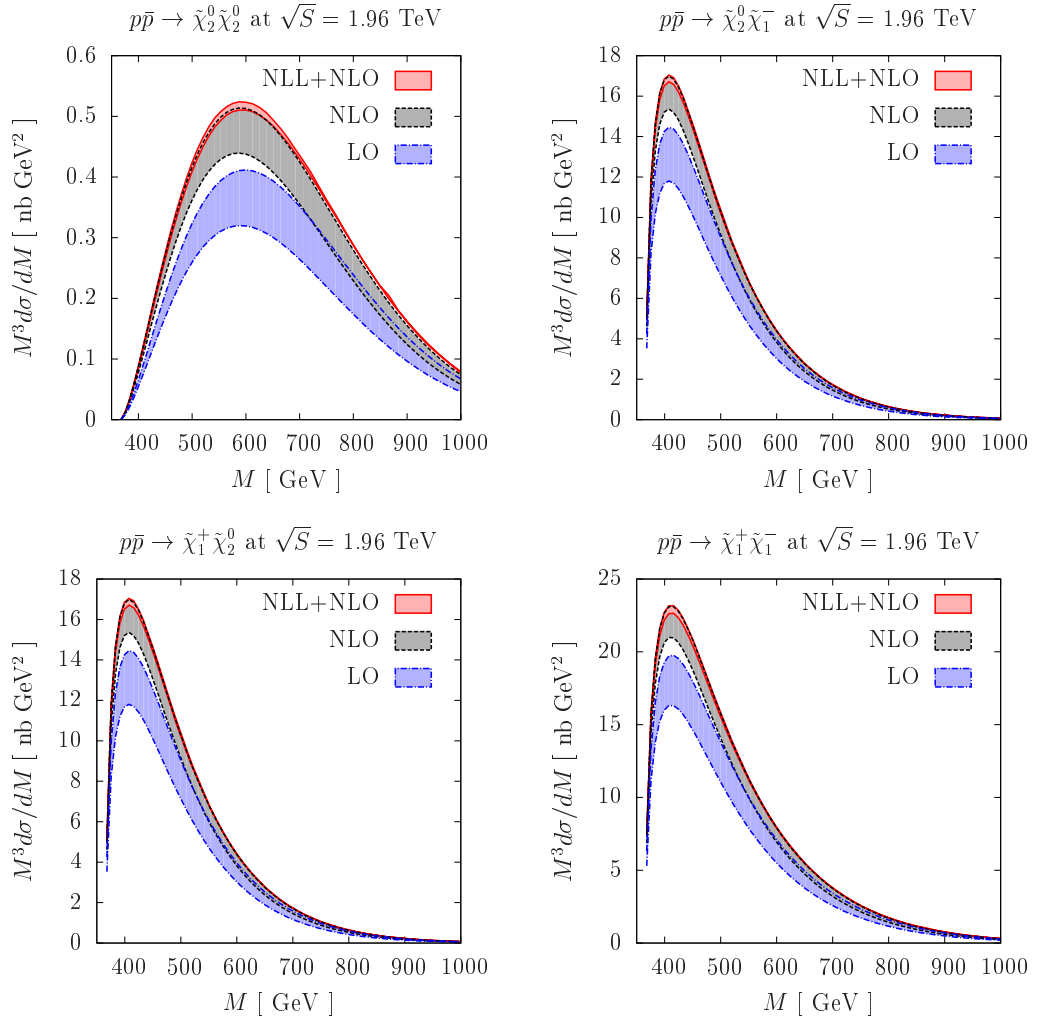


Figure 5.4: Invariant mass spectra for the production of various light gaugino pairs at the Tevatron in the SPS1a' scenario and in the LO (blue), NLO (grey) and NLL+NLO (red) approximation. The corresponding scale uncertainties are represented by the band widths.

5 Gaugino-pair production: Resummed calculations

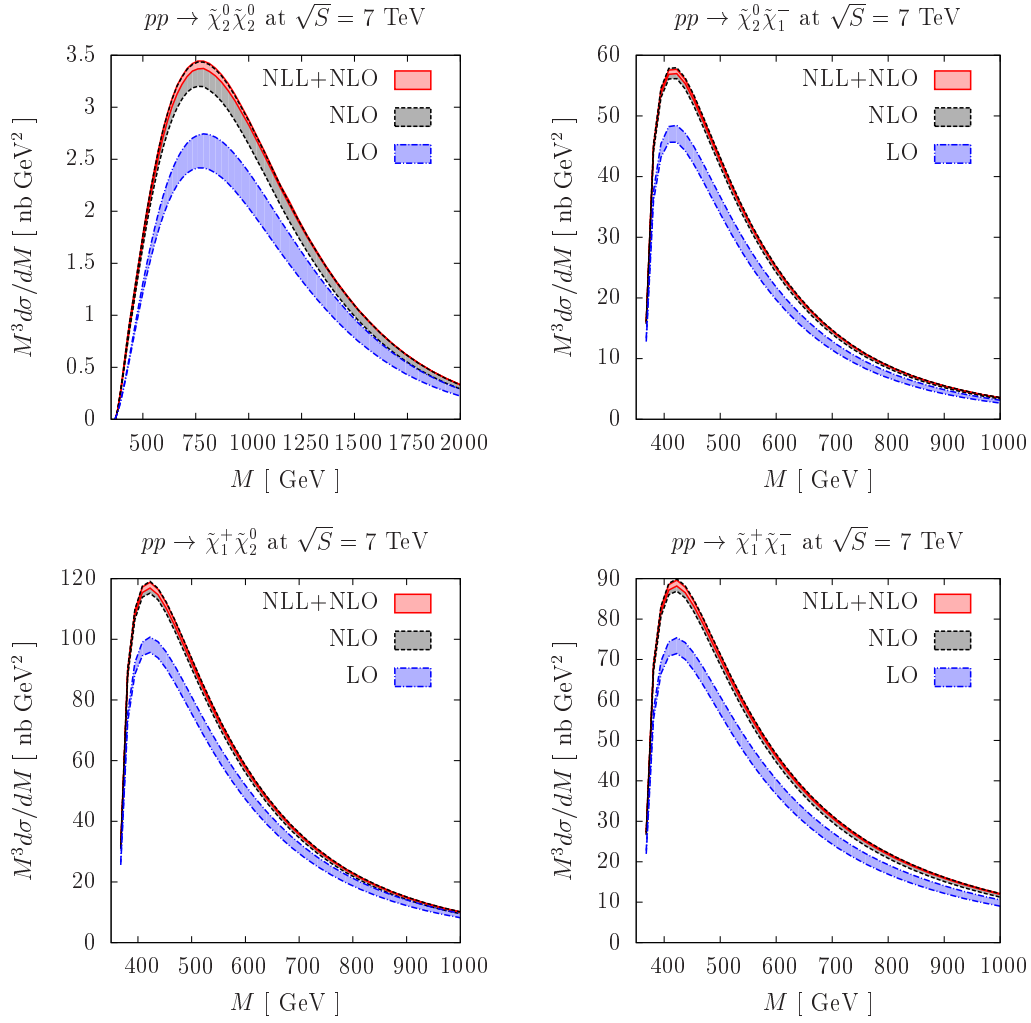


Figure 5.5: Same as Fig. 5.4 for the LHC with its current centre-of-mass energy of $\sqrt{S} = 7$ TeV.

Tevatron. The spectra start at $M = m_{\tilde{\chi}_1^\pm} + m_{\tilde{\chi}_2^0} = 368$ GeV and increase considerably from LO (blue) to NLO (grey), but much less from NLO to NLL+NLO (red). The scale uncertainty is considerably reduced from NLO to NLL+NLO, which indicates good convergence of the reorganized perturbative series. The cross section is smallest for the production of two neutralinos, since they are gaugino-like and couple only weakly to the s -channel Z -boson (see Eq. (4.3)). Since the Tevatron is a $p\bar{p}$ collider, the cross sections are identical for $\tilde{\chi}_2^0 \tilde{\chi}_1^-$ and $\tilde{\chi}_1^+ \tilde{\chi}_2^0$ pairs. The largest cross section is obtained for chargino pairs due to the s -channel photon contribution. Threshold resummation should be most important as $M \rightarrow \sqrt{s}$ and $z \rightarrow 1$, but its effects on the partonic cross section are, of course, reduced in the hadronic cross section shown here by the parton densities, which tend to 0 as $x_{a,b}$ and $z \rightarrow 1$. Nevertheless, on close inspection one observes that the NLL+NLO cross section for two neutralinos no longer overlaps with the one at NLO for relatively large invariant masses of $M \simeq \sqrt{S}/2$.

A similar hierarchy of the different production channels is observed in Fig. 5.5 for the

5.3 Invariant-mass distribution

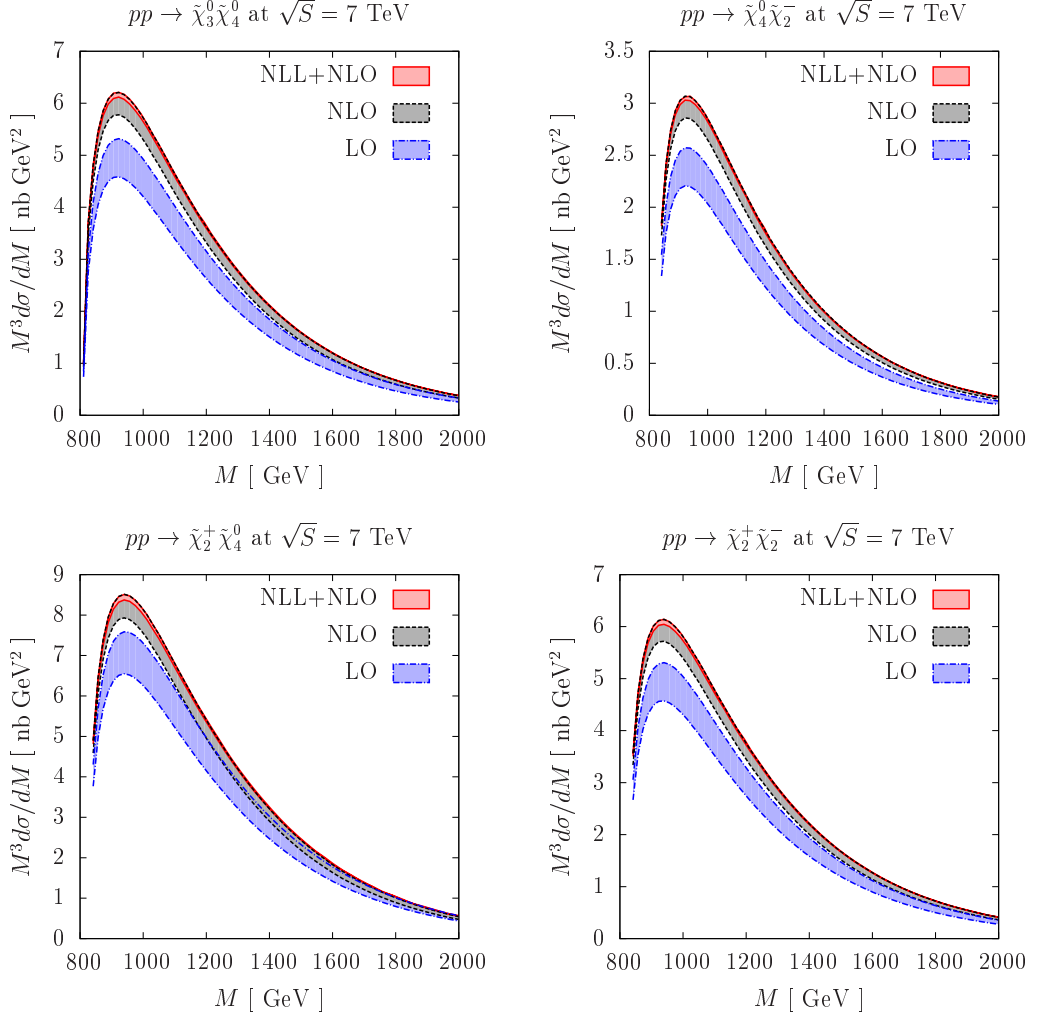


Figure 5.6: Same as Fig. 5.4 for the production of heavy gaugino pairs at the LHC with its current centre-of-mass energy of $\sqrt{S} = 7$ TeV.

LHC with its current centre-of-mass energy of $\sqrt{S} = 7$ TeV. There are, however, two notable differences. First, the LHC is a pp collider, so that the cross section for $\tilde{\chi}_1^+ \tilde{\chi}_2^0$ exceeds the one for $\tilde{\chi}_1^- \tilde{\chi}_2^0$ by a factor of two and becomes even larger than the one for chargino pairs. Second, the NLO band is separated by a wider gap from the LO band than it was the case at Tevatron, whereas the NLL+NLO and NLO bands overlap considerably more. This is, of course, due to the fact that the light gauginos are now produced further away from the threshold of the 7 TeV collider, so that the importance of soft-gluon resummation is reduced. However, one still observes a sizeable reduction of the scale uncertainty from NLO to NLL+NLO.

Heavier gaugino pairs can only be produced with sizeable cross sections at the LHC. We therefore show in Figs. 5.6 and 5.7 the invariant mass spectra $M^3 d\sigma/dM$ for the production of various combinations of $\tilde{\chi}_{3,4}^0$ and $\tilde{\chi}_2^\pm$ at the LHC with $\sqrt{S} = 7$ TeV and 14 TeV and with $m_{\tilde{\chi}_3^0} = 400$ GeV and $m_{\tilde{\chi}_2^\pm} \simeq m_{\tilde{\chi}_4^0} = 415$ GeV in the SPS1a' scenario. The spectra start at $M \simeq 800 - 830$ GeV, and their magnitudes are considerably smaller than in the light gaugino

5 Gaugino-pair production: Resummed calculations

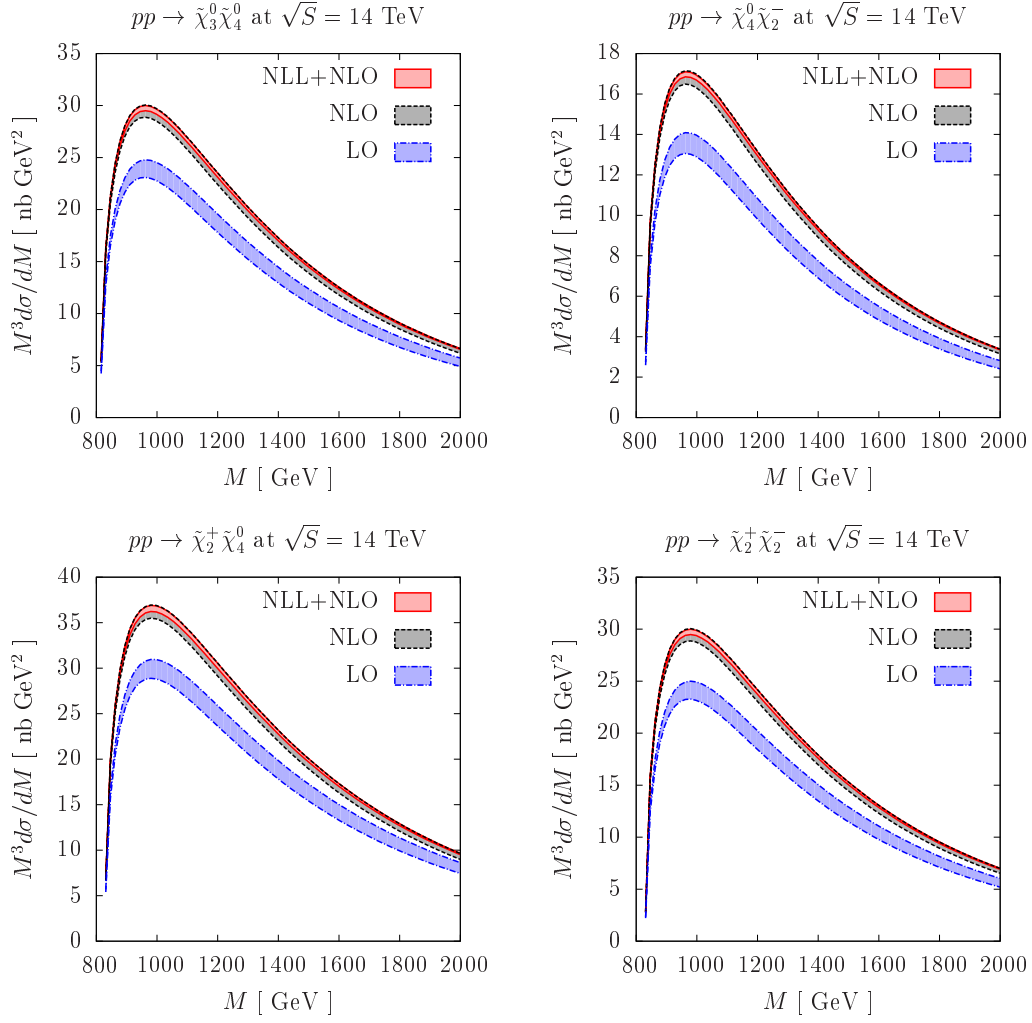


Figure 5.7: Same as Fig. 5.4 for the production of heavy gaugino pairs at the LHC with its design centre-of-mass energy of $\sqrt{S} = 14$ TeV.

5.3 Invariant-mass distribution

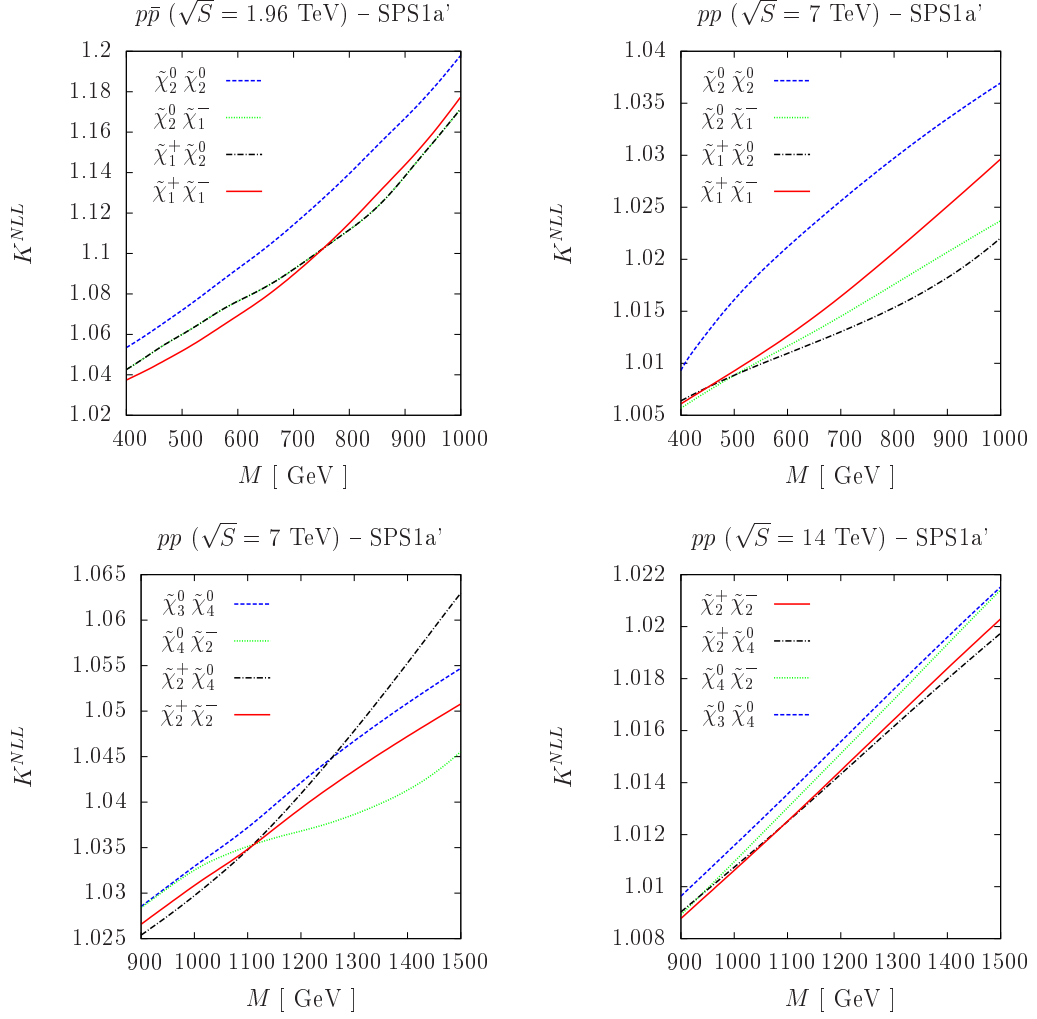


Figure 5.8: Ratios K^{NLL} of NLL+NLO over NLO differential cross sections as a function of the invariant mass M of a gaugino pair at the Tevatron (top left) and LHC with $\sqrt{S} = 7$ TeV (top right and bottom left) and $\sqrt{S} = 14$ TeV (bottom right) in the SPS1a' scenario.

case. However, they are now of comparable size for neutralino and chargino pairs due to the fact that the dominantly higgsino $\tilde{\chi}_3^0$ and $\tilde{\chi}_4^0$ now have sizeable couplings to the s -channel Z -boson (see Eq. (4.3)). The associated production of a neutralino and a chargino is again much larger for the positive chargino eigenstate than for its negative counterpart. The cross sections for $\tilde{\chi}_3^0 \tilde{\chi}_2^\pm$ pairs are very similar to those for $\tilde{\chi}_4^0 \tilde{\chi}_2^\pm$ pairs and therefore not shown. Higgsino-like neutralinos and charginos with large s -channel contributions are produced as S -waves, so that the invariant mass spectra rise more steeply at low M than P -wave produced gaugino-like neutralinos and charginos.

From Figs. 5.4–5.7, the impact of threshold resummation effects is difficult to estimate. We therefore present in Fig. 5.8 the relative size

$$K^{\text{NLL}} = \frac{d\sigma^{\text{NLL+NLO}}}{d\sigma^{\text{NLO}}} \quad (5.14)$$

of the NLL+NLO prediction with respect to the NLO prediction. As one expects, the cor-

5 Gaugino-pair production: Resummed calculations

Colliders	$\sigma^{\text{NLL+NLO}}$ [fb]	σ^{NLO} [fb]	σ^{LO} [fb]
$p\bar{p}(\sqrt{S} = 1.96 \text{ TeV})$	$30.9^{+0.1 +1.5}_{-0.2 -1.9}$	$31.2^{+0.9 +1.5}_{-1.2 -1.9}$	$27.2^{+3.6}_{-3.0}$
$pp(\sqrt{S} = 7 \text{ TeV})$	$263.3^{+0.6 +11.4}_{-1.3 -13.2}$	$265.5^{+5.0 +11.5}_{-4.3 -13.2}$	$223.1^{+6.9}_{-7.1}$
$pp(\sqrt{S} = 10 \text{ TeV})$	$470.7^{+1.4 +17.7}_{-2.3 -19.3}$	$474.0^{+8.3 +17.7}_{-6.0 -19.4}$	$387.4^{+2.5}_{-4.3}$
$pp(\sqrt{S} = 14 \text{ TeV})$	$772.7^{+1.6 +25.5}_{-3.1 -26.7}$	$777.5^{+11.9 +25.5}_{-7.4 -26.7}$	$623.7^{+4.7}_{-9.3}$

Table 5.2: Total cross sections for the production of $\tilde{\chi}_1^+ \tilde{\chi}_2^0$ pairs in the SPS1a' scenario at different hadron colliders and centre-of-mass energies in the LO, NLO and NLL+NLO approximation, together with the corresponding scale and PDF uncertainties.

rection is larger at the Tevatron with its lower centre-of-mass energy (top left) than at the LHC (top right) and increases with the invariant mass. The relatively small differences among the K^{NLL} -factors for neutralino pair production and the channels involving at least one chargino can be traced to the fact that the former receives most of its contributions from t - and u -channel squark exchanges, which are more sensible to strong corrections than the exchanges of electroweak bosons in the s -channel.

The K^{NLL} -factors for the production of heavy gaugino pairs at the LHC with $\sqrt{S} = 7$ TeV (14 TeV) are presented in Fig. 5.8 bottom left (bottom right). since the gaugino masses as well as the invariant masses M are now closer to the hadronic centre-of-mass energies. In addition, the result for the $\tilde{\chi}_3^0 \tilde{\chi}_4^0$ channel differs no longer substantially from the other channels, since the heavy neutralinos are now higgsino-like and their production is now also dominated by the s -channel exchange of a weak gauge boson.

5.4 Total cross section

The stability of the perturbative series and its reorganization is traditionally checked by varying the factorisation and renormalisation scales μ_F and μ_R about a central value μ_0 . We therefore present now the total cross sections for the production of light gaugino pairs at the Tevatron (Figs. 5.9 and 5.10) and at the LHC with $\sqrt{S} = 7$ TeV (Fig. 5.11 and 5.12) as a function of the ratio $\mu_{F,R}/\mu_0$, where the central scale μ_0 is now chosen to be the average mass of the produced gaugino pair. The LO prediction (blue, dot-dashed) of the electroweak processes under consideration is, of course, independent of the renormalisation scale μ_R (right part of the figures), whereas the NLO prediction (black, dashed) depends inversely on the logarithm of μ_R through the strong coupling $\alpha_s(\mu_R)$. At NLL accuracy (red, full), the resummed soft corrections attenuate this dependence and introduce a plateau region, so that the prediction is stabilized. The factorisation scale μ_F (central part of the figures) enters the hadronic cross section already at LO through the largely logarithmic dependence of the PDFs, which is then attenuated by the factorisation of initial-state singularities at NLO and further at NLL accuracy. In all cases, the resulting total NLL+NLO prediction is thus much less dependent on the common scale $\mu_F = \mu_R = \mu$ (left part of the figures) than the LO and NLO estimates.

In Tab. 5.2 we present the total cross sections for the trilepton channel in the SPS1a' scenario at the Tevatron ($\sqrt{S} = 1.96$ TeV) and LHC ($\sqrt{S} = 7, 10$ and 14 TeV). Besides the central values (in fb) at LO, NLO and NLL+NLO, we also present the scale and PDF uncertainties. The former are estimated as described above by a common variation of the

5.4 Total cross section

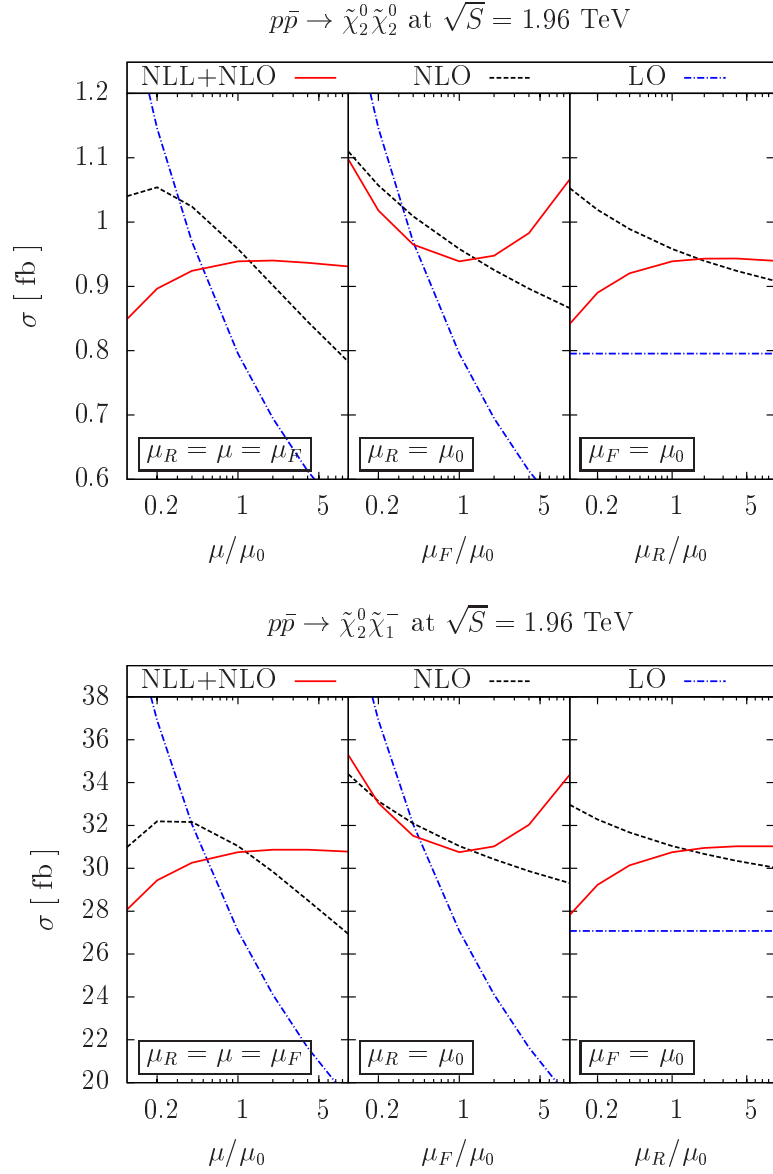


Figure 5.9: Total cross sections for the production of neutralino (top) and chargino-neutralino (bottom) at the Tevatron with $\sqrt{S} = 1.96$ TeV in the LO (blue, dot-dashed), NLO (black, dashed) and NLL+NLO (red, full) approximation.

5 Gaugino-pair production: Resummed calculations

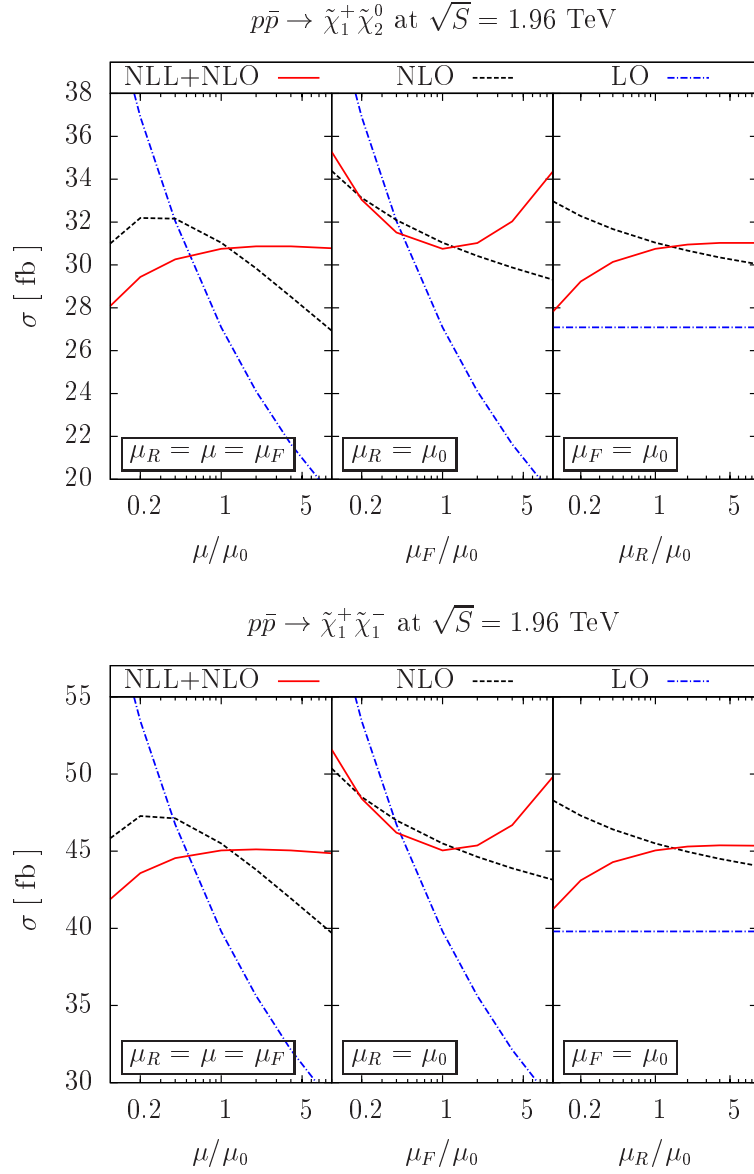


Figure 5.10: Total cross sections for the production of chargino-neutralino (top) and chargino pairs (bottom) at the Tevatron with $\sqrt{S} = 1.96$ TeV in the LO (blue, dot-dashed), NLO (black, dashed) and NLL+NLO (red, full) approximation.

5.4 Total cross section

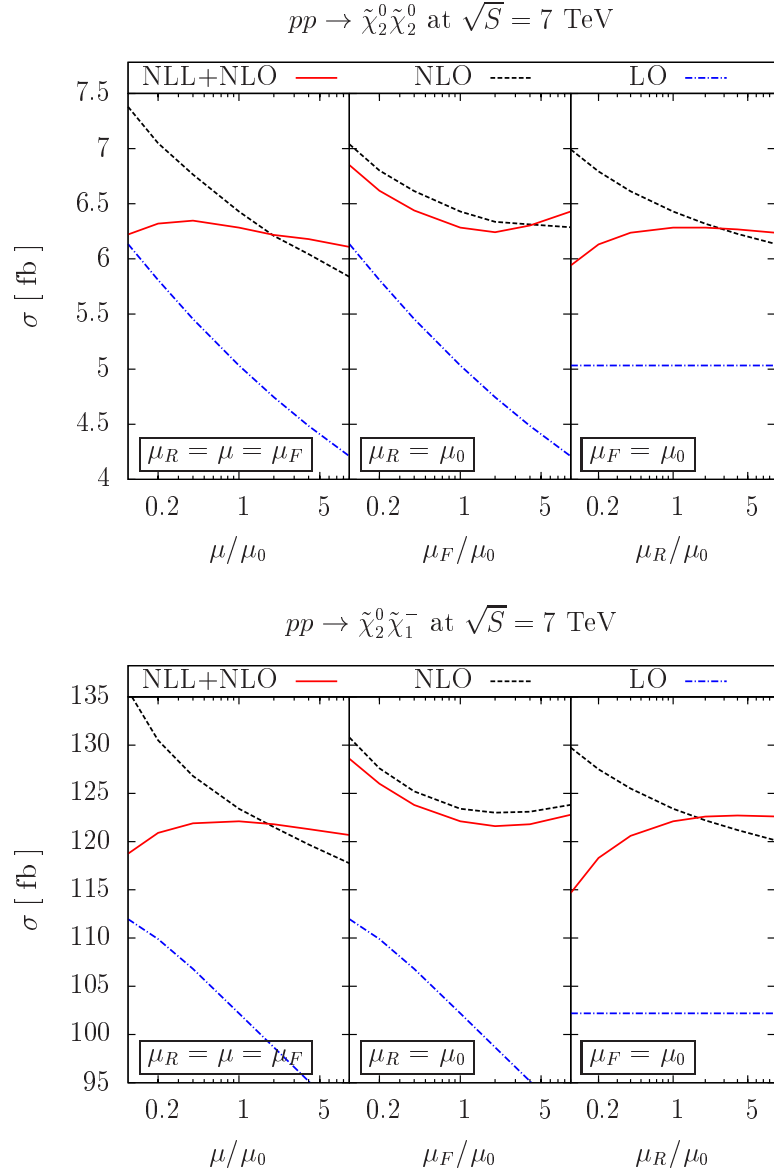


Figure 5.11: Same as Fig. 5.9 for the LHC with its current centre-of-mass energy of $\sqrt{S} = 7$ TeV.

5 Gaugino-pair production: Resummed calculations

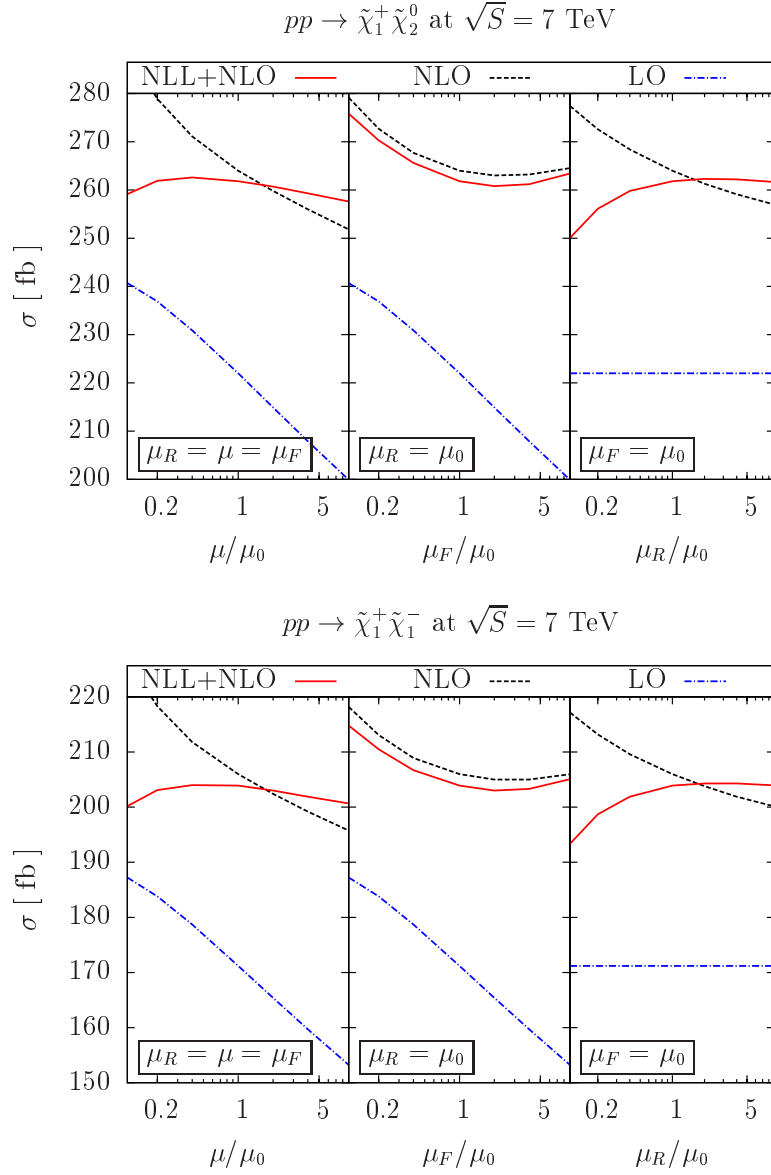


Figure 5.12: Same as Fig. 5.10 for the LHC with its current centre-of-mass energy of $\sqrt{S} = 7$ TeV.

5.4 Total cross section

Gaugino pair	$\sigma^{\text{NLL+NLO}}$ [fb]	σ^{NLO} [fb]	σ^{LO} [fb]
$\tilde{\chi}_2^0 \tilde{\chi}_2^0$	$25.1^{+0.3+1.2}_{-0.2-0.7}$	$25.5^{+0.8+1.3}_{-0.6-0.7}$	$19.2^{+0.3}_{-0.4}$
$\tilde{\chi}_1^+ \tilde{\chi}_1^-$	$665.8^{+1.0+20.6}_{-2.2-20.6}$	$671.1^{+10.8+20.7}_{-6.6-20.6}$	$533.4^{+3.4}_{-7.3}$
$\tilde{\chi}_2^0 \tilde{\chi}_1^-$	$433.3^{+0.6+17.9}_{-0.8-16.0}$	$436.9^{+7.2+17.9}_{-3.5-16.1}$	$348.3^{+2.2}_{-4.9}$
$\tilde{\chi}_1^+ \tilde{\chi}_2^0$	$772.7^{+1.6+25.5}_{-3.1-26.7}$	$777.5^{+11.9+25.5}_{-7.4-26.7}$	$623.7^{+4.7}_{-9.3}$
$\tilde{\chi}_3^0 \tilde{\chi}_4^0$	$14.6^{+0.0+0.7}_{-0.1-0.7}$	$14.8^{+0.3+0.7}_{-0.3-0.7}$	$12.1^{+0.5}_{-0.5}$
$\tilde{\chi}_2^+ \tilde{\chi}_2^-$	$14.0^{+0.1+0.7}_{-0.0-0.6}$	$14.2^{+0.3+0.7}_{-0.3-0.6}$	$11.7^{+0.5}_{-0.5}$
$\tilde{\chi}_3^0 \tilde{\chi}_2^-$	$8.5^{+0.0+0.6}_{-0.0-0.5}$	$8.6^{+0.2+0.6}_{-0.2-0.5}$	$6.9^{+0.3}_{-0.3}$
$\tilde{\chi}_2^+ \tilde{\chi}_3^0$	$19.1^{+0.1+0.9}_{-0.1-1.0}$	$19.3^{+0.4+0.9}_{-0.4-1.0}$	$16.0^{+0.7}_{-0.7}$
$\tilde{\chi}_4^0 \tilde{\chi}_2^-$	$7.8^{+0.0+0.5}_{-0.0-0.5}$	$7.9^{+0.2+0.5}_{-0.2-0.5}$	$6.4^{+0.3}_{-0.3}$
$\tilde{\chi}_2^+ \tilde{\chi}_4^0$	$17.7^{+0.1+0.8}_{-0.1-0.9}$	$17.8^{+0.4+0.8}_{-0.3-0.9}$	$14.9^{+0.7}_{-0.6}$

Table 5.3: Total cross sections for the production of various gaugino pairs in the SPS1a' scenario at the LHC with its design centre-of-mass energy of $\sqrt{S} = 14$ TeV. The central predictions are given at LO, NLO and NLL+NLO together with the corresponding scale and PDF uncertainties.

renormalisation and factorisation scales by a factor of two about the average mass of the two gauginos, the latter through

$$\Delta\sigma_{\text{PDF}+} = \sqrt{\sum_{i=1}^{22} \left[\max(\sigma_{+i} - \sigma_0, \sigma_{-i} - \sigma_0, 0) \right]^2} \quad \text{and} \quad (5.15)$$

$$\Delta\sigma_{\text{PDF}-} = \sqrt{\sum_{i=1}^{22} \left[\max(\sigma_0 - \sigma_{+i}, \sigma_0 - \sigma_{-i}, 0) \right]^2} \quad (5.16)$$

along the 22 eigenvector directions defined by the CTEQ collaboration. Since these are available only for the NLO fit CTEQ6.6M, but not for the LO fit CTEQ6.6L1, we do not present a PDF uncertainty for the LO prediction. Furthermore, the same PDF set enters at NLO and NLL+NLO, so that the PDF uncertainties for these two predictions coincide. The most important result is again the considerable reduction of the scale uncertainty from LO to NLO and then to NLL+NLO. The total cross sections increase with the available centre-of-mass energy due to the higher parton luminosity at smaller values of x . A crude estimate gives

$$\sigma_{pp} = \int_{m^2/S}^1 d\tau f_{q/p}(x_q) f_{\bar{q}/p}(x_{\bar{q}}) \sigma_{q\bar{q}} \sim \int_{m^2/S}^1 d\tau \tau^{-1.8} \frac{1}{\tau S}, \sim \sqrt{S}^{1.6} \quad (5.17)$$

which agrees with the cross sections given in Tab. 5.2 surprisingly well.

In Tab. 5.3 we fix the LHC centre-of-mass energy to its design value of $\sqrt{S} = 14$ TeV and show the total production cross sections for light and heavy gaugino pairs in LO, NLO and NLL+NLO together with the corresponding theoretical uncertainties. As it was already mentioned above, the cross section for the higgsino-like $\tilde{\chi}_3^0 \tilde{\chi}_4^0$ pairs is about as large as the one for $\tilde{\chi}_2^+ \tilde{\chi}_2^-$ pairs, and it is in fact not much smaller than the one for the considerably lighter gaugino-like $\tilde{\chi}_2^0 \tilde{\chi}_2^0$ pairs. In general, the heavy gaugino cross sections are, however, significantly smaller than those for light gauginos.

In Tab. 5.4, we present finally total cross sections for the trilepton channel in our different benchmark scenarios at the LHC with its current centre-of-mass energy of $\sqrt{S} = 7$ TeV.

5 Gaugino-pair production: Resummed calculations

Scenario	$\sigma^{\text{NLL+NLO}}$ [fb]	σ^{NLO} [fb]	σ^{LO} [fb]
LM1	$294.6^{+0.8+12.8}_{-1.4-14.5}$	$297.0^{+5.8+12.8}_{-4.8-14.5}$	$248.2^{+7.1}_{-7.5}$
LM7	$538.9^{+2.4+23.9}_{-3.5-26.7}$	$543.8^{+12.8+24.0}_{-10.7-26.8}$	$441.2^{+14.0}_{-14.3}$
LM9	$1736.2^{+8.0+68.8}_{-12.1-74.3}$	$1750.3^{+38.8+69.0}_{-28.8-74.4}$	$1374.4^{+8.4}_{-15.7}$
SU2	$171.7^{+0.5+8.5}_{-0.9-9.8}$	$173.4^{+4.2+8.5}_{-3.9-9.8}$	$145.0^{+7.4}_{-7.0}$
SU3	$116.9^{+0.1+5.6}_{-0.4-6.4}$	$118.0^{+2.2+5.6}_{-2.1-6.4}$	$101.6^{+4.6}_{-4.4}$
SU2+JV	$170.4^{+0.2+8.6}_{-0.7-9.8}$	$172.0^{+3.9+8.6}_{-3.6-9.9}$	$145.0^{+7.4}_{-7.0}$
SU3+JV	$115.4^{+0.1+5.6}_{-0.1-6.4}$	$116.6^{+1.9+5.6}_{-1.8-6.4}$	$101.6^{+4.6}_{-4.4}$

Table 5.4: Total cross sections for the production of $\tilde{\chi}_1^+ \tilde{\chi}_2^0$ pairs at the LHC with its current centre-of-mass energy of $\sqrt{S} = 7$ TeV for different SUSY benchmark points. The central predictions are given at LO, NLO and NLL+NLO together with the corresponding scale and PDF uncertainties.

Since the masses of $\tilde{\chi}_1^\pm$ and $\tilde{\chi}_2^0$ are always rather similar, one expects also similar total cross sections. This is indeed confirmed by the $\sqrt{S} = 7$ TeV results in Tab. 5.2 and the numbers in Tab. 5.4 with the notable exceptions of LM7 and LM9, where the cross section is about a factor of two and one order of magnitude larger than for the other points, respectively. This is partly due to the lower gaugino masses at LM9 and partly to the much heavier squark masses, which suppress the t - and u -channels and thus their destructive interference with the s -channel amplitudes. The additional jet veto (JV), i.e. the rejection of events containing jets with transverse momentum $p_T > 20$ GeV, envisaged by the ATLAS collaboration to suppress the background from top quark pair production, has obviously no consequences at LO, since gauginos are exclusively produced at this order. An additional quark or gluon can only be present at NLO or NLL+NLO, and restricting its transverse momentum to low values reduces the total cross sections slightly with respect to the unrestricted predictions. The small reduction of the signal cross section in combination with a large reduction of the background should therefore indeed lead to a much better significance.

6

Conclusion

Weak-scale supersymmetry is a very well motivated extension of the SM of particle physics. It offers a natural explanation of the large hierarchy between electroweak and gravitational interactions and allows for the grand unification of the local gauge symmetry of the strong and electroweak interactions. Among the new particles predicted by the MSSM, the fermionic partners of the neutral and charged gauge and Higgs bosons, called neutralinos and charginos, may be relatively light. Indeed, the lightest neutralino, stabilized by an at least approximate R -symmetry, represents one of the most promising dark matter candidates, whose gaugino/Higgsino decomposition has important consequences for cosmology. The search for SUSY particles and the identification of their properties have thus become defining tasks of the current hadron collider program. Particular attention has since long been paid to the production of gauginos, which are produced either directly or through squark/gluino decays. Gauginos may decay leptonically and be thus easily identifiable at the Tevatron and at the LHC. Gaugino-pair production is therefore a very important SUSY discovery channel at both currently running hadron colliders.

In this thesis, we have presented the MSSM, with its field content, its Lagrange density and the resulting mass eigenstates and mixing. Then, we have presented threshold and transverse-momentum resummation techniques with improvements to resum collinear sub-dominant contributions and the necessary prescriptions to get well-defined differential cross sections. The second part of this document has been dedicated to the gaugino-pair production at present pp and $p\bar{p}$ colliders. We have studied the polarisation effects and the effects of the SUSY-QCD corrections, generalising the existing results by allowing the virtual squarks to mix. We have then performed an extensive analysis of the resummation effects for gaugino-pair production in minimal supergravity scenarios. The threshold enhanced corrections have been found to increase the invariant-mass and total cross sections only slightly, but stabilised the reorganised perturbative series with respect to the fixed-order calculation. We have also calculated the transverse-momentum spectrum of gaugino pairs at NLL accuracy and investigated in detail the theoretical uncertainties coming from scale and parton-density function variations. We have found that this renders the perturbative prediction finite, modifies considerably the traditional Monte Carlo predictions, and reduces the theoretical uncertainties to the level of 5–10%. These calculations have a direct impact on the extraction of the gaugino masses and properties, which are potentially related to dark matter properties.

Quite recently, we have entered the era of the NLO Monte Carlo event generators. These programs are often preferred, especially by experimentalists, because they allow to compare

6 Conclusion

experimental data to theoretical predictions, or to simulate experimental signatures when they are no data yet. It is expected that both the resummation and the parton showers implemented in Monte Carlo generators correctly describe the effects of soft-gluon emission from the incoming partons. Nevertheless, resummation techniques provide analytic formulations, and are therefore complementary to the parton shower techniques in the sense that they allow for testing and improving the latter.

As perspectives, comparisons between resummed NLL+NLO and NLO Monte Carlo predictions would be very interesting in order to improve our understanding of parton showering. This last study would also permit to investigate the relevant cuts for the optimisation of signal to background, including the discriminant cut on \cancel{E}_T , and see what is the real impact of our calculations on the experimental determination of the gaugino properties.

The resummation of both the threshold enhanced and small- p_T contributions have been incorporated in a single formalism, namely the joint resummation [46, 58, 110]. An implementation of that formalism is in progress and a comparison with the results presented in this document will then be performed.

Resummation techniques have already been applied to other SUSY processes. Indeed, threshold resummation has been applied to the production of squarks and gluinos [111, 112]. The soft-gluon enhancements have been found to be larger than for the gaugino case, because of larger total colour charges of the produced particle pairs. For slepton-pair production, transverse-momentum, threshold and joint resummations have been applied [113, 114, 115]. A single resummation code for all the SUSY processes would then be a very useful tool.

Bibliography

- [1] S. L. Glashow, “Partial Symmetries of Weak Interactions,” *Nucl. Phys.* **22** (1961) 579–588.
- [2] A. Salam, “Weak and Electromagnetic Interactions,”. Originally printed in *Svartholm: Elementary Particle Theory, Proceedings Of The Nobel Symposium Held 1968 At Lerum, Sweden*, Stockholm 1968, 367-377.
- [3] S. Weinberg, “A Model of Leptons,” *Phys. Rev. Lett.* **19** (1967) 1264–1266.
- [4] D. J. Gross and F. Wilczek, “Ultraviolet behavior of non-abelian gauge theories,” *Phys. Rev. Lett.* **30** (1973) 1343–1346.
- [5] H. D. Politzer, “Reliable perturbative results for strong interactions?,” *Phys. Rev. Lett.* **30** (1973) 1346–1349.
- [6] F. Englert and R. Brout, “Broken symmetry and the mass of gauge vector mesons,” *Phys. Rev. Lett.* **13** (1964) 321–322.
- [7] P. W. Higgs, “Broken symmetries and the masses of gauge bosons,” *Phys. Rev. Lett.* **13** (1964) 508–509.
- [8] H. P. Nilles, “Supersymmetry, Supergravity and Particle Physics,” *Phys. Rept.* **110** (1984) 1–162.
- [9] H. E. Haber and G. L. Kane, “The Search for Supersymmetry: Probing Physics Beyond the Standard Model,” *Phys. Rept.* **117** (1985) 75–263.
- [10] **Boomerang** Collaboration, A. H. Jaffe *et al.*, “Cosmology from Maxima-1, Boomerang and COBE/DMR CMB Observations,” *Phys. Rev. Lett.* **86** (2001) 3475–3479, arXiv:astro-ph/0007333.
- [11] **WMAP** Collaboration, D. N. Spergel *et al.*, “Wilkinson Microwave Anisotropy Probe (WMAP) three year results: Implications for cosmology,” *Astrophys. J. Suppl.* **170** (2007) 377, arXiv:astro-ph/0603449.
- [12] J. R. Ellis, K. A. Olive, Y. Santoso, and V. C. Spanos, “Supersymmetric Dark Matter in Light of WMAP,” *Phys. Lett.* **B565** (2003) 176–182, arXiv:hep-ph/0303043.
- [13] LEPSUSYWG, ALEPH, DELPHI, L3 and OPAL experiments, note LEPSUSYWG/01-03.1 and LEPSUSYWG/04-01.1 (<http://lepsusy.web.cern.ch/lepsusy/Welcome.html>).

Bibliography

- [14] **CDF** Collaboration, T. Aaltonen *et al.*, “Search for Supersymmetry in ppbar Collisions at $\sqrt{s} = 1.96$ -TeV Using the Trilepton Signature of Chargino-Neutralino Production,” *Phys. Rev. Lett.* **101** (2008) 251801, arXiv:0808.2446 [hep-ex].
- [15] **D0** Collaboration, V. M. Abazov *et al.*, “Search for associated production of charginos and neutralinos in the trilepton final state using 2.3 fb⁻¹ of data,” *Phys. Lett.* **B680** (2009) 34–43, arXiv:0901.0646 [hep-ex].
- [16] H. Baer, V. Barger, A. Lessa, and X. Tata, “Capability of LHC to discover supersymmetry with $\sqrt{s} = 7$ TeV and 1 fb⁻¹,” arXiv:1004.3594 [hep-ph].
- [17] J. C. Collins, D. E. Soper, and G. Sterman, “Heavy Particle Production in High-Energy Hadron Collisions,” *Nucl. Phys.* **B263** (1986) 37.
- [18] G. Sterman, “Summation of Large Corrections to Short Distance Hadronic Cross-Sections,” *Nucl. Phys.* **B281** (1987) 310.
- [19] S. R. Coleman and J. Mandula, “All possible symmetries of the s matrix,” *Phys. Rev.* **159** (1967) 1251–1256.
- [20] R. Haag, J. T. Lopuszanski, and M. Sohnius, “All Possible Generators of Supersymmetries of the s Matrix,” *Nucl. Phys.* **B88** (1975) 257.
- [21] Y. A. Golfand and E. P. Likhtman, “Extension of the Algebra of Poincare Group Generators and Violation of p Invariance,” *JETP Lett.* **13** (1971) 323–326.
- [22] D. V. Volkov and V. P. Akulov, “Is the Neutrino a Goldstone Particle?,” *Phys. Lett.* **B46** (1973) 109–110.
- [23] J. Wess and B. Zumino, “Supergauge Transformations in Four-Dimensions,” *Nucl. Phys.* **B70** (1974) 39–50.
- [24] J. Wess and B. Zumino, “A Lagrangian Model Invariant Under Supergauge Transformations,” *Phys. Lett.* **B49** (1974) 52.
- [25] J. Wess and B. Zumino, “Supergauge Invariant Extension of Quantum Electrodynamics,” *Nucl. Phys.* **B78** (1974) 1.
- [26] S. P. Martin, “A Supersymmetry Primer,” arXiv:hep-ph/9709356.
- [27] P. Fayet and J. Iliopoulos, “Spontaneously Broken Supergauge Symmetries and Goldstone Spinors,” *Phys. Lett.* **B51** (1974) 461–464.
- [28] L. Girardello and M. T. Grisaru, “Soft Breaking of Supersymmetry,” *Nucl. Phys.* **B194** (1982) 65.
- [29] A. H. Chamseddine, R. L. Arnowitt, and P. Nath, “Locally Supersymmetric Grand Unification,” *Phys. Rev. Lett.* **49** (1982) 970.
- [30] R. Barbieri, S. Ferrara, and C. A. Savoy, “Gauge Models with Spontaneously Broken Local Supersymmetry,” *Phys. Lett.* **B119** (1982) 343.
- [31] L. J. Hall, J. D. Lykken, and S. Weinberg, “Supergravity as the Messenger of Supersymmetry Breaking,” *Phys. Rev.* **D27** (1983) 2359–2378.

Bibliography

- [32] G. J. Gounaris, C. Le Mouel, and P. I. Porfyriadis, “A description of the neutralino observables in terms of projectors,” *Phys. Rev.* **D65** (2002) 035002, [arXiv:hep-ph/0107249](#).
- [33] M. M. El Kheishen, A. A. Aboshousha, and A. A. Shafik, “Analytic formulas for the neutralino masses and the neutralino mixing matrix,” *Phys. Rev.* **D45** (1992) 4345–4348.
- [34] J. C. Collins, D. E. Soper, and G. Sterman, “Factorization of Hard Processes in QCD,” *Adv. Ser. Direct. High Energy Phys.* **5** (1988) 1–91, [arXiv:hep-ph/0409313](#).
- [35] W. E. Caswell, “Asymptotic Behavior of Nonabelian Gauge Theories to Two Loop Order,” *Phys. Rev. Lett.* **33** (1974) 244.
- [36] G. Altarelli and G. Parisi, “Asymptotic Freedom in Parton Language,” *Nucl. Phys.* **B126** (1977) 298.
- [37] W. Furmanski and R. Petronzio, “Lepton - Hadron Processes Beyond Leading Order in Quantum Chromodynamics,” *Zeit. Phys.* **C11** (1982) 293.
- [38] F. Bloch and A. Nordsieck, “Note on the Radiation Field of the electron,” *Phys. Rev.* **52** (1937) 54–59.
- [39] S. Catani and L. Trentadue, “Resummation of the QCD Perturbative Series for Hard Processes,” *Nucl. Phys.* **B327** (1989) 323.
- [40] J. C. Collins, D. E. Soper, and G. Sterman, “Transverse Momentum Distribution in Drell-Yan Pair and W and Z Boson Production,” *Nucl. Phys.* **B250** (1985) 199.
- [41] G. Bozzi, S. Catani, D. de Florian, and M. Grazzini, “Transverse-momentum resummation and the spectrum of the Higgs boson at the LHC,” *Nucl. Phys.* **B737** (2006) 73–120, [arXiv:hep-ph/0508068](#).
- [42] W. R. Frazer and J. F. Gunion, “Scale breaking for quark and gluon distributions in QCD: a diagrammatic analysis,” *Phys. Rev.* **D19** (1979) 2447.
- [43] J. G. M. Gatheral, “Exponentiation of eikonal cross-sections in nonabelian gauge theories,” *Phys. Lett.* **B133** (1983) 90.
- [44] S. Catani and L. Trentadue, “Comment on QCD exponentiation at large x,” *Nucl. Phys.* **B353** (1991) 183–186.
- [45] M. Krämer, E. Laenen, and M. Spira, “Soft gluon radiation in Higgs boson production at the LHC,” *Nucl. Phys.* **B511** (1998) 523–549, [arXiv:hep-ph/9611272](#).
- [46] A. Kulesza, G. Sterman, and W. Vogelsang, “Joint resummation in electroweak boson production,” *Phys. Rev.* **D66** (2002) 014011, [arXiv:hep-ph/0202251](#).
- [47] J. Kodaira and L. Trentadue, “Summing Soft Emission in QCD,” *Phys. Lett.* **B112** (1982) 66.

Bibliography

- [48] S. Catani, E. D’Emilio, and L. Trentadue, “The gluon form-factor to higher orders: gluon gluon annihilation at small Q -transverse,” *Phys. Lett.* **B211** (1988) 335–342.
- [49] J. C. Collins and D. E. Soper, “Back-To-Back Jets in QCD,” *Nucl. Phys.* **B193** (1981) 381.
- [50] J. C. Collins and D. E. Soper, “Back-To-Back Jets: Fourier Transform from B to K-Transverse,” *Nucl. Phys.* **B197** (1982) 446.
- [51] S. Catani, D. de Florian, and M. Grazzini, “Universality of non-leading logarithmic contributions in transverse momentum distributions,” *Nucl. Phys.* **B596** (2001) 299–312, [arXiv:hep-ph/0008184](#).
- [52] D. de Florian and M. Grazzini, “Next-to-next-to-leading logarithmic corrections at small transverse momentum in hadronic collisions,” *Phys. Rev. Lett.* **85** (2000) 4678–4681, [arXiv:hep-ph/0008152](#).
- [53] D. de Florian and M. Grazzini, “The structure of large logarithmic corrections at small transverse momentum in hadronic collisions,” *Nucl. Phys.* **B616** (2001) 247–285, [arXiv:hep-ph/0108273](#).
- [54] G. A. Ladinsky and C. P. Yuan, “The Non-perturbative regime in QCD resummation for gauge boson production at hadron colliders,” *Phys. Rev.* **D50** (1994) 4239, [arXiv:hep-ph/9311341](#).
- [55] F. Landry, R. Brock, G. Ladinsky, and C. P. Yuan, “New fits for the nonperturbative parameters in the CSS resummation formalism,” *Phys. Rev.* **D63** (2001) 013004, [arXiv:hep-ph/9905391](#).
- [56] F. Landry, R. Brock, P. M. Nadolsky, and C. P. Yuan, “Tevatron Run-1 Z boson data and Collins-Soper-Sterman resummation formalism,” *Phys. Rev.* **D67** (2003) 073016, [arXiv:hep-ph/0212159](#).
- [57] A. V. Konychev and P. M. Nadolsky, “Universality of the Collins-Soper-Sterman nonperturbative function in gauge boson production,” *Phys. Lett.* **B633** (2006) 710–714, [arXiv:hep-ph/0506225](#).
- [58] E. Laenen, G. Sterman, and W. Vogelsang, “Higher-order QCD corrections in prompt photon production,” *Phys. Rev. Lett.* **84** (2000) 4296–4299, [arXiv:hep-ph/0002078](#).
- [59] S. Catani, M. L. Mangano, P. Nason, and L. Trentadue, “The Resummation of Soft Gluon in Hadronic Collisions,” *Nucl. Phys.* **B478** (1996) 273–310, [arXiv:hep-ph/9604351](#).
- [60] H. Contopanagos and G. Sterman, “Principal value resummation,” *Nucl. Phys.* **B419** (1994) 77–104, [arXiv:hep-ph/9310313](#).
- [61] J. Debove, B. Fuks, and M. Klasen, “Gaugino-pair production in polarized and unpolarized hadron collisions,” *Phys. Rev.* **D78** (2008) 074020, [arXiv:0804.0423 \[hep-ph\]](#).

Bibliography

- [62] J. Debove, B. Fuks, and M. Klasen, “Threshold resummation for gaugino pair production at hadron colliders,” *arXiv:1005.2909* [Unknown].
- [63] V. D. Barger, R. W. Robinett, W.-Y. Keung, and R. J. N. Phillips, “Production of gauge fermions at colliders,” *Phys. Lett.* **B131** (1983) 372.
- [64] S. Dawson, E. Eichten, and C. Quigg, “Search for Supersymmetric Particles in Hadron - Hadron Collisions,” *Phys. Rev.* **D31** (1985) 1581.
- [65] S. Y. Choi, A. Djouadi, H. S. Song, and P. M. Zerwas, “Determining SUSY parameters in chargino pair-production in e^+e^- collisions,” *Eur. Phys. J.* **C8** (1999) 669–677, *arXiv:hep-ph/9812236*.
- [66] G. J. Gounaris, J. Layssac, P. I. Porfyriadis, and F. M. Renard, “Neutralino pair production at LHC,” *Phys. Rev.* **D70** (2004) 033011, *arXiv:hep-ph/0404162*.
- [67] G. Bozzi, B. Fuks, B. Herrmann, and M. Klasen, “Squark and gaugino hadroproduction and decays in non- minimal flavour violating supersymmetry,” *Nucl. Phys.* **B787** (2007) 1–54, *arXiv:0704.1826* [hep-ph].
- [68] W. Beenakker *et al.*, “The Production of charginos / neutralinos and sleptons at hadron colliders,” *Phys. Rev. Lett.* **83** (1999) 3780–3783, *arXiv:hep-ph/9906298*.
- [69] G. Bunce *et al.* RHIC Spin Group, <http://www.phy.bnl.gov/rhicspin/documents/4year.pdf>.
- [70] **SPIN** Collaboration, R. Baiod, P. S. Martin, and A. D. Russell, “Polarized protons in the Tevatron Collider,”. Prepared for 10th Topical Workshop on Proton-Antiproton Collider Physics, Batavia, Illinois, 9-13 May 1995.
- [71] A. De Roeck and P. R. Newman. Private communications.
- [72] M. Glück, E. Reya, and A. Vogt, “Dynamical parton distributions revisited,” *Eur. Phys. J.* **C5** (1998) 461–470, *arXiv:hep-ph/9806404*.
- [73] M. Glück, E. Reya, M. Stratmann, and W. Vogelsang, “Models for the polarized parton distributions of the nucleon,” *Phys. Rev.* **D63** (2001) 094005, *arXiv:hep-ph/0011215*.
- [74] D. de Florian, R. Sassot, M. Stratmann, and W. Vogelsang, “Global Analysis of Helicity Parton Densities and Their Uncertainties,” *Phys. Rev. Lett.* **101** (2008) 072001, *arXiv:0804.0422* [hep-ph].
- [75] **D0** Collaboration, V. M. Abazov *et al.*, “Search for squarks and gluinos in events with jets and missing transverse energy in $p\bar{p}$ collisions at $\sqrt{s} = 1.96$ -TeV,” *Phys. Lett.* **B638** (2006) 119–127, *arXiv:hep-ex/0604029*.
- [76] **CDF** Collaboration, T. Aaltonen *et al.*, “Search for chargino-neutralino production in $p\bar{p}$ collisions at 1.96-TeV with high- $p(T)$ leptons,” *Phys. Rev.* **D77** (2008) 052002, *arXiv:0711.3161* [hep-ex].
- [77] **OPAL** Collaboration, G. Abbiendi *et al.*, “Search for nearly mass-degenerate charginos and neutralinos at LEP,” *Eur. Phys. J.* **C29** (2003) 479–489, *arXiv:hep-ex/0210043*.

Bibliography

- [78] **DELPHI** Collaboration, J. Abdallah *et al.*, “Searches for supersymmetric particles in e^+e^- collisions up to 208-GeV and interpretation of the results within the MSSM,” *Eur. Phys. J.* **C31** (2003) 421–479, arXiv:hep-ex/0311019.
- [79] **Particle Data Group** Collaboration, W. M. Yao *et al.*, “Review of particle physics,” *J. Phys.* **G33** (2006) 1–1232.
- [80] S. P. Martin, K. Tobe, and J. D. Wells, “Virtual effects of light gauginos and higgsinos: A precision electroweak analysis of split supersymmetry,” *Phys. Rev.* **D71** (2005) 073014, arXiv:hep-ph/0412424.
- [81] T. Moroi, “The Muon Anomalous Magnetic Dipole Moment in the Minimal Supersymmetric Standard Model,” *Phys. Rev.* **D53** (1996) 6565–6575, arXiv:hep-ph/9512396.
- [82] V. Buescher and K. Jakobs, “Higgs boson searches at hadron colliders,” *Int. J. Mod. Phys.* **A20** (2005) 2523–2602, arXiv:hep-ph/0504099.
- [83] J. F. Gunion, L. Poggioli, R. J. Van Kooten, C. Kao, and P. Rowson, “Higgs boson discovery and properties,” arXiv:hep-ph/9703330.
- [84] D. Denegri, W. Majerotto, and L. Rurua, “Constraining the minimal supergravity model parameter $\tan(\beta)$ by measuring the dilepton mass distribution at LHC,” *Phys. Rev.* **D60** (1999) 035008, arXiv:hep-ph/9901231.
- [85] T. Roser, “RHIC and its Upgrade Programs,” *Conf. Proc.* **C0806233** (2008) frxagm01.
- [86] B. Surrow and f. t. S. Collaboration, “Recent STAR results in high-energy polarized proton-proton collisions at RHIC,” arXiv:1004.4884 [hep-ex].
- [87] A. D. Krisch, “Accelerating polarized protons with Siberian snakes,” *Acta Phys. Polon.* **B29** (1998) 1357–1370.
- [88] F. Zimmermann, “LHC upgrade scenarios,”. Prepared for Particle Accelerator Conference (PAC 07), Albuquerque, New Mexico, 25-29 Jun 2007.
- [89] M. M. Nojiri, G. Polesello, and D. R. Tovey, “Measuring the mass of the lightest chargino at the CERN LHC,” arXiv:hep-ph/0312318.
- [90] G. Passarino and M. J. G. Veltman, “One Loop Corrections for e^+e^- Annihilation Into $\mu^+\mu^-$ in the Weinberg Model,” *Nucl. Phys.* **B160** (1979) 151.
- [91] M. Böhm, A. Denner, and H. Joos, “Gauge theories of the strong and electroweak interaction,”. Stuttgart, Germany: Teubner (2001) 784 p.
- [92] W. Beenakker, R. Höpker, M. Spira, and P. M. Zerwas, “Squark and gluino production at hadron colliders,” *Nucl. Phys.* **B492** (1997) 51–103, arXiv:hep-ph/9610490.
- [93] J. A. Aguilar-Saavedra *et al.*, “Supersymmetry parameter analysis: SPA convention and project,” *Eur. Phys. J.* **C46** (2006) 43–60, arXiv:hep-ph/0511344.

Bibliography

- [94] S. Catani and M. H. Seymour, “A general algorithm for calculating jet cross sections in NLO QCD,” *Nucl. Phys.* **B485** (1997) 291–419, arXiv:hep-ph/9605323.
- [95] C. S. Li, Z. Li, R. J. Oakes, and L. L. Yang, “Threshold Resummation Effects in the Associated Production of Chargino and Neutralino at Hadron Colliders,” *Phys. Rev.* **D77** (2008) 034010, arXiv:0707.3952 [hep-ph].
- [96] P. M. Nadolsky *et al.*, “Implications of CTEQ global analysis for collider observables,” *Phys. Rev.* **D78** (2008) 013004, arXiv:0802.0007 [hep-ph].
- [97] B. C. Allanach *et al.*, “The Snowmass points and slopes: Benchmarks for SUSY searches,” *Eur. Phys. J.* **C25** (2002) 113–123, arXiv:hep-ph/0202233.
- [98] A. Djouadi, J.-L. Kneur, and G. Moultaka, “SuSpect: A Fortran code for the supersymmetric and Higgs particle spectrum in the MSSM,” *Comput. Phys. Commun.* **176** (2007) 426–455, arXiv:hep-ph/0211331.
- [99] **Particle Data Group** Collaboration, C. Amsler *et al.*, “Review of particle physics,” *Phys. Lett.* **B667** (2008) 1.
- [100] **Tevatron Electroweak Working Group** Collaboration, “Combination of CDF and D0 Results on the Mass of the Top Quark,” arXiv:0903.2503 [hep-ex].
- [101] J. Debove, B. Fuks, and M. Klasen, “Transverse-momentum resummation for gaugino-pair production at hadron colliders,” *Phys. Lett.* **B688** (2010) 208–211, arXiv:0907.1105 [hep-ph].
- [102] W. Porod, “SPheno, a program for calculating supersymmetric spectra, SUSY particle decays and SUSY particle production at e+ e- colliders,” *Comput. Phys. Commun.* **153** (2003) 275–315, arXiv:hep-ph/0301101.
- [103] M. Battaglia *et al.*, “Updated post-WMAP benchmarks for supersymmetry,” *Eur. Phys. J.* **C33** (2004) 273–296, arXiv:hep-ph/0306219.
- [104] **CMS** Collaboration, G. L. Bayatian *et al.*, “CMS technical design report, volume II: Physics performance,” *J. Phys.* **G34** (2007) 995–1579.
- [105] **The ATLAS** Collaboration, G. Aad *et al.*, “Expected Performance of the ATLAS Experiment - Detector, Trigger and Physics,” arXiv:0901.0512 [hep-ex].
- [106] T. Sjöstrand, S. Mrenna, and P. Z. Skands, “PYTHIA 6.4 Physics and Manual,” *JHEP* **05** (2006) 026, arXiv:hep-ph/0603175.
- [107] **CDF** Collaboration, R. Field, “CDF Run II Monte-Carlo tunes,”. Proceedings of TeV4LHC 2006 Workshop 4th meeting, Batavia, Illinois, 20-22 Oct 2006.
- [108] I. Hinchliffe, F. E. Paige, M. D. Shapiro, J. Soderqvist, and W. Yao, “Precision SUSY measurements at CERN LHC,” *Phys. Rev.* **D55** (1997) 5520–5540, arXiv:hep-ph/9610544.
- [109] C. G. Lester and D. J. Summers, “Measuring masses of semiinvisibly decaying particles pair produced at hadron colliders,” *Phys. Lett.* **B463** (1999) 99–103, arXiv:hep-ph/9906349.

Bibliography

- [110] E. Laenen, G. Sterman, and W. Vogelsang, “Recoil and threshold corrections in short distance cross-sections,” *Phys. Rev.* **D63** (2001) 114018, arXiv:hep-ph/0010080.
- [111] A. Kulesza and L. Motyka, “Soft gluon resummation for the production of gluino-gluino and squark-antisquark pairs at the LHC,” *Phys. Rev.* **D80** (2009) 095004, arXiv:0905.4749 [hep-ph].
- [112] W. Beenakker *et al.*, “Soft-gluon resummation for squark and gluino hadroproduction,” *JHEP* **12** (2009) 041, arXiv:0909.4418 [hep-ph].
- [113] G. Bozzi, B. Fuks, and M. Klasen, “Transverse-momentum resummation for slepton-pair production at the LHC,” *Phys. Rev.* **D74** (2006) 015001, arXiv:hep-ph/0603074.
- [114] G. Bozzi, B. Fuks, and M. Klasen, “Threshold Resummation for Slepton-Pair Production at Hadron Colliders,” *Nucl. Phys.* **B777** (2007) 157–181, arXiv:hep-ph/0701202.
- [115] G. Bozzi, B. Fuks, and M. Klasen, “Joint resummation for slepton pair production at hadron colliders,” *Nucl. Phys.* **B794** (2008) 46–60, arXiv:0709.3057 [hep-ph].

Abstract

Weak-scale Supersymmetry (SUSY) is a very well motivated extension of the Standard Model of particle physics. Linking bosons and fermions in an elegant formalism, SUSY allows for a natural solution of the hierarchy problem and for accurate unification of the three Standard Model gauge couplings at a high unification scale. Furthermore, if R-parity is conserved, it provides a convincing candidate for the large amount of cold dark matter observed in the Universe. In the Minimal Supersymmetric Standard Model, this is generally the lightest neutralino, one of the spin-1/2 supersymmetric partners of the electroweak gauge bosons (gauginos) and of the Higgs bosons (Higgsinos), which mix to form four neutral (neutralino) and two charged (chargino) mass eigenstates. After an introduction to supersymmetry, we present the transverse-momentum and threshold resummation formalisms. We then consider the gaugino-pair production at current hadron colliders, i.e. at RHIC, Tevatron and LHC. We study the corresponding effects of polarised initial hadrons and full SUSY-QCD corrections. We finally apply transverse-momentum and threshold resummations to gaugino-pair production, and show that they have important impact on the transverse-momentum and invariant-mass distributions. Throughout these studies, we also investigate the theoretical uncertainties coming from scale and parton-density function variations.

Keywords: supersymmetry, neutralino, chargino, resummation, QCD, cross section, polarisation, collider.

Résumé

L'ajout de la supersymétrie au Modèle Standard (MS) de la physique des particules est très bien motivée. Reliant les bosons aux fermions dans un formalisme élégant, la supersymétrie propose une solution naturelle au problème de hiérarchie et permet l'unification des trois constantes de couplages du MS à grande échelle d'énergie. De plus, si la R-parité est conservée, elle fournit un candidat naturel pour expliquer la grande quantité de matière noire observée dans l'univers. Dans le MS supersymétrique minimal, c'est généralement le neutralino, l'un des partenaires supersymétriques des bosons électrofaibles (jauginos) et des bosons de Higgs (Higgsinos), qui se mélangent pour former quatre états propres de masses neutres (neutralinos) et deux chargés (charginos). Après une introduction sur la supersymétrie, nous présentons les formalismes de resommation au seuil et en impulsion transverse. Ensuite, nous considérons la production de paires de jauginos aux collisionneurs hadroniques actuellement en marche, i.e. RHIC, Tevatron et LHC. Nous étudions les effets dus à la polarisation des hadrons initiaux et aux corrections QCD supersymétriques complètes. Finalement, nous appliquons les resommations au seuil et en impulsion transverse à la production de paires de jauginos, et nous montrons qu'elles ont un impact important sur les distributions de masses invariantes et d'impulsion transverses. Tout au long de ces études, nous analysons en détail les erreurs théoriques venant des variations d'échelles et des fonctions de densités de partons.

Mots-clés: supersymétrie, neutralino, chargino, resommation, QCD, section efficace, polarisation, collisionneur.